Analyses of Heat Transfer and Temperature-induced Behaviour in Geotechnics

Dissertation

as a requirement of the degree of
Doktor-Ingenieur (Dr.-Ing.)

at the Faculty of
Civil and Environmental Engineering
Ruhr-Universität Bochum

submitted by
Yang Yang
from Anhui, China

Reviewers
Prof. Dr.-Ing. habil. Tom Schanz
Assoc. Prof. Dr. Doc. Maria Datcheva
Prof. Dr. rer. nat. habil. Klaus Gürlebeck
Prof. Dr.-Ing. Holger Steeb
Prof. Dr. Annette Hafner

Bochum, December 2016

Vorwort des Herausgebers

Thermisch-Hydraulisch-Mechanisch (THM) gekoppelte Prozesse spielen bei zahlreichen Aufgabenstellungen der Geotechnik und darüber hinaus (Biomechanik, Geowissenschaften etc.) eine sehr wichtige Rolle. Die diese Probleme beschreibenden Gruppen von gekoppelten Differentialgleichungen werden sehr häufig mittels numerischer Verfahren behandelt. Herr Dr. Yang geht in seiner Arbeit hingegen einen eher klassischen Weg. Unter der Verwendung der Grundlagen der Poroelastizität fügt er seinen analytischen Herleitungen die notwendigen thermischen und hydraulischen Prozesse hinzu und erzielt mittels unterschiedlicher numerischer Verfahren letztendlich Lösungen für die transiente Entwicklung der zu Grunde liegenden Zustandsgrößen. Die verwendeten numerischen Verfahren werden von ihm modifiziert und erfolgreich implementiert. Derartige analytische Lösungen erlauben effiziente Systembetrachtungen unter Variation der Systemparameter und können zusätzlich als Referenzlösungen im Rahmen der Validierung von numerischen Verfahren dienen.

Herr Dr. Yang präsentiert die allgemeine Lösung für einen geschichteten gesättigten Halbraum unter Berücksichtigung der Thermo-Osmose (hier als Kopplung zwischen dem Temperaturfeld und dem sowohl konvektiven als auch diffusen hydraulischen Transport verstanden) und dem lokalen Ungleichgewicht der Temperaturen von Porenfluid und Festkörper. Es zeigt sich, dass besonders im Nahfeld einer Temperaturquelle die Berücksichtigung dieser Prozesse zu signifikant erhöhten temperaturinduzierten Porenwasserdrücken, Verformungen und hydraulischen Gradienten führt.

Die grundlegenden allgemeinen Gleichungen werden für eine thermische Quelle sowohl im Halbraum als auch auf dessen Rand formuliert und numerisch gelöst. Zur Lösung der Gleichungssysteme modifiziert Herr Dr. Yang zwei etablierte Verfahren der Mathematik ("propagator matrix method" und "higher-order adaptive Gaussian quadrature method") erfolgreich. Ein solches System bildet näherungsweise die Situation von einem Endlager für radioaktiven Abfall ab. Mittels einer Variation der Systemparameter gelingt es Herrn Dr. Yang, die außerordentliche Bedeutung der Berücksichtigung der genannten Effekte im Zusammenhang mit Materialien geringer Permeabilität aufzuzeigen.

Univ. Prof. Dr.-Ing. habil. Tom Schanz

Bochum, Dezember 2016

This work is dedicated to my beloved grandmother and parents

Acknowledgements

This PhD thesis is a result of five-year research work carried out in the Chair of Foundation Engineering, Soil and Rock Mechanics, Ruhr-Universität Bochum. First and foremost, I would like to thank my supervisor Professor Tom Schanz who gave me a chance to start my study in RUB and provided me a lot of precious scientific support during my research work. I would like to give my sincere gratitude to Assoc. Prof. Maria Datcheva from Bulgarian Academy of Sciences for her continuous help and lots of constructive suggestions for my research work especially for my journal papers. Her prudential and earnest scientific attitude also impresses me very much. I appreciate Prof. Klaus Gürlebeck from Bauhaus Universität Weimar for his nice discussion, constructive suggestions and great help in the review of my journal paper. My thanks are also going to Prof. Feng-Lin Guo from Shanghai Jiao Tong University and Prof. Lu-Wu He from East China University for the ever fruitful discussions and valuable help with my scientific work.

I would like to appreciate Prof. Steinar Nordal from Norwegian University of Science and Technology for his invitation to visit his chair and his valuable suggestions regarding the numerical simulation in my work.

I would also give my warm gratitude to my colleagues in RUB who provide me so much help in my work and even in my life in Germany.

I would like to appreciate the support of the China Scholarship Council offered to me during my stay at RUB.

At last, I sincerely thank my grandmother and parents who are always around me giving me their endless love.

Bochum, Germany

December 2016

Yang Yang

Abstract

The goal of this research is to investigate the heat transfer mechanism and the influence of temperature field on the behaviour of coupled thermo-hydro-mechanical system. In this thesis, three problems in geosciences related to heat transfer and temperature-induced behaviour are considered and these problems are thermo-osmosis effects in saturated porous media with a cylindrical borehole subjected to impulse thermal and mechanical loadings, the analysis of multilayered thermoelastic media subjected to surface loadings containing a heat source with application to heat-emitting high level nuclear waste repository and heat transfer in geothermal heat-pump system in a single vertical borehole. These three case studies related to problems in geosciences involving heat transfer and temperature-induced behaviour are theoretically and numerically investigated.

The mathematical-physical models including geometrical approximations, governing equations for the considered physical processes, and the boundary and initial conditions for these problems are formulated first. The analytical solutions for temperature, heat flux and corresponding variables, e.g., displacement, pore pressure, fluid flux and stress, are obtained and followed by a parametric study for each of the investigated problems aiming to investigate the distribution of temperature field and the relevant temperature-induced behaviour. Two special effects which closely relate with temperature field, i.e., thermo-osmosis effect and the local thermal non-equilibrium effect, are taken into account and numerically investigated for a kind of low-permeability clay. An improved propagator matrix method and a numerical scheme of high-order adaptive Gaussian quadrature method with continued fraction expansions are introduced in the analysis of multilayered geological structure. The conclusions drawn could help to improve the design of the borehole heat exchanger system and the repository of heat-emitting high level nuclear waste.

Zusammenfassung

Das Ziel dieser Arbeit ist die Untersuchung von Wärmetransportmechanismen und des Einflusses von Temperaturfeldern auf das Verhalten von thermisch hydraulisch mechanisch gekoppelten Systemen. Drei geowissenschaftliche Fragestellungen, in denen Wärmetransport und temperaturabhängiges Systemverhalten relevant sind, werden betrachtet. Zunächst werden am Beispiel eines zylindrischen Bohrlochs in einem Halbraum aus gesättigten porösen Material unter thermischen und mechanischen Impulslasten thermo-osmosische Effekte erfasst. Dann werden geschichtete thermoelastische Materialien im Hinblick auf Lagerstätten für wärmeproduzierende hochnukleare Abfälle analysiert. Abschließend wird der Wärmetransport eines geothermischen Wärmepumpensystems in einem vertikalen Bohrloch abgebildet. Diese drei Fragestellungen zum Wärmetransport und temperaturabhängigen Verformungen werden theoretisch und numerisch untersucht.

Zunächst werden die mathematisch-physikalischen Modelle einschließlich der geometrischen Annahmen, die grundlegenden Gleichungen zur Beschreibung der physikalischen Prozesse und die Rand- und Anfangsbedingungen formuliert und dargelegt. Anschließend werden die Gleichungen auf die drei Randwertprobleme angewendet. Für jede Fragestellung werden die analytischen Lösungen für Temperaturverteilungen, Wärmefluss und den dazugehörigen Größen, welche das temperaturabhängige Systemverhalten beschreiben, wie Verschiebungen, Porenwasserdrücke, Flüssigkeitsbewegung und Spannungen, angegeben. Mit Hilfe dieser Lösungen werden die Einflüsse einzelner Parameter auf die Temperaturfelder und das Systemverhalten durch eine Parameterstudie analysiert. Zwei spezielle Aspekte, thermo-osmosische Effekte und der lokale thermische Ungleichgewichtseffekt, werden dabei berücksichtigt und für ein wenig durchlässiges Tonmaterial numerisch untersucht. Zur Beschreibung von mehrfach geschichteten geologischen Strukturen wird eine verbesserte Propagatormatrixmethode und die numerische Umsetzung einer adaptiven Gauß-Quadratur höherer Ordnung eingeführt. Die gewonnenen Ergebnisse können Hinweise zur Verbesserung des Entwurfes von Bohrlochwärmetauschern und Lagerstätten für wärmeerzeugende hochradioaktive Abfällen geben.

Contents

List of Figures

List of Tables

Nomenclature

a_{fs}	Specific surface area
b	Body force
c_s, c_f	Specifit heat capacities of solid and fluid phases
d_p	Particle diameter
e	Euler's number
g	Gravity
G	Shear modulus
h	Internal heat transfer coefficient
$H(t)$	Heaviside step function
H, L	Constant length and characteristic scale length
J_i	i-th order Bessel function of first kind
k, k_s, k_f	Overall, solid and fluid thermal conductivities
k_h, K_h	Intrinsic permeability and hydraulic conductivity
K, K_s	Bulk modulus of solid skeleton and solid grain
K_i	i-th order Bessel function of second kind
p	Pore fluid pressure
q_f, q_H	Fluid and heat flux
q_b	Heating rate per unit length

q_{geo} Geothermal heat flux

Q Heating source

r Radius

R Thermal resistance

s Frequency

S_f Thermo-filtration coefficient

S_w Thermo-osmosis coefficient

u Solid displacement

V, V_s, V_f Volume

V_p Pumping velocity

w Displacement of pore fluid with respect to solid skeleton

$\alpha, \alpha_s, \alpha_f$ Overall, solid and fluid thermal expansion coefficients

β_f Bulk modulus of fluid

γ_f Specific gravity of fluid

δ Dirac delta function

ε Strain

η Wave number

$\theta, \theta_s, \theta_f, \theta_0$ Equilibrium, solid, fluid and reference temperatures

$\kappa, \kappa_s, \kappa_f$ Overall, solid and fluid thermal diffusivities

λ Lame parameter

μ Fluid viscosity

ν Poisson's ratio

ξ Biot-Willis coefficient

ρ, ρ_s, ρ_f Overall, solid and fluid densities

σ Stress

ϕ Porosity

φ Angle

ψ Auxiliary function

ω Decay constant of radioactive element

∇ Gradient

1 Introduction

1.1 Introduction

Heat transfer is the process of energy exchange in physical systems. The rate of heat transfer depends on the temperature differences and the physical properties of the intervening medium through which the heat is transferred. The transfer direction is normally from a region of high temperature to the one of low temperature. The process will cease until all the involved systems reach the thermal equilibrium state. Generally speaking, there are three fundamental modes of heat transfer:

- Heat conduction. By means of molecular agitation, energy will transfer between systems which are directly in physical contact. Fourier's law is primarily to describe the mechanism of heat conduction.
- Heat convection. Due to the mass motion of the fluid such as air or water, energy will be carried and transferred between the system and its environment.
- Heat radiation. In a vacuum or transparent medium, energy will transfer by means of emission of photons in electromagnetic waves. The Stefan-Boltzmann equation is used to describe the radiant transfer rate in a vacuum.

Heat transfer and a temperature-induced behaviour commonly exist both in nature and engineering. Various industrial activities are closely concerned with heat transfer and temperature fields. For instance, the investigation of heat conduction process always plays an important role in geothermal energy exploitation (Figure 1.1) where heat is generated from radioactive decay and continual heat loss from earth's formation. The usage of solar energy will largely encourage our contributions on the study of radiant heat transfer. In the daily life, various of heat exchangers used for more efficient heat transfer or to dissipate heat are widely used in refrigeration, air conditioning, space heating, power generation, car's radiator, etc.

Due to the common existence of heat, the temperature-induced/coupled behaviour should be carefully reconsidered. A vivid example is about radioactive waste management, where

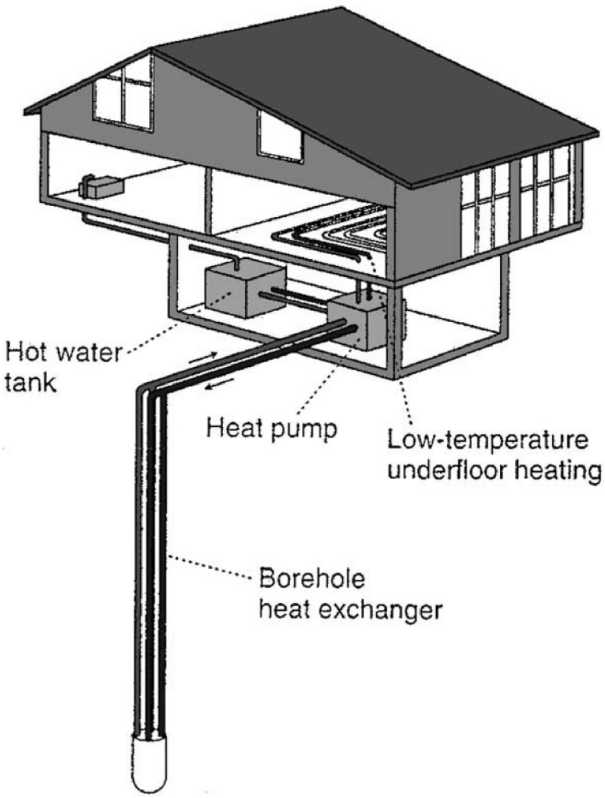

Figure 1.1: Typical application of a BHE/heat pump system in a Central European home (Sanner et al. 2003)

the waste is regarded as a decaying heat source as shown in Figure 1.2 and a deep geological repository is usually suggested. In this case, a thermoelastic or thermoporoelastic model should be established and the temperature-induced behaviour should be carefully investigated. As the development of interdisciplinary, numerous complex coupled processes become more and more obvious and get increasing attentions. The commonly used models for the coupled processes are thermo-hydro-mechanical model (THM) (Gawin & Schrefler 1996; Bai & Abousleiman 1997), thermo-hydro-chemo-mechanical model (THCM) (Kolditz et al. 2012) and thermo-electro-mechanical model (TEM) (Liew et al. 2003). Recently, scientists even try to establish a more complete and complex thermo-hydro-chemo-bio-magneto-electro-mechanical coupled model to describe the transfer mechanism in porous media. However, the temperature field must be introduced and the temperature-induced behaviour are of great interest to be concerned with in all the upper mentioned models.

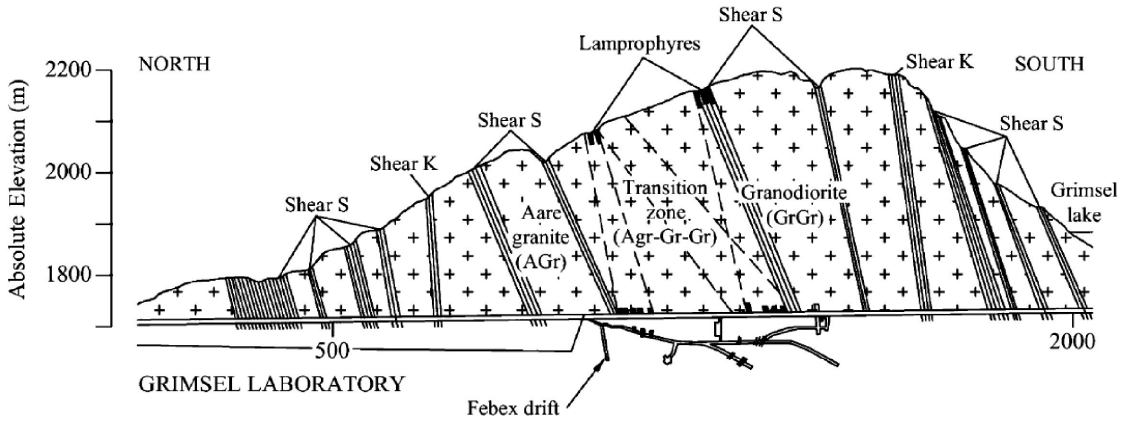

Figure 1.2: Geological cross-section for radioactive waste repository in the Grimsel area (Alonso et al. 2005)

1.2 Scope and objectives

The study mainly focuses on the analytical and numerical investigation of a THM coupled model in saturated porous media and the corresponding engineering applications. The effect of coupled flow (thermo-osmosis) on the THM coupled saturated porous media fulfilling local thermal non-equilibrium condition (LTNE), is investigated first. For the partially decoupled thermoelastic model, the multilayered thermoelastic half space with application to a repository for heat-emitting high-level nuclear waste in a geological formation is studied. The temperature field is important for both of the up-mentioned problems, and thus we will investigate the heat transfer mechanism considering a particular application in geothermal energy exploitation. The major objective of this study is to investigate the heat transfer mechanism and the temperature-induced behaviour in porous media with application in geotechnics. In order to achieve this objective, the following three problems will be studied and finished step by step:

- Modelling. Based on the in-situ model, a suitable geometrical approximation to real geotechnical project will be established with the relevant governing equations and initial and boundary conditions.

- Theoretical study. The most important task is to get the analytical solutions for all the variable fields, i.e., temperature field, deformation field, stress field, pore pressure field, etc. The analytical study could enhance our understanding on the heat transfer mechanism and temperature-induced behaviour in porous media with particular application in geotechnics.

- Numerical study. As case studies, series of numerical simulations, based on the upper analytical solutions, will be implemented out with specified geophysical parameters to investigate the heat transfer and temperature-induced behaviour.

The objectives of this study can be summarized as:

- First, a critical literature review on the theoretical and numerical study on the coupled THM behaviour is presented. A coupled THM model in saturated porous media with the consideration of thermo-osmosis effect and the thermal local non-equilibrium condition is established. The analytical solutions of temperature, pore pressure, stress, displacement and fluid flux are obtained. Numerical simulations are carried out to investigate the coupled effects of thermo-osmosis in saturated porous media. The effects of LTNE on temperature, pore pressure, stress, displacement and fluid flux are also discussed.

- Next, the thermoelasticity theory will be adopted to establish a multilayered thermoelastic geophysical model with containing sources and surface loads. The analytical solutions for temperature, stress and displacement are obtained with the help of propagator matrix method. With a specified kind of clay material which is used as the buffer in radioactive waste repository, numerical simulations are performed to investigate the temperature distribution and the temperature-induced behaviour under a decaying heat source.

- In order to better reveal the heat transfer mechanism in geotechnics, we establish a geotechnical model of a single vertical borehole heat exchanger system. The analytical solution of the heat transfer problem in the system of semi-infinite ground with a finite line heat exchange source are derived. The model parameter study for the temperature distribution in the ground and in the water for long operation time is performed.

1.3 Organization of the dissertation

This dissertation consists of seven chapters, of which the content can be briefly summarized as:

- Chapter 1: Introduce the background, the scope and the objective and the organization of this dissertation.

- Chapter 2: Present a literature overview on the applications of coupled THM model and the decoupled thermoelastic model. The previous theoretical works on the analytical solutions for the coupled THM model are discussed.
- Chapter 3: The governing equations of the initial boundary value problem (IBVP) for heat transfer, fluid flow and constitutive mechanical relation are presented and discussed.
- Chapter 4: Present an analytical study on thermo-osmosis effect in THM coupled saturated porous medium which fulfills the local thermal non-equilibrium condition.
- Chapter 5: A multilayered thermoelastic half space is established and analytically and numerically investigated with an application to nuclear waste disposal in a geological formation.
- Chapter 6: An analytical study on heat transfer in a geothermal heat-pump system is presented.
- Chapter 7: Based on the works in this study, conclusions are drawn and the works in the next step are suggested.

2 State of the art

2.1 Application of a coupled THM models in geomechanics

As the development of multi-discipline approach, a lot of complicated coupled processes become more important and attractive. One of the most important coupled processes is a coupled thermo-hydro-mechanical (THM) process which gets increasing attentions in engineering. The non-isothermal condition is common in some engineering circumstances, such as radioactive waste repository, geothermal energy exploit, energy storage in deep ground, petroleum extraction and so on. The coupling effects among heat flow, pore fluid flow and solid skeleton deformation under these circumstances are actually very significant. The traditional models, just like the elastic, poroelastic (Biot 1956; Biot & Willis 1957) or thermoelastic (Biot 1955; Nowacki 1962) models cannot precisely describe these coupling effect between the deformation, hydrology and temperature fields, thus the THM coupling theory is presented and widely used to analyze the coupling effect in saturated/unsaturated porous media.

A very important application of coupled THM model in geotechnics is the assessment of radioactive waste disposal (Yang, Guerlebeck & Schanz 2014) both in saturated/unsaturated soil or rock where temperature field plays an important role in the coupling behaviour. Booker & Savvidou (1985) established a three-dimensional time-dependent fluid saturated thermoporoelastic model with a containing point heat source and analytically investigated the effect of temperature field on the responses of stress and pore pressure. Kurashige (1989) extended Rice-Cleary theory (Rice & Cleary 1976) and established a one-dimensional model of a spherical cavity in saturated infinite thermoporoelastic media and investigated the effect of heat transportation due to fluid flow on the temperature distribution and thermal stresses in rock. Giraud & Rousset (1995) developed a solution scheme for an one-dimensional consolidation problem of a saturated thermoporoelastic medium and used analytical solutions to treat a problem of radioactive waste disposal in

compressible clay. The numerical results showed that coupling effects among thermal, hydraulic and mechanical behaviors are significant for porous media with low permeability coefficient such as compressed clay. Thomas & Cleall (1999) discussed the development of a coupled THM model considering the coupled flow of heat, moisture and air in expansive unsaturated clays. Wu et al. (2004) proposed a THM constitutive model for unsaturated soils considering thermal softening phenomenon and compared the numerical results by means of the finite element method of the constitutive behaviour with the existing experimental results. Francois et al. (2009) carried out finite element modelling of an in situ thermal experiment to investigate the effect of temperature on the response of a candidate host formation for radioactive waste disposal. Kodashima & Kurasbige (2009) presented a saturated thermoporoelastic hollow sphere whose inner surface is exposed to burning gas and outer surface is cooled by the fluid injection. They investigated the effect of heat advection due to active fluid injection on the reduction of temperature and thermal stresses and got the conclusion that the active fluid pressurization and injection are effective in suppressing the maximum thermal hoop stress at the outer surface and avoiding the occurrence of the excess compressional stress at the inner surface. Based on the coupled THM theory (Giraud & Rousset 1995), Liu, Xie & Zheng (2010) presented a nonlinear model for the thermohydroelastic dynamic (THED) response in saturated porous media and solved a problem of one-dimensional cylindrical cavity in homogeneous isotropic poroelastic medium subjected to a time-dependent thermal/mechanical shock. They investigated the effects of Biot-Willis coefficient and thermo-osmosis on displacement and compared the thermohydroelastic dynamic response with the simplified thermoelastic dynamic (TED) response as shown in Figure 2.13. Furthermore, they (Liu et al. 2009; Liu, Xie & Ye 2010) investigated the thermohydroelastic and thermoelastic dynamic responses of a two-dimensional saturated poroelastic media under a time-dependent non-torsional thermal/mechanical source or time harmonic loads with the help of Legendre polynomials and Fourier transform schemes.

Maghoul et al. (2010) derived analytical transient fundamental solutions for a three-dimensional THM coupled unsaturated porous media, and discussed how to simplify the solutions to investigate the responses in three special cases, i.e., steady-state thermo-hydro-mechanical, steady-state hydro-mechanical and elastostatic cases. With the Boundary Integral Method, Maghoul et al. (2011) extend their work to numerically investigate the dynamic response in frequency domain for a two-dimensional THM coupled unsaturated porous media. Rutqvist et al. (2001) presented the coupled THM model in saturated and unsaturated geologic formations such as fractured rock and compared four finite element codes including ROCMAS, THAMES, FRACON and AQCLAY for simulating such

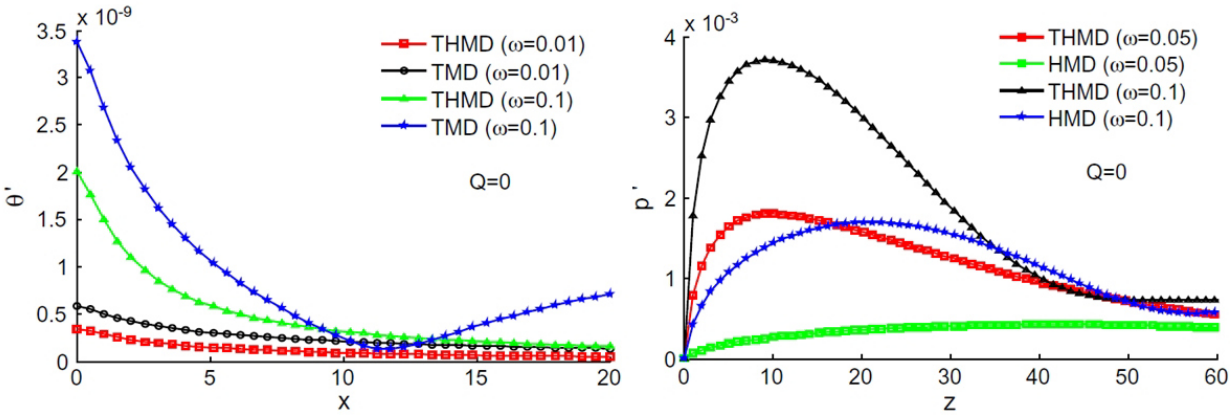

Figure 2.1: Variations of temperature and pore pressure with z (normal force).(Liu, Xie & Zheng 2010)

coupled process. Chen, Zhou & Jing (2009) established a three-dimensional numerical model with the help of the Galerkin finite element method to investigate a fully coupled multiphase flow, thermal transport and stress/deformation in unsaturated porous media (as shown in Figure 2.2), with the consideration of six processes and their coupling, i.e., stress-strain, fluid flow, gas flow, vapor flow, heat transport and porosity evolution processes. Chen, Tan, Yu, Wu & Jia (2009) presented a fully coupled THM model in unsaturated porous media considering of the effect of temperature on the dynamic viscosity of the fluid and void ratio, the effect of thermo-osmosis, effects on fluid flow and the influence of heat flow due to thermal convection, and numerically investigated the coupled behavior of a tunnel in unsaturated argillite during excavation, ventilation and concrete lining stages with FEM method. Sanchez et al. (2012) carried out a large-scale heating test to study the THM behaviour of a clay barrier subjected to heating and hydration over a long period of time. Kolditz et al. (2012) presented an open-source project OpenGeoSys as shown in Figure 2.3 to simulate the thermo-hydro-mechanical-chemical (THMC) process in porous media and showed the potential of THMC modelling in geotechnics and hydrology, as well as geothermal energy extraction and storage. Gatmiri et al. (2010) derived the fundamental solutions of two-dimensional non-isothermal unsaturated multiphase porous media in frequency and time domains, and utilized these solutions to investigate three limiting cases including the steady state thermo-hydro-mechanical response, steady-state hydro-mechanical response and elastostatic response.

With the help of FEM (finite element method), FDM (finite difference method) and Newton-Raphson method, Gawin & Schrefler (1996) established a THM coupled numerical model regarding phase change phenomenen to simulate slow transient phenomenen

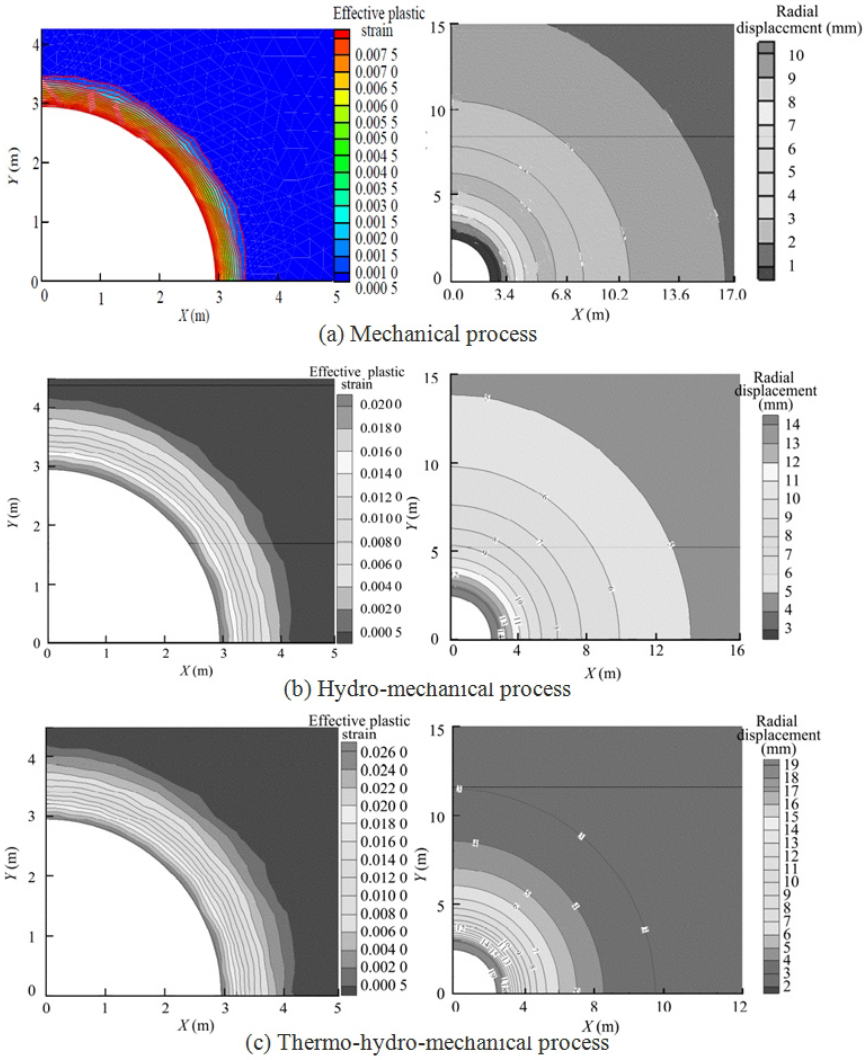

Figure 2.2: Distributions of effective plastic strain and radial displacement (Chen, Zhou & Jing 2009)

involving flow of heat, fluid and gas in unsaturated porous media. Schrefler et al. (2002) presented a coupled THM model for normal high-performance concrete (HPC) and ultra-high performance concrete (UHPC) structures subjected to heating, in which the concrete is a multiphase material consisting of a solid phase (cement paste and aggregates), two gaseous constituents (water vapour and dry air) and water in three forms (chemically bound water, adsorbed water, capillary water). A series of experiments and numerical simulations were carried out to investigate the temperature and gas pressure development and hydro-thermal and mechanical performance of HPC and UHPC under high temperature. Jussila & Ruokolainen (2007) established a THM coupled numerical model with the considerations of non-linear elastic strain and moisture swelling, and studied the coupled

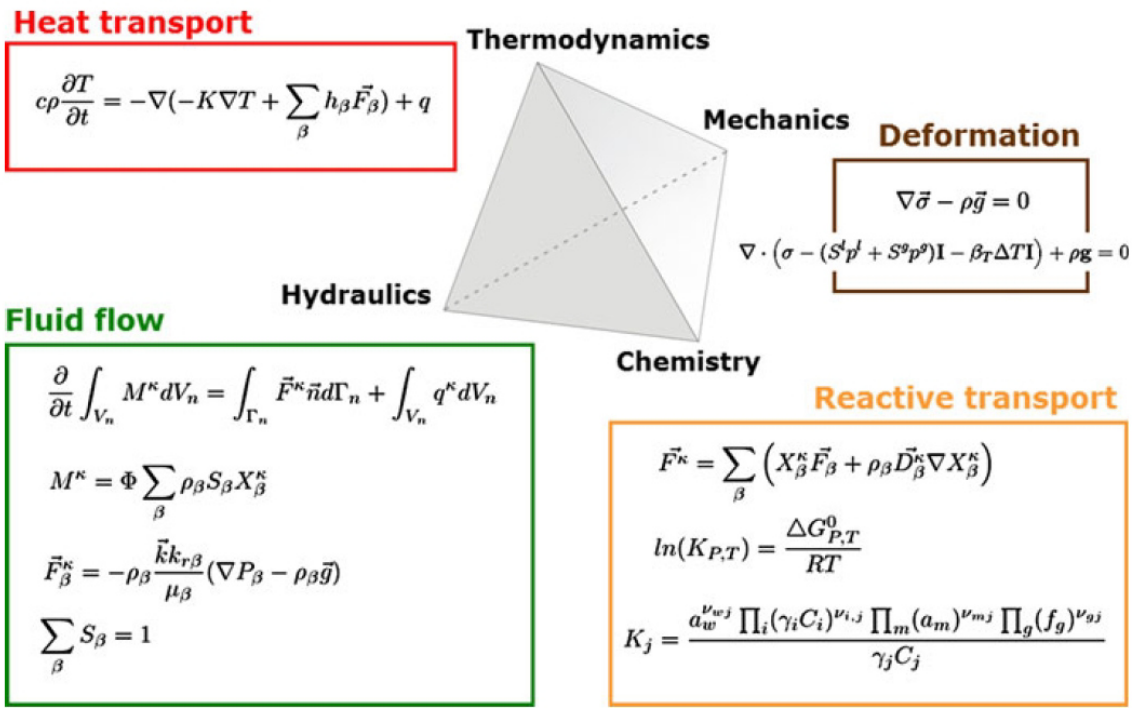

Figure 2.3: Mathematical framework for coupled THMC modeling (Kolditz et al. 2012)

effects in swelling compacted bentonite with FEM method. Nowak et al. (2011) used FEM to investigate a three-dimensional simultaneous THM coupled model of two full scale in-situ experiments aimed to the assess of the complex coupling behavior of engineered and geologic barrier systems in possible nuclear waste repositories.

Although the fully THM coupled models are relatively more strict, the analytical solutions for these models can rarely be obtained due to the mathematical difficulty especially for the THM coupled models in unsaturated porous media. Thus, some other partially decoupled models are still popular nowadays. For a one-dimensional consolidation problem, Bai & Abousleiman (1997) presented a fully coupled thermoporoelastic formulation and discussed the general conditions where the coupling should be maintained, and where a partial coupling or decoupling technique could be applied. One of the most popular models is the thermoelasticity. It is widely used in the analysis of multilayered geological structure.

Multilayered structures widely exist in nature and are closely relevant to different engineering problems. For instance, the geological structure can be considered for simplicity as multilayered half space due to the geological formation and sedimentary history as shown in Figure 2.4. There are also various man-made materials or structures that can

be regarded as multilayered structures for modelling applications in fields ranging from e.g. civil, mechanical and biomechanical engineering to microelectronics and optics. Moreover, parts of human and animal organs and tissues can be considered as stratified media.

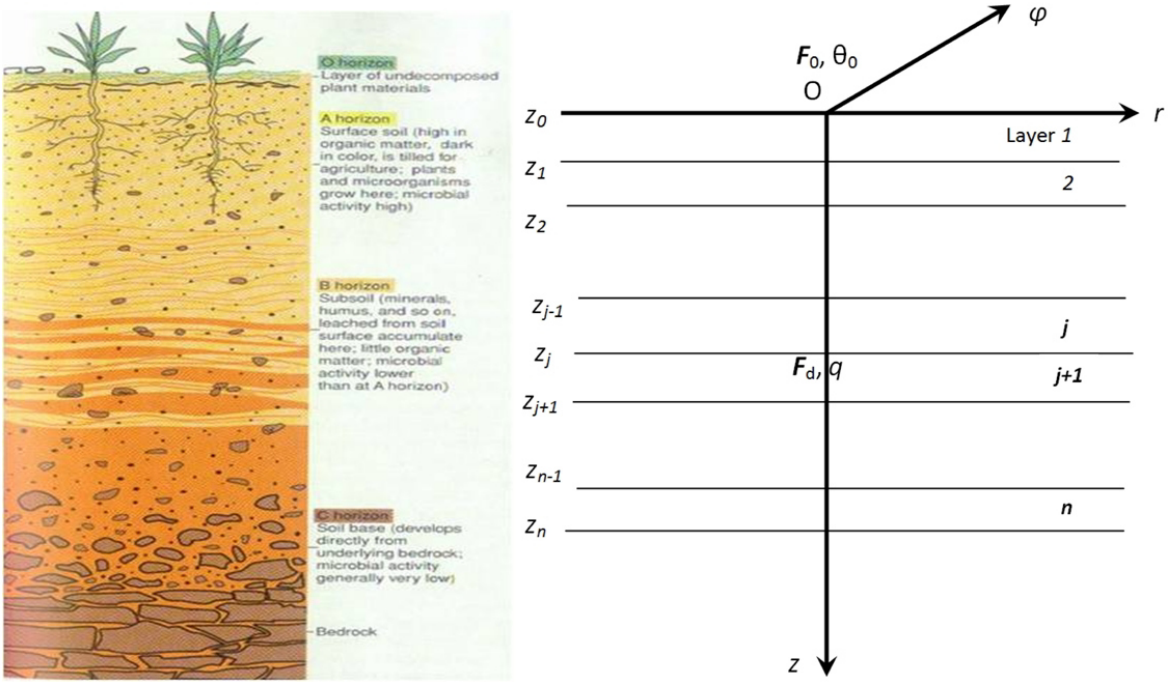

Figure 2.4: The multilayered geological structure (Pan 1989*b*)

More often the multilayered structure is assumed to be composed of homogeneous parallel layers. Several approaches exist to solve the static and dynamic problems for multilayered structures (Yang et al. 2016). The most common numerical and semi-analytical methods are the finite element method (FEM) and the boundary element method (BEM). It is well accepted that BEM is more suited compared to FEM to cases where the domain of interest is infinite.

As an alternative one can consider the finite layer method (FLM) Small & Booker (1984, 1986*a*) and its improved version – the exact stiffness matrix method Senjuntichai & Rajapakse (1995); Degrande et al. (1998), and the analytical layer-element method (ALEM) Ai et al. (2015*b*). However, these methods require an assembling of a global propagator matrix whose size is proportional to the number of layers n and thus the methods are becoming inefficient if the number n increases or the length of the layer is large Pan (1989*b*, 1997). One of the best method to treat problems related to processes in multilayered structures is the propagator matrix method (PMM) (Singh 1970). PMM was first used

by Thomson Thomson (1950) and further developed by Haskell (1953) and Gilbert & Backus (1966) to solve problems in elastodynamics. The essential principle is to formulate the solution for a group of ordinary differential equations which are written in the format of matrix as following:

$$\frac{\mathrm{d}}{\mathrm{d}z}\mathbf{f} = \mathbf{M}\mathbf{f} \tag{2.1}$$

where $\mathbf{f}$ is the variables array, $\mathbf{M}$ is a matrix containing the material parameters and the relevant independent variables in a homogeneous layer. The corresponding solution is then:

$$\mathbf{f}(z) = e^{\mathbf{M}(z-z^*)}\mathbf{f}(z^*) = \mathbf{P}^z_{z^*}\mathbf{f}(z^*) \tag{2.2}$$

where the matrix $\mathbf{P}^z_{z^*}$ is called propagator because it propagates the solutions from z^* to z. With the above iterative relation we can get the general solution for multilayered structure if all the variables at the interfaces are continuous:

$$\begin{aligned}\mathbf{f}(z) &= e^{\mathbf{M}_1(z-z_1)}\mathbf{f}(z_1) = e^{\mathbf{M}_1(z-z_1)} \cdot e^{\mathbf{M}_2(z_1-z_2)}\mathbf{f}(z_2) \\ &= e^{\mathbf{M}_1(z-z_1)} \cdot e^{\mathbf{M}_2(z_1-z_2)} \cdots e^{\mathbf{M}_n(z_{n-1}-z_n)}\mathbf{f}(z_n) = \mathbf{P}^z_{z_n}\mathbf{f}(z_n)\end{aligned} \tag{2.3}$$

where $\mathbf{P}^z_{z_n}$ is a global propagator matrix assembling by the independent propagator matrix in each of the layer. In addition, the variables can also propagate in the opposite direction with a suitable choice of global propagator matrix expressed as:

$$\mathbf{f}(z_n) = \mathbf{P}^{z_n}_z\mathbf{f}(z) \tag{2.4}$$

where $\mathbf{P}^{z_n}_z = [\mathbf{P}^z_{z_n}]^{-1}$.

The method successfully overcomes the difficulty in FLM for large n, and has the advantage of high computational efficiency. Although PMM is superior to the previous methods, the solutions were reported to be numerically unstable in the far evanescent regime for high frequency and large layer thickness (Kennett 1974, 2009; Wang 1999; Wang & Kuempel 2003). To overcome such instability issues there were used the following modifications of PMM – delta matrix method (Dunkin 1965), transmission and reflection matrix method (TRM) (Kennett 1974) and the orthogonalization method (Wang 1999).

There are many authors presenting solutions of various problems involving stratified structures. For the pure elastic multilayered structures, Small & Booker (1984, 1986*b*) applied the finite layer method and Fourier or Hankel transform technique to investigate the 2D and 3D static problems for cases with strip, circular and rectangular surface loads, and compared with the relevant analytical solutions as verification. With the same method, Booker & Small (1985) studied the three-dimensional problem subjected to circular and general loadings in multilayered viscoelastic soil. Singh & Garg (1985) investigated the

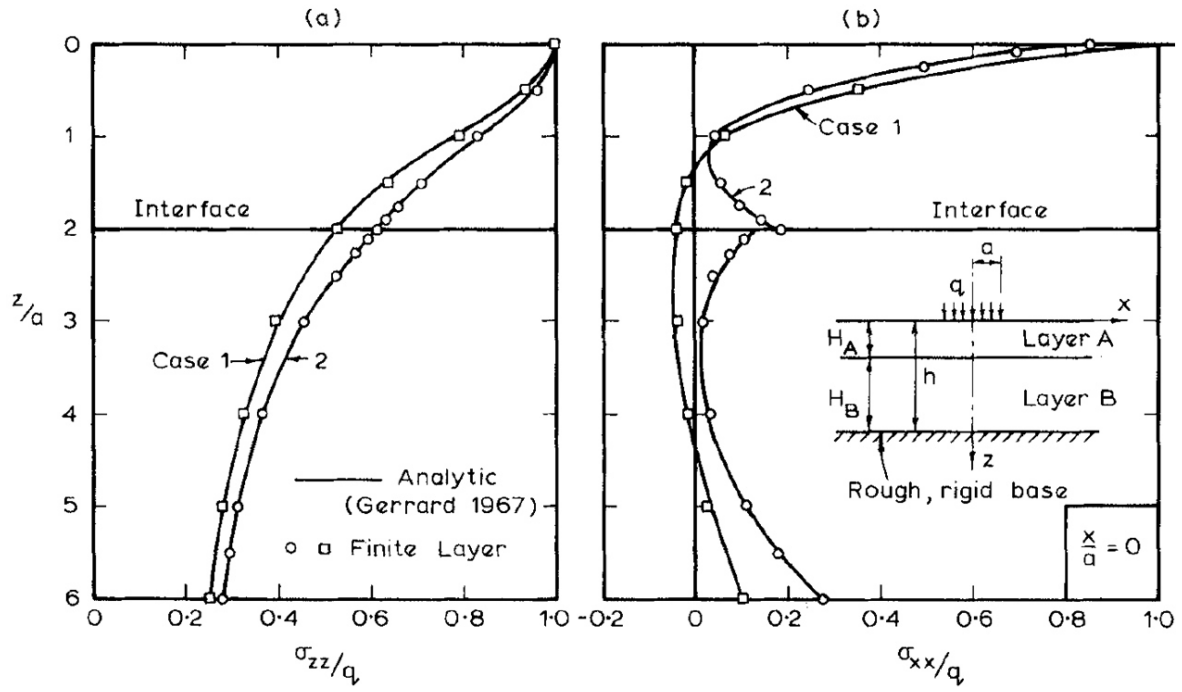

Figure 2.5: Stresses on axis beneath uniform strip loading (Small & Booker 1984)

The two-dimensional static problem of a long displacement dislocation in a multilayered half space with Thomson – Haskell matrix method. The analytical solution for the surface displacements due to dip-slip and strike-slip faults of arbitrary dip are derived for the plain strain and antiplane strain situations. Singh (1986) studied the three-dimensional axisymmetric problem of static deformation in a multilayered half space subjected to surface loads and derived the explicit expressions for the displacements and stresses due to a vertical force and a torque. Pan (1989*b*,*a*) analytically studied the static deformations in three-dimensional problems for multilayered elastic medium with general surface loads and internal dislocation sources. Based on Singh's (Singh 1970) theoretical work, Jovanovich et al. (1974*a*,*b*) examined the effect of earth structure on earthquake displacement, strain and tilt fields at the Earth's surface due to point dislocation sources. Rundle (1980) investigated a problems of static elastic-gravitational deformations in layered half space due to various point sources. Zhu & Rivera (2002) studied elasto-dynamic and elasto-static problems in multilayered half space with displacement-stress discontinuities. They rederived the propagator matrices for both the dynamic and static cases and showed that the dynamic propagator matrix and the solution can converge to their static counterparts at near-zero frequency by using Jordan canonical forms of matrices.

For poroelastic multilayered media, Senjuntichai & Rajapakse (1995) presented an analysis of a 3D quasi–static problem. For deriving the solution of the problem they applied the stiffness matrix method that is an improvement of FLM. The stiffness matrix method is also used to evaluate the dynamic response of multilayered medium to a time-harmonic load including existing fluid source (Rajapakse & Senjuntichai 1995*a*). Degrande et al. (1998) investigated the harmonic and transient wave propagation problem for porous medium with different degrees of saturation solving the problem using the said exact stiffness matrix method and numerically investigated effect of partial saturation and a moving water table on harmonic and transient wave propagation. Wang & Fang (2003) studied the non-axisymmetric Biot consolidation problem in saturated poroelastic media under three different drained and undrained boundary conditions using PMM. Lu & Hanyga (2005) adopted TRM to investigate a 3D axisymmetric dynamic problem with applied vertical point force with a fluid source in a point. Furthermore, Liu & Zhao (2013) adopted PMM to analyze the dynamic response of poroelstic media and compared the results with the solution obtained using FLM Senjuntichai & Rajapakse (1995). The related numerical examples demonstrated PMM is more accurate and stable than FLM, and is an alternative approach to conducting the dynamic analysis of multilayered poroelastic media. Recently, Zheng et al. (2013*a*,*b*) studied the 3D dynamic problem defined for a multilayered poroelastic half space under the action of an internal point force, fluid injection and harmonic surface traction as shown in Figure 2.6. There they applied the orthogonalization technique developed by Wang (1999)and a high-order adaptive integration method with continued fraction expansions to accelerate the convergence of the truncated integral in numerical simulation. To validate the accuracy and efficiency of this method a comparison is presented between the numerical results and the analytical solution for a uniform poroelastic half space.

The next type of coupled field problems involving multilayered structures is that of thermoelasticity. Rundle (1982) studied the static and pseudo static nonisothermal deformation problems in multilayered elastic media with a heat source. Small & Booker (1986*a*) considered a 2D axisymmetric problem for multilayered thermoelastic half space with a heat source using FLM and applied their analytical solutions to treat a problem of nuclear waste depositary as shown in Figure 2.7. Pan (1990) developed a general analytical method to investigate the problem of transient thermoelastic deformation in multilayered half space subjected to general surface loads and internal sources with the help of PMM. Wang & Ai (2015) introduced a new method – precise integration method (PIM) to investigate the thermo-elastic response with buried decaying heat sources in multilayered materials. Furthermore, Haartsen & Pride (1997) numerically determined the wave prop-

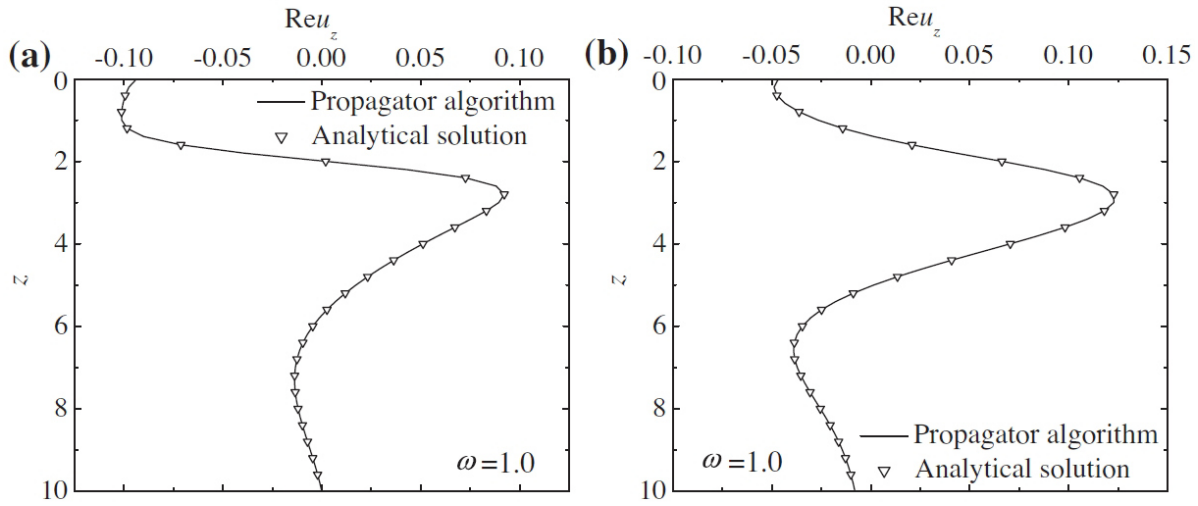

Figure 2.6: Depth profiles of vertical displacements for $r = 1, h = 0$ due to (a) a horizontal point force and (b) a fluid injection point source (Zheng et al. 2013*a*)

agation in porous media as a solution to a coupled hydro-mechanical-electro-magnetical problem for stratified porous medium with an embedded full-waveform electroseismic point-source.

The next of the few available references are those of Small & Booker (1986*a*) as FLM application example, of Ai et al. (2015*b*) as ALEM application example, of Wang & Ai (2015) as PIM application example and of Rundle (1982) where conventional propagator matrix method was used. On the other hand, there are sufficient references on thermoelastic homogeneous models. However, it can be concluded that the studies on multilayered structures mainly focus on the elastic and poroelastic models while the temperature field is rarely taken into account.

For both THM coupled model and the parcially decoupled thermoelastic model, the temperature filed all plays a very important role. Compared with the mechanical load, the temperature load/source sometimes worth more our attention just like the investigation of the nuclear waste disposal. The study in the heat transfer mechanism is quite important which could benefit our understanding about the temperature-related engineering, for instance the geothermal energy exploitation.

The geothermal energy generates from the original formation of the Earth and the radioactive decay of materials. It is roughly estimated that the temperature of the Earth's core is between 3000^0C to 5000^0C. The temperatures in excess of 500^0C can be discovered in the Earth's crust just a few thousand meters below the surface. The geothermal gradi-

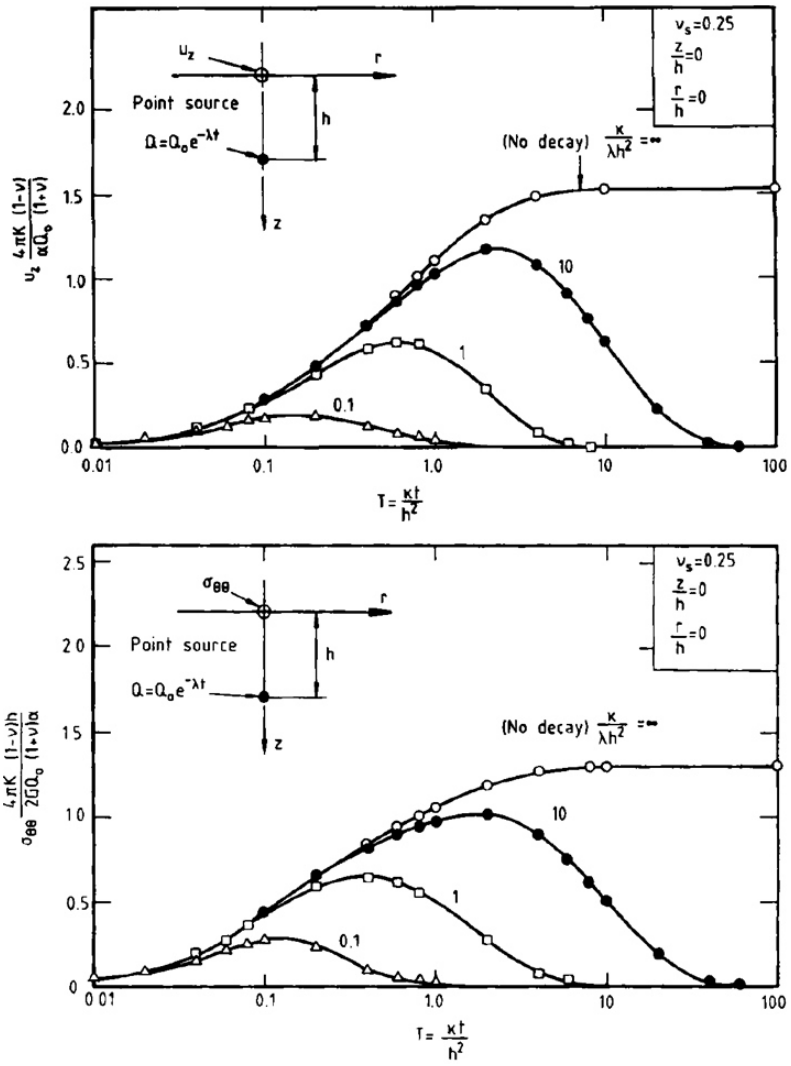

Figure 2.7: Distribution of temperature, displacement and stress (Small & Booker 1986*a*)

ent, which is the difference in temperature between the core of the Earth and its surface, drives a continuous conduction of geothermal energy in the form of heat from the core to the surface. There is a long history to utilize the geothermal energy. Since Paleolithic times people have used hot spring for bathing and heating. Nowadays, the utilization of geothermal energy gets a significant growth. It is reported that (Lund & Boyd 2015), the total installed capacity for geothermal utilization worldwide is 70,329 MWt up to the end of 2014 with an annual growth rate of 7.7%. The total annual energy use is 587,786 TJ (163,287 GWh) with an annual growth rate of 6.8% as shown in Figures 2.8 and 2.9.

Geothermal heat pumps (GHPs) which are a highly efficient, renewable and environmental friendly energy technology are used for space heating and cooling and other applications.

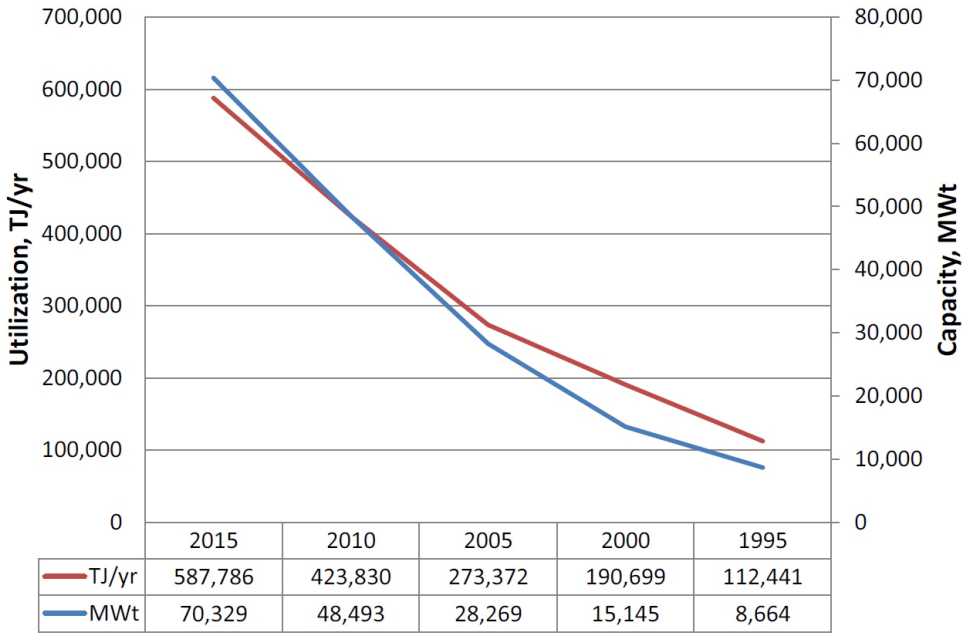

Figure 2.8: The installed direct-use geothermal capacity and annual utilization from 1995 to 2015 (Lund & Boyd 2015)

Geothermal heat pump can utilize the ground as heat source or heat sink and transfer heat for space heating during winter, and transfer heat out of the space for cooling during summer. Bose et al. (1985) generally presented the design manual for ground-coupled heat pump in details. A geothermal heat pump consists of three fundamental elements in general: an earth connection system, a heat pump system and a heat distribution system as shown in Figure 2.10.

- Earth connection system. The earth connection system usually contains a series of closed and buried loop of pipes, horizontally or vertically, which we call closed-loop system. The fluid circulates through these pipes, allowing heat but not fluid itself to be transferred between building and the ground. The circulating fluid is generally water or a water/antifreeze mixture. Less commonly, the earth connection system can also be configured with an open loop of pipes connecting to a surface water body or an aquifer that directly transfers water between the heat exchanger and water source. However, this open-loop system is politically forbidden for the sake of environmental protection.

- Heat pump. This element contains three main parts:

  – The evaporator, which takes the heat from the water in the ground loop.

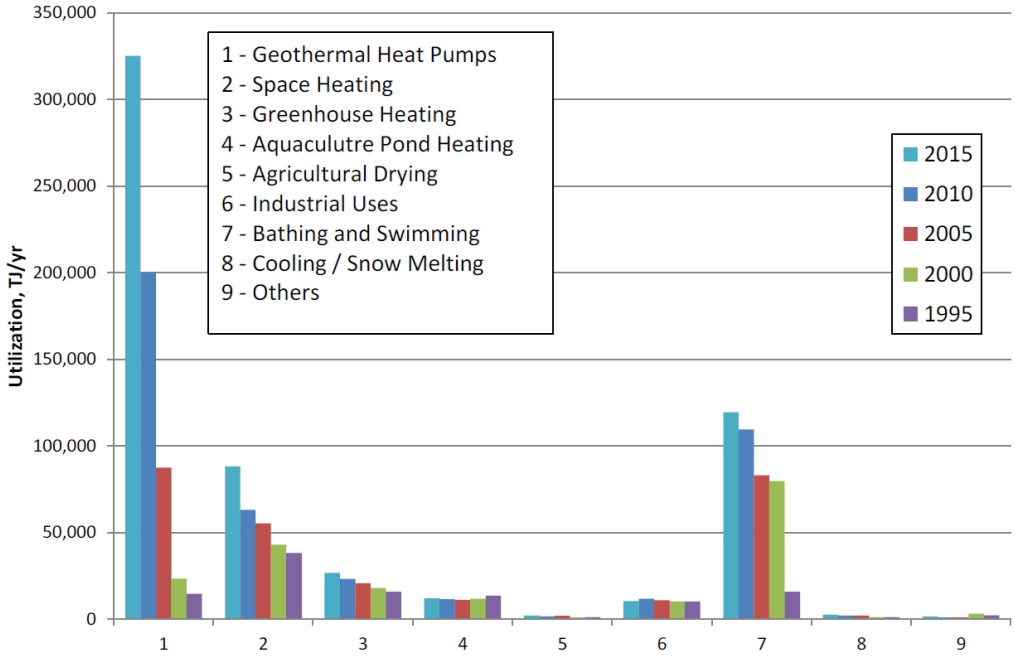

Figure 2.9: Comparison of worldwide direct-use geothermal energy in TJ/yr from 1995, 2000, 2005, 2010 and 2015 (Lund & Boyd 2015)

  - The compressor, which moves the refrigerant round the heat pump and compresses the gaseous refrigerant to the temperature needed for the heat distribution circuit.
  - The condenser, which gives up heat to a hot water tank to feed the distribution system.

- Heat distribution system, consisting of under floor heating or radiators for space heating and in some cases water storage for hot water supply.

In the past, a lot of theoretical and experimental works were carried out to investigate the heat transfer mechanism in this GHP system (Yang, Datcheva, Koenig & Schanz 2014). For a classical GHP with vertically configured U-tube in deep borehole exchanger (BHE) as shown in Figure 2.11, Ingersoll & Plass (1948) and Ingersoll et al. (1954) developed Kelvin's line-source theory and provided several novel analytical approaches to design the heat exchanger system. The line-source approach approximates the deep borehole with the U-tube as an infinite line with radial heat flow. A more accurate method is the cylinder-source method developed by Carslaw & Jaeger (1947), which assumes the borehole as a cylinder with a constant radial heat flux at the radius of the cylinder. However both of these theories neglect the axial heat flow along depth and are only adequate for short

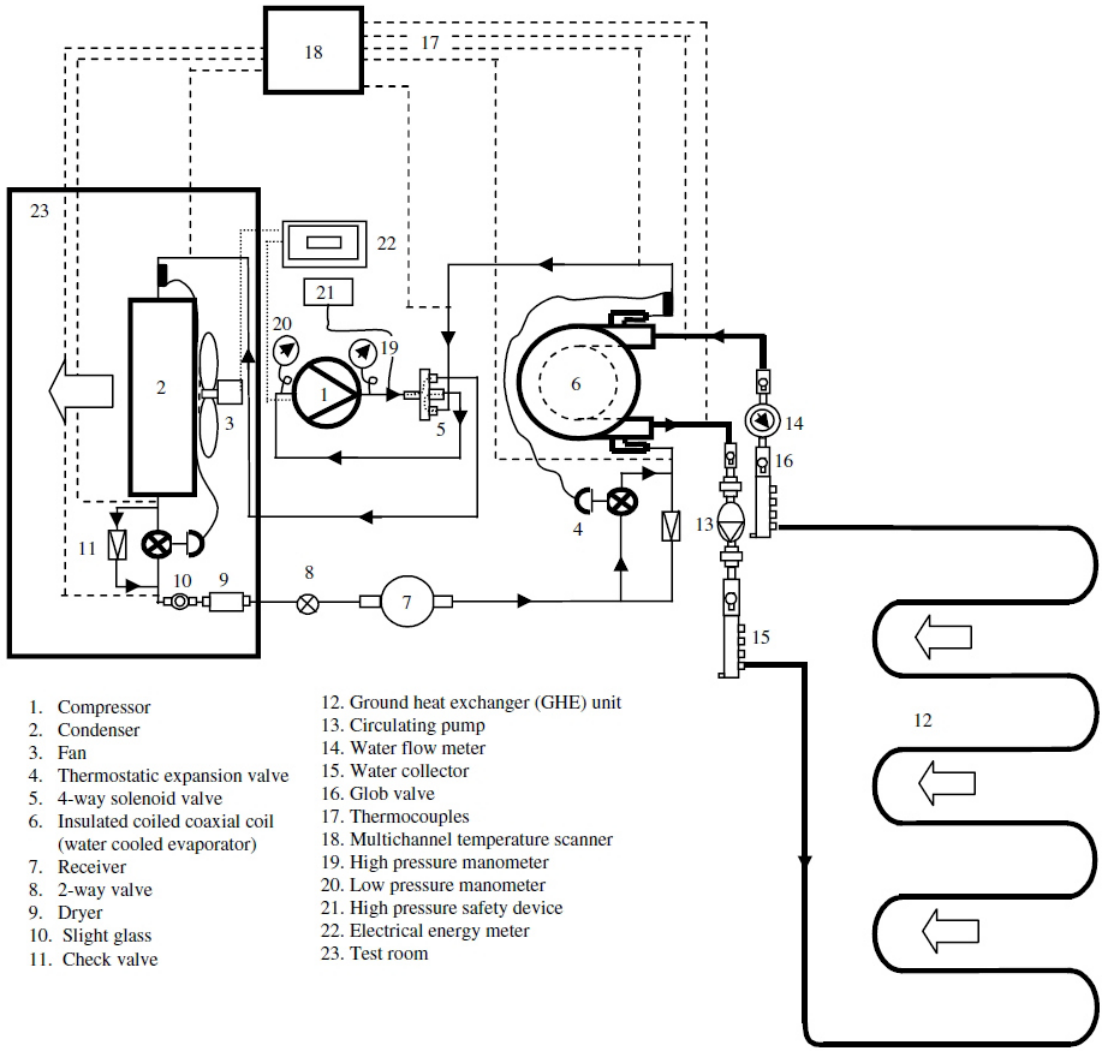

Figure 2.10: Complete schematic description of the geothermal heat pump system (Pulat et al. 2009)

duration operation from hours to months, ground temperature cannot reach a steady state value for long duration operation. A finite line-source theory was then developed by Eskilson (1987), which takes axial heat flow condition into consideration and can be valid for both short or long duration operations.

Based on the study of thermal response of a borehole exchanger to a constant heat injection or extraction, the in-situ tests called thermal response tests (TRTs) are commonly carried out to detect the thermal properties of the ground, grouting materials and the heat exchanger. Eskilson & Claesson (1988) analytically investigated dimensioning rules and the effects of stratification of the ground, climatic variations, geothermal gradient and

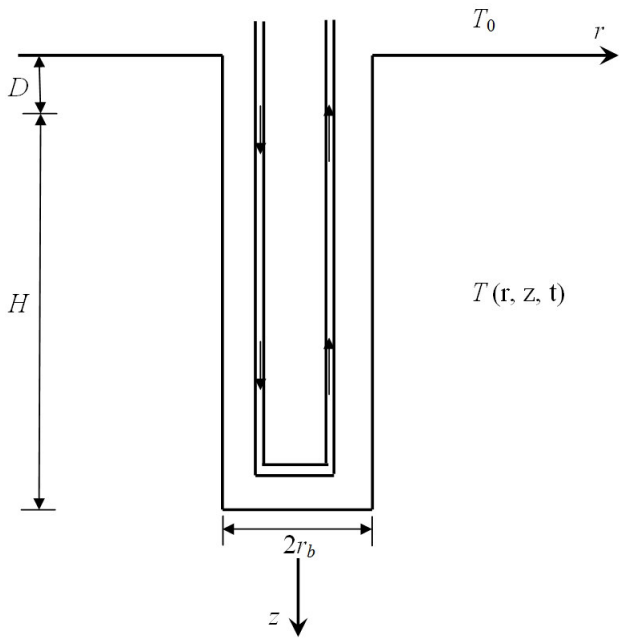

Figure 2.11: Heat extraction using U-tube in deep borehole (Eskilson 1987)

groundwater filtration on the heat extraction step. They used TRTs to determine three important parameters: average thermal conductivity in the ground, borehole thermal resistance, and average undisturbed ground temperature. Eskilson & Claesson (1988) designed a computational model with suitable choice of mesh to simulate a symmetry group of boreholes based on the intricate superposition technique. Based on Eskilson's (Eskilson 1987) theoretical work, Yavuzturk & Spitler (1999) developed non-dimensional short time-step temperature response factors with an analytically validated two-dimensional transient implicit finite volume model. Lamarche & Beauchamp (2007) introduced a modified approach of A- and B-integrals to evaluate Eskilson's g-function for long duration analyses of BHE system. Bandos et al. (2009) improved Eskilson's g-function (Eskilson 1987) and presented a new analytical formulae for asymptotic behavior of thermal response with the consideration of surface temperature oscillations. They established an efficient model to assess the TRTs data by improving the asymptotic expression of the mean borehole temperature. Accounting for the thermal interference between the two legs of U-tube, Diao et al. (2004) derived the explicit analytical solution of the finite line source in semi-finite medium and then calculated of the thermal resistance both outside and inside the borehole for long time steps. With the finite element technique, Al-Khoury et al. (2010) established a three-dimensional time-dependent model to investigate the heat transfer in a double U-tube BHE system buried in multilayered soil mass both for long- and short-

duration operations. The effect of the grout thermal conductivity in relation to the fluid flow rate is studied too. Zeng et al. (2003) established a quasi-three-dimensional model and then derived analytical solutions of the fluid temperature and borehole resistance for single and double U-tube BHE system with the consideration of fluid axial convective heat. Diao et al. (2004) established a conduction-advection model to estimate the impact of groundwater flow on performance of U-tube BHE system. Their numerical results as shown in Figure 2.12 demonstrated that water advection in the porous media could significantly change the conductive temperature distribution, and the hydraulic and thermal properties of soils and rocks can also influence the advection heat transfer. Similar study was also implemented by Fan et al. (2007, 2008).

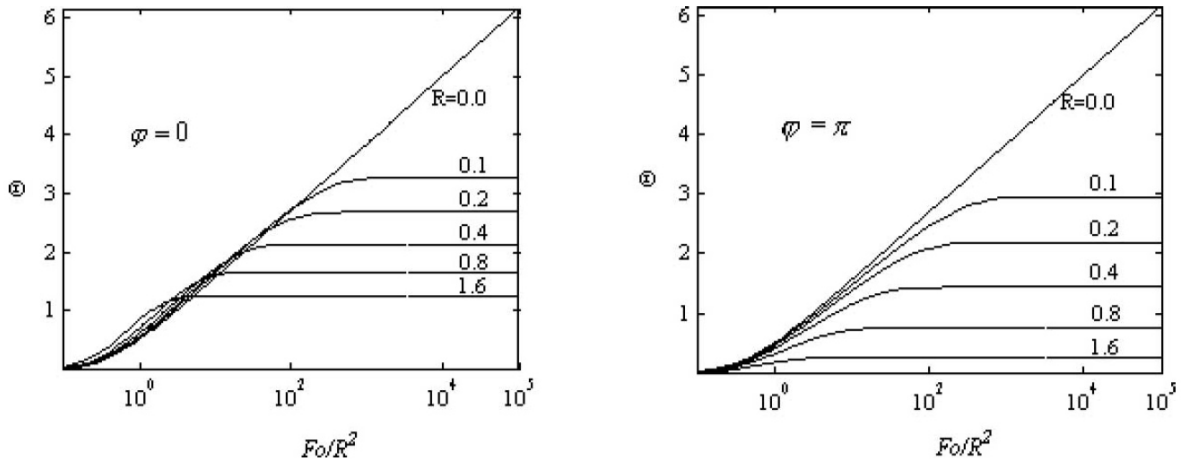

Figure 2.12: Temperature responses to the line-source heating with and without water advection (Diao et al. 2004)

For a horizontally configured stretch, the heat transfer mechanism is different from the one for vertically buried BHE system, because such stretch is always buried at the superficial ground and the temperature factors just like sunshine hour and precipitation will influence the heat transfer process significantly. Chung et al. (1999) established a two-dimensional model to study the problem of steady state heat transfer from a constant wall temperature circular pipe with a plane surface exposed to a fluid flow by means of alternating direction implicit (ADI) finite difference method. Demir et al. (2009) used ADI finite difference method to investigate the effect of boundary condition, e.g., Meteorological soil, weather temperatures and solar radiation, on the thermal response of a two-dimensional time-dependent model, and compared the numerical results with the experimental data. Esena, Inalli & Esen (2007); Esena, Inalli, Esen & Pihtili (2007) carried out a series of experiments to investigate the temperature distribution in the vicinity of

the horizontally stretched pipes and to determine the coefficient of performance (COP) of the geothermal heat pump system. The experimental results were compared and agreed well with a two-dimensional time-dependent numerical model by means of finite difference method. Taking the heat and moisture transfer in the soil into account, Piechowski (1999) introduced a new approach to simulate the horizontal type GHP with special attention on the pipe-soil interface. With the effect of outdoor temperature on system capacities and COP values with respect to outdoor air and mean soil temperatures, Pulat et al. (2009) experimentally studied the performance of horizontal GHP with various system parameters. The variations of circulating antifreeze solution temperatures, extracted and rejected heat, super heat rate in evaporator and sub-cooling rate in condenser, total power consumption and the COP values for both the entire system and heat pump unit were obtained.

2.2 Analytical solutions for coupled THM model

The analytical solutions for the THM model can well reveal the mechanism of the coupled behaviour in porous media, and can also be a benchmark for the numerical simulation. Although not all the analytical solutions can be obtained for THM model, there are still a lot of theoretical works with some meaningful analytical solutions published in the past.

2.2.1 Analytical solutions for coupled THM model in porous media

McTigue (1986) first presented a linear theory and a general solution scheme for saturated thermoporoelastic media. The constitutive relation takes the compressibility and thermal expansion of both the fluid and solid skeleton into account which reads:

$$\sigma_{ij} = 2G\varepsilon_{ij} + \lambda\varepsilon_{kk}\delta_{ij} - \xi p\delta_{ij} - K\alpha\theta\delta_{ij} \tag{2.5}$$

where σ_{ij} is the total stress, ε_{ij} is infinitesimal strain, p is pore pressure, θ is temperature change, respectively, G, λ, $\xi(=1-\frac{K_s}{K})$, K, K_s and α and are shear modulus, Lame parameter, Biot-Willis coefficient, bulk modulus, bulk modulus of solid skeleton and thermal expansion coefficient, respectively. δ is Kronecker delta.

Booker & Savvidou (1985) developed an analytical solution for the consolidation problem of 3D homogeneous cylinder under non-isothermal conditions. Booker & Savvidou (1985) established a three-dimensional time-dependent fluid saturated THM model with a containing point heat source and got the analytical solutions for displacement, pore pressure,

stress and temperature by means of Laplace and Fourier transform. Rajapakse & Senjuntichai (1995*b*) studied the three-dimensional quasi-static response of a multilayered poroelastic half-space with compressible constituents. Bai & Abousleiman (1997) discussed the coupling theory and simplification method, and studied one dimensional consolidation behaviour of soil column as a practical application. Giraud & Rousset (1995) obtained the analytical solutions for the static response in one-dimensional semi-infinite multilayered porous media with a point heat decaying point source. Giraud (1998) presented the solutions for the behaviour of a two-layered porous space, which contains a deep low permeability layer with decaying heating source and a superficial layer, to examine the effects of contrasts of permeability, thermal conductivity and specific heat capacities between the two layers on the large-scale behaviour of the porous space. Zhang et al. (1999) studied the consolidation problem of a thermoporoelastoplastic model and compared with thermoporoelastic model. Vafai & Sheikh (2004) presented the exact mathematical solution for heat transfer in the models of parallel plate channel and circular duct based on Brinkman's theory. Kanj & Abousleiman (2005) established an unjacked hollow cylinder with anisotropic materials subjected to non-isothermal conditions, and investigated the thermal and material anisotropy effects on the quasi-static response of pore pressure and stress. Ekbote & Abousleiman (2005) presented an anisotropic porochemothermoelastic inclined borehole subjected to non-isothermal conditions, and studied the thermochemical effects on pore pressure and stress. Liu (2010) studied the dynamic response of a 2D thermo-hydro-elastic model and compared with the thermoelastic model. However, when soil and rock are subjected to rapid heating or cooling, the rate of heat transfer between soil/rock and pore fluid may not be fast enough for the two phases to achieve local thermal equilibrium (He & Jin 2011). The physical properties of soil and fluid are independent, different from the mixture material. This phenomenon is even more obvious in heat insulation materials. Under this condition, the local thermal non-equilibrium (LTNE) transfer theory is better than LTE transfer theory to describe the temperature distributions. In this field, Nield (1998) investigated the forced convection processes in a channel between parallel planes. Vafai & Alazmi (2002) investigated the effects of variant boundary conditions on constant wall heat flux under LTNE conditions. Nield & Bejan (2006) published a book to describe the development of LTNE transfer theory in details. He & Jin (2011) investigated the distributions of temperatures, pore pressure and thermal stresses on an one-dimensional spherical model fulfilling LTNE condition and also compared LTNE transfer theory with LTE transfer theory. For an one-dimensional semi-infinite model, Liu, Xie & Zheng (2010) got the solutions of dynamic response under mechanical/thermal shock in Laplace transform domain.

Most of the analytical solutions are for the saturated porous media, while numerical approximations with the help of FEM, FVM, DEM,FDM and so on are obtained for the unsaturated porous media. However, there are still some limited analytical solutions following some necessary simplifications are obtained. For the study of unsaturated porous media, the relevant constitutive equation should be changed with the introduction of gas pressure written as (Maghoul et al. 2010):

$$\sigma - p_g\mathbf{I} = \mathbf{DE} - F(p_g - p_w)\mathbf{I} - C\theta\mathbf{I} \tag{2.6}$$

where p_g and p_w are pore gas and water pressure, respectively, $\mathbf{I}$ is identity tensor, and the definitions of $\mathbf{D}$, F and C can be found in their article. Gatmiri & Jabbari (2005*a*,*b*) derived the fundamental solution for the nonlinear hydro-mechanical governing differential equations for static and quasi-static porous media for both two and three-dimensional problems. Jabbari & Gatmiri (2007) derived the thermoporoelastic fundamental solution for the nonlinear governing differential equations for static and for both two and three-dimensional problems. Maghoul et al. (2010) derived analytical transient fundamental solutions for a three-dimensional THM coupled unsaturated porous media by applying the Laplace transform and using the Kupradze method.

2.2.2 Analytical solutions for multilayered thermoelastic model

If the hydraulic field is decoupled from the THM model, that means the porous media is dry, so we can get the classic Duhamel-Neumann relation which can be written as follows

$$\sigma_{ij} = 2G\varepsilon_{ij} + \lambda\varepsilon_{kk}\delta_{ij} - K\alpha\theta\delta_{ij} \tag{2.7}$$

More often the multilayered thermoelastic structure is assumed to be composed of homogeneous parallel layers. Several approaches exist to solve the static and dynamic problems for multilayered structures. The most common numerical and semi-analytical methods are the finite element method (FEM) and the boundary element method (BEM). It is well accepted that BEM is more suited compared to FEM to cases where the domain of interest is infinite.

As an alternative one can consider the finite layer method (FLM) (Small & Booker 1984, 1986*a*) and its improved version – the exact stiffness matrix method (Senjuntichai & Rajapakse 1995; Degrande et al. 1998), and the analytical layer-element method (ALEM) (Ai et al. 2015*b*; Ai & Wang 2015; Ai et al. 2015*a*). However, both methods require an assembling of a stiffness matrix whose size is proportional to the number of layers N and

thus the methods are becoming inefficient if the number N is large (Pan 1989*b*, 1997). One of the best methods to treat problems related to processes in multilayered structures is the propagator matrix method (PMM) (Singh 1970). PMM was first used by Thomson (1950) and further developed by Haskell (1953) and Gilbert & Backus (1966) to solve problems in elastodynamics. The method successfully overcomes the difficulty in FLM for large N, and has the advantage of high computational efficiency. Although PMM is superior to the previous methods, the solutions were reported to be numerically unstable in the far evanescent regime for high frequency and large layer thickness (Kennett 1974, 2009; Wang 1999; Wang & Kuempel 2003). To overcome such instability issues there were used the following modifications of PMM – delta matrix method (Dunkin 1965), transmission and reflection matrix method (TRM) (Kennett 1974), the orthogonalization method (Wang 1999), the backward transfer matrix method (BTM) (Yue 1995) and the method suggested by Ai et al. (2002).

There are many authors presenting solutions of various problems involving stratified structures. For the pure elastic multilayered structures, Small & Booker (1984, 1986*b*) applied the finite layer method to investigate the 2D and 3D static problems for cases with strip, circular and rectangular surface loads. Singh & Garg (1985), Pan (1989*b*), Singh (1970, 1986) and Pan (1989*a*) studied the static deformations in 2D and 3D problems for multilayered elastic medium with internal dislocation sources and surface loads. Based on Singh (1970), Jovanovich et al. (1974*a*,*b*) and Rundle (1980) investigated problems of static deformations in earth structure with point dislocation sources.

For poroelastic multilayered media, Senjuntichai & Rajapakse (1995) presented an analysis of a 3D quasi–static problem. For deriving the solution of the problem they applied the stiffness matrix method that is an improvement of FLM. Degrande et al. (1998) investigated the wave propagation problem for porous medium with different degrees of saturation solving the problem using the said exact stiffness matrix method.Wang & Fang (2003) studied the non-axisymmetric Biot consolidation problem under three different boundary conditions using PMM. Recently, Zheng et al. (2013*a*) studied the 3D axisymmetric problem defined for a multilayered poroelastic half space under the action of an internal point force and fluid injection. There they applied the orthogonalization technique developed by Wang (1999). To validate the accuracy and efficiency of this method a comparison is presented between the numerical results and the analytical solution for a uniform poroelastic half space.

The next type of coupled field problems involving multilayered structures is that of thermoelasticity. Rundle (1982) studied the static and pseudo static nonisothermal deforma-

tion problems in multilayered elastic media with a heat source. Small & Booker (1986*a*) considered a 3D axisymmetric problem for multilayered thermoelastic half space with a heat source. Pan (1990) developed a general analytical method to investigate the problem of transient thermoelastic deformation in multilayered half space subjected to surface loads and internal sources with the help of PMM. However, there is a slight mistake in Equation (16) for the expression of X_{ij} which is further discussed in appendix C. Zhong & Geng (2009) used transfer matrix method to study the thermal stresses in multilayered asphalt pavement with temperature-dependent material parameters. Recently, Wang & Ai (2015) and Ai et al. (2016) introduced a new method – precise integration method (PIM) to investigate the thermo-elastic response with buried decaying heat sources in multilayered materials.

The next of the few available references are those of Small & Booker (1986*a*) as FLM application example, of Ai et al. (2015*b*); Ai & Wang (2015) and Ai et al. (2015*a*) as ALEM application examples, of Wang & Ai (2015) and Ai et al. (2016) as PIM application examples and of Rundle (1982) where conventional propagator matrix method was used. On the other hand, there are sufficient references on thermoelastic homogeneous models. However, it can be concluded that the studies on multilayered structures mainly focus on the elastic and poroelastic models while the temperature field is rarely taken into account.

2.2.3 Analytical solutions for heat transfer in geotechnics

In the field of heat transfer, a lot of different theories are developed and applied to the geothermal energy utilization. The first matured and well-known theory is Kelvin's line-source theory (Ingersoll & Plass 1948). Accordingly, the temperature response θ in the ground due to a constant heat rate in polar coordinate reads:

$$\theta(r,t) - \theta_0 = \frac{q_l}{4\pi k} \int_{\frac{r^2}{4\kappa t}} \frac{e^{-u}}{u} \mathrm{d}u \tag{2.8}$$

where θ_0 the initial temperature of the ground, q_l the heating rate per length of the line source, k and κ are the thermal conductivity and diffusivity of the ground.

Carslaw & Jaeger (1947) improved this theory and presented a cylinder-source method, which assumes the borehole as a cylinder with a constant radial heat flux at the radius of the cylinder. The temperature response in the ground can be presented in the cylindrical

coordinate:

$$\begin{cases} \dfrac{\partial^2\theta}{\partial r^2}+\dfrac{1}{r}\dfrac{\partial\theta}{\partial r}=\dfrac{1}{\kappa}\dfrac{\partial\theta}{\partial t} & r_b<r<\infty \\ -2\pi r_b k\dfrac{\partial\theta}{\partial r}=q_l & r=r_b, t>0 \\ \theta-\theta_0=0 & r>r_b, t=0 \end{cases} \tag{2.9}$$

where r_b is the borehole radius.

Eskilson (1987) took axial heat flow condition into consideration and developed a finite line-source theory which demonstrate to be valid for both short or long duration operations. The basic governing equations of the temperature response in the ground in cylindrical coordinates read:

$$\begin{cases} \dfrac{\partial^2\theta}{\partial r^2}+\dfrac{1}{r}\dfrac{\partial\theta}{\partial r}+\dfrac{\partial^2\theta}{\partial z^2}=\dfrac{1}{\kappa}\dfrac{\partial\theta}{\partial t} \\ \theta(r,0,t)=T_0 \\ \theta(r,z,0)=T_0 \\ q_l(t)=\dfrac{1}{H}\displaystyle\int_0^H 2\pi r k\frac{\partial\theta}{\partial r}|_{r=r_b}\mathrm{d}z \end{cases} \tag{2.10}$$

The final expression of the temperature response at the borehole wall to a unit step heat pulse can be expressed with respect to a g-function as:

$$\theta_b-\theta_0=-\frac{q_l}{2\pi k}g(t/t_s, r_b/H) \tag{2.11}$$

where $t_s = H^2/9\kappa$ means the steady-state time. The g-function is used to describe the thermal response factor of the borehole to a heat pulse and to estimate the three-dimensional temperature distribution of a multiple borehole configuration which is closely related with the thermal resistance R and could be calculated numerically. Moreover, two asymptotic approximations for g-function were also presented by Eskilson (1987), to better develop the computational code:

$$g(t/t_s, r_b/H)=\begin{cases} \ln\left(\dfrac{H}{2r_b}\right)+\dfrac{1}{2}\ln\left(\dfrac{t}{t_s}\right) & 5r_b^2/\kappa<t<t_s \\ \ln\left(\dfrac{H}{2r_b}\right) & t>t_s \end{cases} \tag{2.12}$$

Based on the finite-line source theory, Zeng et al. (2002) gave the analytical solution for temperature response in the ground which reads:

$$\theta(r,z,t)-\theta_0=\frac{q_l}{4\pi k}\int_0^H \frac{erfc\left(\dfrac{\sqrt{r^2+(z-h)^2}}{2\sqrt{\kappa t}}\right)}{\sqrt{r^2+(z-h)^2}}-\frac{erfc\left(\dfrac{\sqrt{r^2+(z+h)^2}}{2\sqrt{\kappa t}}\right)}{\sqrt{r^2+(z+h)^2}}\,\mathrm{d}h \tag{2.13}$$

where H is the depth, $erfc()$ is complementary error function, the temperature at the mid-borehole depth, i.e., $T(r, 0.5H, t)$ is usually chosen as its representative temperature, .

2.2.4 Analytical study for thermo-osmosis effect

Some special thermal-coupled effects like thermo-osmosis effect are also studied previously. Coupled flows, which consist of thermo-osmosis and thermo-diffusion, mean that fluxes (e.g., water, solute and heat) are driven by non-conjugate thermodynamic forces (Carnahan 1984). According to this definition, thermo-osmosis can be interpreted as fluid flux driven by temperature gradient. Thermo-osmosis was firstly observed experimentally and explained theoretically in Derjaguin & Sidorenkov (1941). Based on this definition, the formula of fluid flow q_f driven by pore pressure and temperature can be written as:

$$q_f = -\frac{k_h}{\mu}\nabla p - S_w \nabla \theta_f \tag{2.14}$$

where θ_f is fluid temperature, μ is the fluid viscosity, $k_h (= K_h/(\rho_f g))$ is the intrinsic permeability, K_h is the hydraulic conductivity, g is gravity acceleration, S_w is a phenomenological coefficient associated with the influence of temperature gradient on the fluid flux, and can be measured directly in the laboratory (Letey & Kemper 1969; Srivastava & Avasthi 1975; Carnahan 1983). The assessment of the phenomenological coefficient S_w needs to be specially discussed as it is one of the model parameters that account the significance of the thermal osmosis in the overall process of the fluid transport. Dividing the hydraulic term in the above equation by the thermo-osmosis term, at zero specific discharge, implies (Rastogi et al. 1964):

$$-\frac{|\nabla p|}{|\nabla \theta_f|} = \frac{S_w \mu}{k_h} = \Gamma \tag{2.15}$$

A series of experimental and theoretical works have shown that the thermo-osmosis effect makes a great contribution to fluid flux especially in these materials whose permeability coefficients are relatively small. Srivastava & Avasthi (1975) showed that, in compacted kaolinite subjected to temperature gradient of $20^0 C m^{-1}$, the water flux associated with this effect can reach to $10^{-8} m s^{-1}$. Carnahan (1984) showed that fluid flux in clay due to this effect is significantly greater than that complying with Darcy's law, the ratio of these two fluxes can be as greater as three orders of magnitudes. Considerable attention on this effect should be put in nuclear waste storage. Because the permeability coefficient of clay barriers for nuclear waste is very low, thermo-osmosis effect derived from

large temperature gradient will generate high pore fluid flux, pore pressure and soil deformation (Hueckel & Pellegrini 1992), which could decrease the strength of clay barriers and even gradually destroy the nuclear waste container. A lot of experiments are also designed to determine the value of the phenomenological coefficients related with thermo-osmosis (Letey & Kemper 1969; Srivastava & Avasthi 1975; McVay 1984). In terms of theoretical works, Carnahan (1984), McTigue (1986) and Liu (2010) mentioned coupled flows but neglected them in numerical simulation. Zhou et al. (1998) presented both the analytical solutions and mixed finite element formulates of 1D thermoporoelastic column with thermodynamically coupled flows. Ekbote & Abousleiman (2005) presented a coupled porochemothermoelastic borehole and investigated the thermo-osmosis effect on the distributions of pore pressure and effective stress. Ghassemi & Diek (2002) adopted the thermoporoelasticity theory to derive the analytical solutions of pore pressure and stresses around a borehole in saturated swelling shale, and extend their work to chemically active rock to investigate the effect of both thermo- and chemical-osmosis on the stability of the borehole under high temperature and high pressure circumstance. They demonstrated that the stress and the pore pressure near the borehole are significantly changed due to thermo-osmosis and suggested that depending on the type of the fluid and the porous media thermal osmosis can cause increase in the inflow that yields a reduction of the effective stress and the strength or can promote the outflow of the fluid from the rock that leads to excessive dehydration.

Based on the physical molecular theory, Julio Goncalves and & Tremosa (2012) developed a new mathematical expression for the thermo-osmotic permeability and investigated the thermo-osmosis effect on the pore pressure and fluid flow in argillaceous media. Their numerical results showed that the thermo-osmotic permeability can be estimated only from surface-charge density, temperature, pore size and salinity, and the thermo-osmosis effect will play a prominent role in compacted shale layer with a temperature gradient.

2.2.5 Analytical study for LTNE heat transfer

Due to the importance of temperature field to the coupled THM model, a lot of contributions on the heat transfer mechanism is also of great interest. The Local Thermal Non-equilibrium (LTNE) effect in heat transfer process, which implies the local temperature of solid skeleton may not be the same with the temperature of pore fluid, becomes attractive recently. Nield made a great contribution to the development in this field. Nield & Bejan (2006) introduced the development of heat transfer fulfilling LTNE effect where

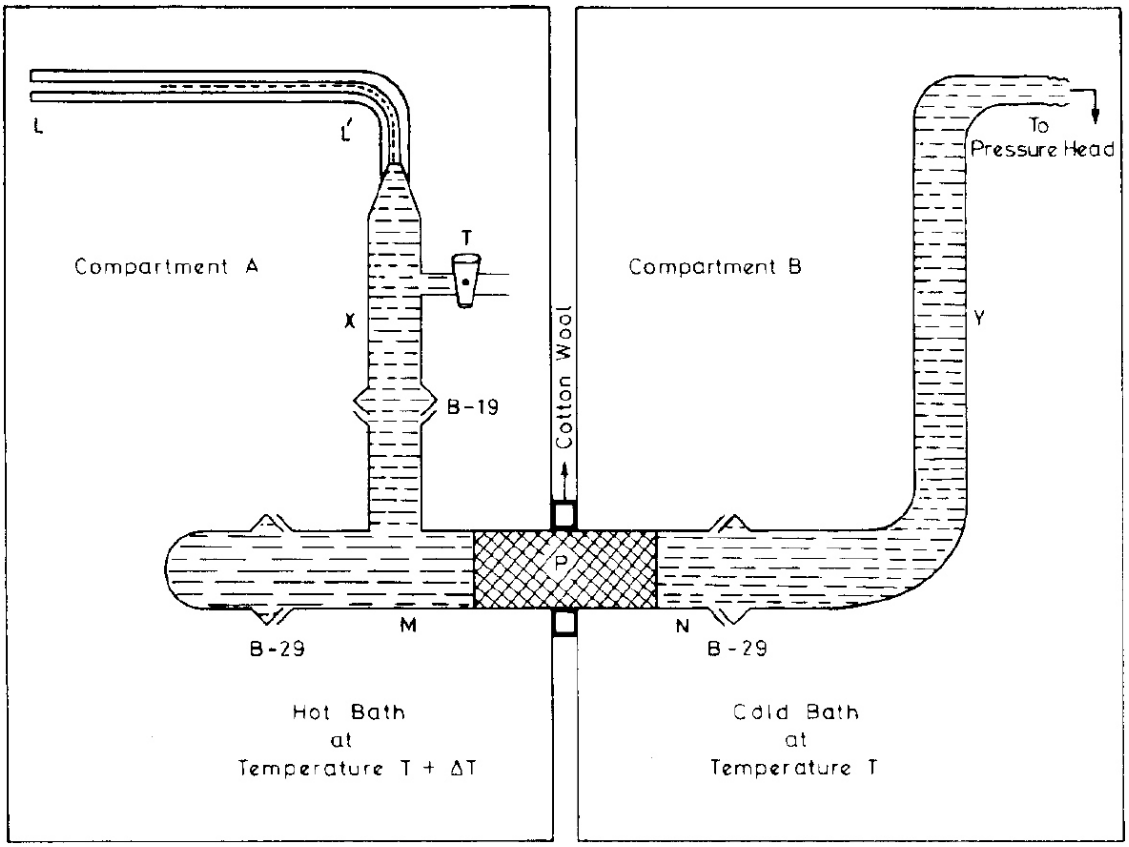

Figure 2.13: Thermo-osmotic cell in the lab (Srivastava & Avasthi 1975)

two constitutive equations for heat conduction in porous media are adopted to describe such process:

$$\begin{cases} (1-\phi)\rho_s c_s \dfrac{\partial \theta_s}{\partial t} = (1-\phi)\nabla \cdot (k_s \nabla \theta_s) + (1-\phi)Q_s + h(\theta_f - \theta_s) \\ \phi \rho_f c_f \dfrac{\partial \theta_f}{\partial t} + (\rho_f c_f) q_f \cdot \nabla \theta_f = \phi \nabla \cdot (k_f \nabla \theta_f) + (1-\phi)Q_f + h(\theta_s - \theta_f) \end{cases} \tag{2.16}$$

where θ_s and θ_f are solid and fluid temperatures, ρ_s and ρ_f are densities of solid and fluid phases, c_s and c_f are specific heat capacities of solid and fluid phases, k_s and k_f are heat conductivities, ϕ is porosity, Q_s and Q_f are sources for solid and fluid phases, h is a exchange heat transfer coefficient and can be determined by (Dixon & Cresswell 1979):

$$\begin{cases} h = a_{fs} h^* \\ a_{fs} = 6(1-\phi)/d_p \\ \dfrac{1}{h^*} = \dfrac{d_p}{N u_{fs} k_f} + \dfrac{d_p}{\beta k_s} \end{cases} \tag{2.17}$$

The definitions of all coefficients can be found in their book (Nield & Bejan 2006). He & Jin (2011) established a one-dimensional saturated thermoporoelastic media to inves-

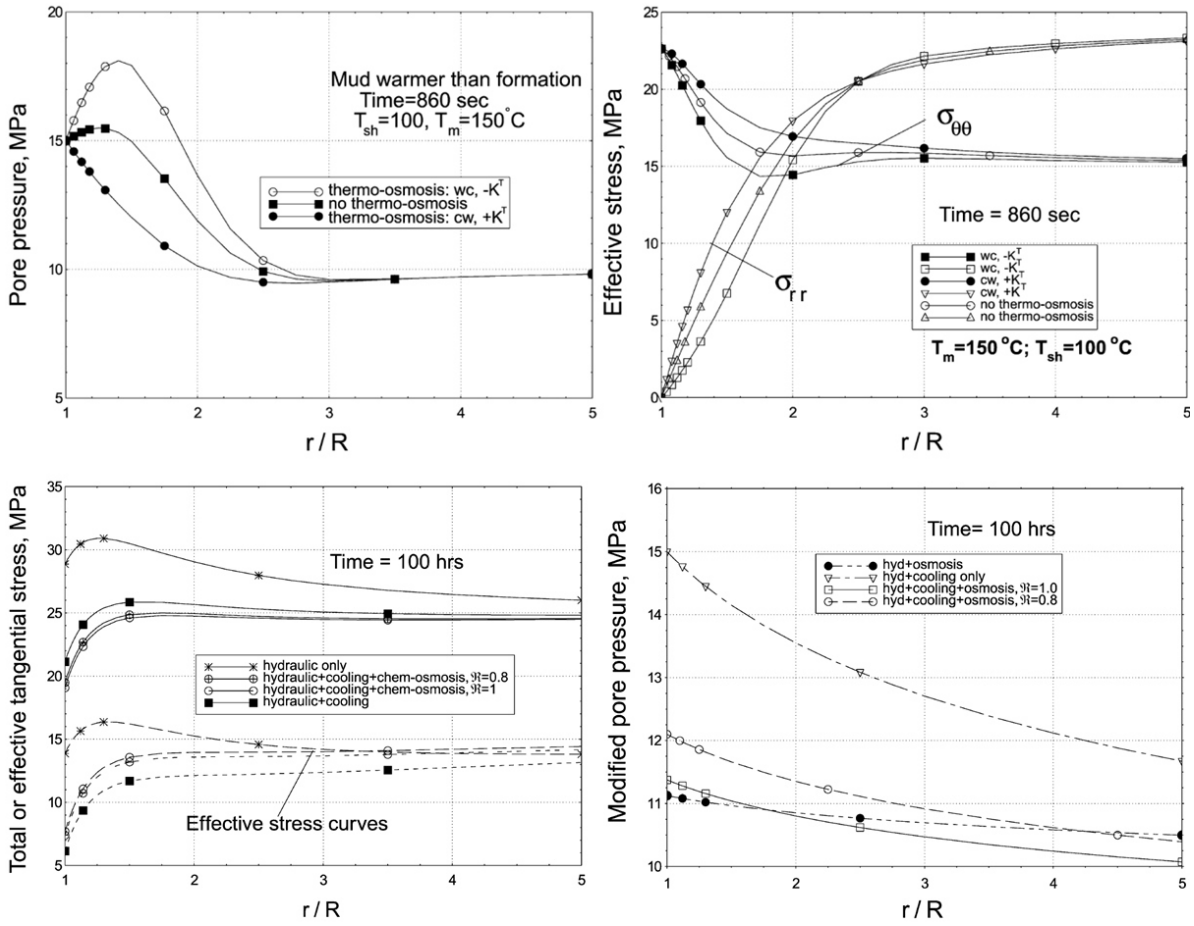

Figure 2.14: Effect of thermal osmosis on pore pressure and stress around the wellbore, cw: cold to warm; wc: warm to cold (shale cooler than mud) (Ghassemi & Diek 2002)

tigated the effect of local thermal non-equilibrium on the responses of temperature, pore pressure and thermal stresses, and compared the LTNE effect with LTE effect as shown in Figure 2.15.

The previous analytical studies on THM coupled generally adopted a single energy conservation equation with the LTE condition, and the thermo-osmosis effect is not always considered due to large value permeability. However, two energy conservation equation fulfilling the LTNE condition can better reveal the heat transfer mechanism in porous media, the thermo-osmosis effect may play an important role in the low-permeability materials like the clay, shale and so on. It is worthy our effort to carefully establish a more complete model with consideration of LTNE condition and thermo-osmosis effect and numerically investigate the THM coupled behaviour in porous media which has a low permeability.

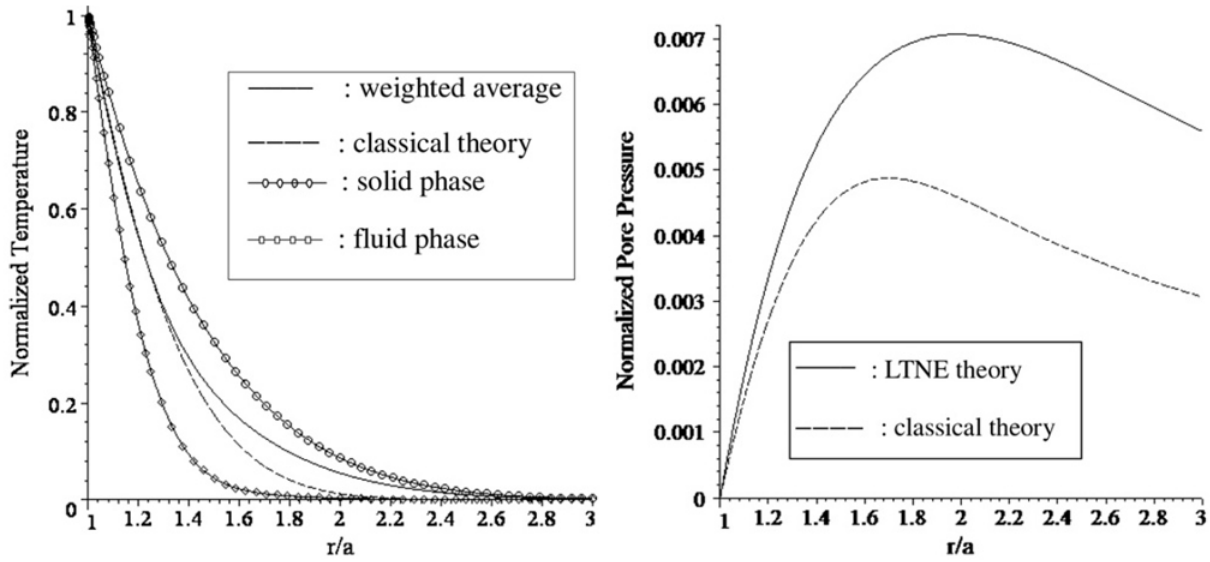

Figure 2.15: Normalized temperature and pore pressure distributions with radial direction (He & Jin 2011)

In this study, we will introduce the thermoporoelasticity theory fulfilling LTNE condition to investigate the quasi-static response of temperatures, pore pressure, stress, displacement and fluid flux around a cylindrical borehole subjected to impact thermal and mechanical loadings in an infinite saturated poroelastic medium. The analytical solutions for all variables will be derived first with the help of Laplace transform scheme. The thermo-osmosis effect will be taken into account to investigate the coupling effect in a typical clay. The difference between the LTNE and LTE heat transfer theories will also be discussed.

Next, we will take temperature field into consideration and extend the application of the generalized propagator matrix method to analyze of temperature-induced deformations in multilayered thermoelastic media. First will be presented the governing equations together with boundary and initial conditions for a 3D formulation of the problem for the static response of multilayered thermoelastic media subjected to general surface loads and containing sources. Second, a set of vector surface harmonics will be introduced, followed by application of PMM with the aid of continuity conditions to derive the general solution for temperature, heat flow, displacements and stress. Moreover, the numerical instability problem in the conventional PMM algorithm will be discussed and resolved. Next, a numerical strategy of high-order adaptive Gaussian quadrature method with continued fraction expansions (Chave 1983) will be employed to approximate the integral–form solution expressed in terms of semi-infinite Hankel-type integrals. Finally, the solution

will be applied to treat the problem of embedded in the geological structure radioactive waste repository where the radioactive waste is regarded as a decaying heat source. The temperature-induced deformations, stresses and the temperature distribution are investigated and also compared with relevant previous results. The influence of source shape on the thermoelastic responses is also discussed.

Then, we will adopt the finite-line theory to investigate a vertical U-tube BHE system with specified boundary and initial conditions. The explicit analytical solutions of temperature responses both in the ground and in the fluid will be presented and the numerical simulations will be implemented to study the temperature variations due to different borehole radius and pumping rate. This work can benefit to optimize the design of the BHE system and provide a fundamental support to increase the working efficiency of the BHE system.

At last, a series of conclusions about the coupled THM behaviour fulfilling LTNE conditions, the influence of thermo-osmosis effect, the principle of numerical optimization for multilayered thermoelastic media and the heat transfer mechanism in the geothermal energy exploitation are drawn. The further works on the n-dimensional dynamic response of coupled THM model, the analytical/numerical study on unsaturated porous media are introduced for further consideration.

3 Governing equations for IBVP formulated

3.1 Introduction

There are sufficient theoretical works for the pure elastic and thermoelastic model in the past. The analytical work on the heat transfer is also matured and widely applied in various engineering fields. However, the theoretical work on coupled THM model is not sufficient up to now. The analytical solutions for THM models can well reveal the mechanism of the coupled behaviour in porous media, and can also be a benchmark for the numerical simulation. The existing solutions for coupled THM model generally have some simplifications. For instance, the material parameters are assumed to be constant, the deformation is infinitesimal, the temperature change is limited, the constitutive relationship is linear and so on. Although not all the problems for the coupled THM model can be formulated, there are still a lot of theoretical works with some meaningful analytical solutions published in the past.

3.2 Heat transfer

Generally speaking, there are three fundamental modes of heat transfer: heat conduction, heat convection and heat radiation. Based on Nield Bejan's work (Nield & Bejan 2006), the constitutive equations for heat transfer in porous media read:

$$\begin{cases} (1-\phi)\rho_s c_s \dfrac{\partial \theta_s}{\partial t} = (1-\phi)k_s \nabla^2 \theta_s + h(\theta_f - \theta_s) + (1-\phi)Q_s \\ \phi \rho_f c_f \dfrac{\partial \theta_f}{\partial t} + \rho_f c_f q_f \nabla \theta_f = \phi k_f \nabla^2 \theta_f - h(\theta_f - \theta_s) + \phi Q_f \end{cases} \tag{3.1}$$

where the term $h(\theta_f - \theta_s)$ reveals the exchange heat transfer between solid and fluid phases. If we assume that $\theta_s = \theta_f = \theta$, that implies the transfer process reaches the LTE

state, the classic energy conservation equation can be obtained by combining the above two equations (McTigue 1986):

$$(\rho c)_m \frac{\partial \theta}{\partial t} + \rho_f c_f q_f \nabla \theta = k \nabla^2 \theta + Q \tag{3.2}$$

where $(\rho c)_m = (1-\phi)\rho_s c_s + \phi \rho_f c_f$, $k = (1-\phi)k_s + \phi k_f$ and $Q = (1-\phi)Q_s + \phi Q_f$ denote the the overall heat capacity per unit volume, overall thermal conductivity, and overall heat production per unit volume of the medium, and the terms in the equation represent

- $\frac{\partial \theta}{\partial t}$: rate of change of temperature over time;
- $\rho_f c_f q_f \nabla \theta$: heat convective transfer;
- $k \nabla^2 \theta$: heat conduction transfer.

When taken the influence of deformation and fluid pressure on temperature field, the more complex THM coupled equation should be adopted as (Liu, Xie & Zheng 2010):

$$(\rho c)_m \frac{\partial \theta}{\partial t} + \rho_f c_f q_f \nabla \theta = \theta_0 K \alpha \frac{\partial e}{\partial t} - \theta_0 \alpha_f K_f k_h \nabla^2 p + k \nabla^2 \theta + Q \tag{3.3}$$

where θ_0 is the reference temperature, $e(= tr\varepsilon)$ is the volumetric strain, α_f is the linear thermal expansion coefficient for fluid, K_f is the bulk modulus for fluid. For the different model, different kinds of equations for heat flux q_H is selected. The Fourier's law is most widely adopted equation for $\mathbf{q}_H$ which reads:

$$\mathbf{q}_H = -k \nabla \theta \tag{3.4}$$

What should be pointed out is that, the above equation is only for the heat conduction, a more complete equation with the considerations of heat convection and thermal-filtration should be written as (Liu, Xie & Zheng 2010):

$$\mathbf{q}_H = -k \nabla \theta + \rho_f q_f c_f \theta - S_f \nabla p \tag{3.5}$$

where S_f is a phenomenological coefficient associated with the influence of water pressure gradient on the heat flux (thermal-filtration).

Before we investigate the heat transfer problem, it is necessary to state the boundary and initial conditions clearly to make the problem manageable. The boundary condition is defined upon the actual circumstance which will discuss in the following in details:

- If the boundary directly contacts with other objective with prescribed temperature, the boundary condition can be easily defined as: $\theta = f_\theta$ where f_θ is a constant or a prescribed function;

- If there is a prescribed heat flux, the boundary condition can be defined as: $\nabla\theta = f_q$, where f_q can be zero, a constant or a prescribed function;
- The linear radiation boundary condition is given by $\nabla\theta + h_r(\theta - f_\theta)$. The radiation condition describes that the flux across the boundary is proportional to the temperature difference between the boundary and the circumstance;
- If the boundary is just the interface of two media with different heat conductivities, so the boundary condition can be defined as: $k_1\nabla\theta_1 = k_2\nabla\theta_2$;
- There still some other boundary types, like the non-linear heat transfer condition which can be found in Carslaw & Jaeger (1947).

The initial condition is usually given by:

$$\theta = f_{\theta 0} \tag{3.6}$$

although $f_{\theta 0}$ can be a function of the coordinate, that implies the objective has not a uniform temperature. In order to well manage the proble, we usually assume $f_{\theta 0}$ =constant.

3.3 Fluid flow

In the field of porous media, the Darcy's law is commonly used to describe the fluid flow which is formulated by Henry Darcy based on the results of experiments (Darcy 1956), and it reads:

$$\mathbf{q}_f = -\frac{k_h}{\mu}\nabla p \tag{3.7}$$

A more complete formulation for the dynamic case with the thermo-osmosis effect could be expressed as (Chen, Tan, Yu, Wu & Jia 2009):

$$\mathbf{q}_f = -\frac{k_h}{\mu}(\nabla p - \rho_f g) - S_w\nabla\theta \tag{3.8}$$

where S_w is a phenomenological coefficient associated with the influence of temperature gradient on the fluid flux (thermo-osmosis) and it has a relationship with S_f known as $S_w = (\theta + \theta_0)S_f$ or $S_w = \theta_0 S_f$ for small temperature change.

We usually define two typical kinds of boundary conditions for the fluid flow:

- If the boundary is free to the circumstance, we give $p = 0$ at the surface;
- If the boundary is impermeable or it is infinite, we usually give $q_f = 0$.

3.4 Constitutive mechanical relation

If the soil is linear elastic isotropic saturated porous media, and take the effect of deformation on the balance of mass and heat, the constitutive relation of an isotropic linear poroelastic media could be depicted in terms of the effective stress and temperature change as (McTigue 1986):

$$\sigma'_{ij} = 2G\varepsilon_{ij} + \frac{2G\nu}{1-2\nu}\varepsilon_{kk}\delta_{ij} - K\alpha\theta\delta_{ij} \tag{3.9}$$

where σ'_{ij} is effective stress and $\sigma'_{ij} = \sigma_{ij} + \xi p\delta_{ij}$. The dynamic equilibrium equation and strain-displacement relation can be expressed as (Liu, Xie & Zheng 2010):

$$\sigma_{ij,j} + b_j = \rho\ddot{u}_i + \rho_f\ddot{w}_i \tag{3.10}$$

$$\varepsilon_{ij} = (u_{i,j} + u_{j,i})/2 \tag{3.11}$$

where b_j is body force, u_i and w_i are displacement of solid skeleton and displacement of pore fluid with respect to solid skeleton. Combining Equations (6.9)–(6.11) can obtain

$$G\nabla^2 u_i + \frac{G}{1-2\nu}u_{j,ji} - \xi p_{,i} - K\alpha\theta_{,i} = \rho\ddot{u}_i + \rho_f\ddot{w}_i \tag{3.12}$$

The above equation can be reduced to the Navier equation for an idea elastic model as

$$G\nabla^2 u_i + \frac{G}{1-2\nu}u_{j,ji} = \rho\ddot{u}_i \tag{3.13}$$

by neglecting the hydraulic and temperature fields from the THM coupled model.

Two typical boundary conditions are discussed here:

- If the boundary is free and subjected to prescribed loads, we give $\sigma = f_\sigma$ at the surface where f_σ is a prescribed mechanical load;
- If the boundary is fixed, we usually give $u = 0$;
- If it is a infinite model, so $\nabla u = 0$ at infinity.

We commonly set the initial displacement and stress equal zero or constant for the pre-stressing case. Although the initial pre-deformation and pre-stress may not be uniform throughout the objective, we prefer to assume it as a uniformed value to make the problem manageable.

The above equations for heat transfer, fluid flow and the constitutive relations together with the initial and boundary conditions constitute the complete mathematical-physical model. In order to get the analytical solutions, we usually make some simplifications, like the material parameters are constant, the deformation is infinitesimal, the temperature change is small and so on.

4 Thermo-Osmosis Effect in Coupled THM Porous Medium

4.1 Introduction

Coupled processes like thermo-hydro-mechanical (THM) coupling widely exist in different branches of engineering, such as geothermal energy extraction, nuclear engineering, geotechnical engineering and so on. These circumstances will generate strong coupling effects in heat flux, fluid flux and soil deformation. Coupled flows, which consists of thermo-osmosis and thermo-diffusion, mean that fluxes (e.g., water, solute and heat) are driven by non-conjugated thermodynamic forces (Carnahan 1984). According to this definition, thermo-osmosis can be interpreted as fluid flux driven by a temperature gradient. Both theoretical and experimental studies demonstrate that the thermo-osmosis effect plays an important role in the response of low permeability materials.

On the other hand, temperature is one important coupling factor while different heat transfer theories result in different temperature field. Traditional researches adopt the local thermal equilibrium (LTE) transfer theory with the assumption that solid and fluid temperatures are identical. In this case, the solid and fluid are blended together as a new mixture, a group of average parameters are endowed to the mixture material as its physical properties. However, the physical properties of soil and fluid are independent, different from the mixture material. Under this condition, the local thermal non-equilibrium (LTNE) transfer theory is better than the LTE transfer theory to describe the temperature distributions.

Contributions on thermal coupled process fulfilling LTNE conditions together with the effect of thermo-osmosis are not so sufficient. And the applications of the local thermal non-equilibrium transfer theory are mainly put in the field of heat transfer itself, the thermal induced pore pressure, stress, deformation and so on are less discussed. In this chapter, thermo-poroelasticity theory fulfilling local thermal non-equilibrium condi-

tion with thermo-osmosis effect is presented in section 4.2 to investigate the quasi-static response of fully saturated poroelastic media. A coefficient h is employed to describe interface heat transfer between the solid and the fluid phases. For a cylindrical borehole subjected to impact thermal and mechanical loadings in an infinite poroelastic medium, the analytical solutions are derived in Laplace transform space in section 4.3. Section 4.4 displays the parameter study for a typical clay. The coupled effects of thermo-osmosis in pore pressure, displacement, radial stress and fluid flux are investigated. The effects of LTNE are also studied and compared with the relevant results fulfilling LTE condition in this section. At last we obtain several conclusions in section 5 which are useful both in theoretical study and practical application.

4.2 Governing equations of coupled THM model fulfilling LTNE condition

4.2.1 Constitutive equations

The quasi-static equilibrium equations for saturated isotropic poroelastic medium based on the framework of Biot theory can be expressed in terms of total stress σ_{ij}, strain ε_{ij}, pore pressure p and solid phase temperature θ_s as follows (McTigue 1986):

$$\sigma_{ij} = 2G\varepsilon_{ij} + \frac{2G\nu}{1-2\nu}\varepsilon_{kk}\delta_{ij} - \xi p\delta_{ij} - K\alpha\theta_s\delta_{ij} \tag{4.1}$$

where δ_{ij} is the Kronecker's delta, $\xi(= 1 - K/K_s)$ is the Biot-Willis coefficient, G is the shear modulus, ν is the Poisson's ratio, K is the drained bulk modulus of solid skeleton, K_s is the drained bulk modulus of solid grain, α is the volumetric thermal expansion coefficient of solid skeleton. Compared with the relevant equation from McTigue (1986), θ_s is more accurate than the weighted average temperature θ to describe the contribution of thermal expansion to total stress.

For the isotropic, homogeneous and linear elastic porous media, the equilibrium equations and strain-displacement relations can be written as:

$$\sigma_{ij,j} = 0 \tag{4.2}$$

$$\varepsilon_{ij} = (u_{i,j} + u_{j,i})/2 \tag{4.3}$$

where u_i denotes the displacement. In addition, inertia terms and body force are neglected here.

Substituting Equation (4.1) into Equation (4.2) results in

$$2G\frac{1-\nu}{1-2\nu}\nabla\varepsilon_{kk} - \xi\nabla p - K\alpha\nabla\theta_s = 0 \tag{4.4}$$

4.2.2 Fluid flow

Consider a saturated poroelastic solid element of volume V which consists of solid grain of volume V_s and voids of volume V_f. The rates of changes of V, V_s and V_f with respect to time satisfy the following relationships:

$$\frac{\partial\varepsilon_{kk}}{\partial t} = \frac{1}{V}\frac{\partial V}{\partial t} = \frac{1}{V}\frac{\partial V_f}{\partial t} + \frac{1}{V}\frac{\partial V_s}{\partial t} \tag{4.5}$$

$$\frac{1}{V}\frac{\partial V_s}{\partial t} = (1-\phi)\alpha_s\frac{\partial\theta_s}{\partial t} - \frac{1-\phi}{K_s}\frac{\partial p}{\partial t} + \frac{\vec{m}}{3K_s}\frac{\partial\vec{\sigma}}{\partial t} \tag{4.6}$$

$$\frac{1}{V}\frac{\partial V_f}{\partial t} = -\nabla q_f + \phi\alpha_f\frac{\partial\theta_f}{\partial t} - \frac{\phi}{\beta_f}\frac{\partial p}{\partial t} \tag{4.7}$$

where α_s and α_f are the volumetric thermal expansion coefficients of solid grain and fluid respectively, β_f is the bulk modulus of fluid, ϕ is the porosity, $\vec{\sigma}$ denotes the effective stress vector, $\vec{m}$ is row vector defined as $\vec{m} = (1 \quad 1 \quad 1 \quad 0 \quad 0 \quad 0)$, and q_f is fluid flux. The three terms on the right hand side of Equation (4.6) represent the volume change of solid grain due to the changes of solid temperature, pore fluid pressure and effective stress, respectively. The three terms on the right hand side of Equation (4.7) represent the volume change of fluid due to the volume of outflow fluid, the changes of fluid temperature and pore fluid pressure, respectively. It should be noticed that, in Equations (4.6) and (4.7), θ_s and θ_f are employed instead of θ to describe the contributions of thermal expansions to volume change of solid and fluid elements, respectively.

Substituting Equations (4.6) and (4.7) into Equation (4.5) results in

$$\nabla q_f = -\frac{\partial\varepsilon_{kk}}{\partial t} + \phi\alpha_f\frac{\partial\theta_f}{\partial t} + (1-\phi)\alpha_s\frac{\partial\theta_s}{\partial t} - (\frac{\phi}{\beta_f} + \frac{1-\phi}{K_s})\frac{\partial p}{\partial t} + \frac{\vec{m}}{3K_s}\frac{\partial\vec{\sigma}}{\partial t} \tag{4.8}$$

Here we take coupled flow phenomena into consideration, so the fluid flux is given by the following equation:

$$q_f = -(k_h/\mu)\nabla p - S_w\nabla\theta_f \tag{4.9}$$

where k_h is the intrinsic permeability μ is fluid viscosity, γ_f is the specific gravity of fluid, S_w is a phenomenological coefficient associated with influence of temperature gradient on fluid flux, and can be measured directly in the laboratory in principle (Srivastava &

Avasthi 1975; Carnahan 1984). The second term on the right side indicates that fluid flux can be driven by fluid temperature gradient (instead of $\nabla\theta$), which is called thermo-osmosis effect. If this term is neglected, Equation (4.9) can be reduced to Darcy's law. In addition, there is another coupled flow called thermo-diffusion or Soret flow, by which solute will diffuse with the effect of temperature gradient. Soret flow is different from Fickian flow induced by concentration gradient, and should be noticed when we study the contaminant transport in underground water. But this effect is neglected here because there is no chemical coupling effect in this study.

Substituting Equations (4.9) and (4.1) into Equation (4.8) yields

$$K_f \nabla^2 p + S_w \nabla^2 \theta_f = \xi \frac{\partial \varepsilon_{kk}}{\partial t} - f_1 \frac{\partial \theta_f}{\partial t} - f_2 \frac{\partial \theta_s}{\partial t} + f_3 \frac{\partial p}{\partial t} \tag{4.10}$$

where $K_f = k_h/\mu$, $f_1 = \phi\alpha_f$, $f_2 = (1-\phi)\alpha_s - \frac{\alpha K}{K_s}$, $f_3 = \frac{\phi}{\beta_f} + \frac{1-\phi}{K_s}$. Without consideration of compressibility of the constituents, that is $K_s, \beta_f \to \infty$, $\xi = 1$ and $f_3 = 0$.

4.2.3 Heat flow

Under the LTNE condition, the solid phase temperature and fluid phase temperature are different both in transient and steady situations. The governing equations of heat conduction can be expressed as (Nield, 2006; He, 2011)

$$(1-\phi)\rho_s c_s \frac{\partial \theta_s}{\partial t} = (1-\phi) k_s \nabla^2 \theta_s + h(\theta_f - \theta_s) \tag{4.11}$$

$$\phi \rho_f c_f \frac{\partial \theta_f}{\partial t} = \phi k_f \nabla^2 \theta_f - h(\theta_f - \theta_s) \tag{4.12}$$

where θ_f is the fluid temperature, k_s and k_f are heat conductivities of solid and fluid respectively, ρ_s and ρ_f are the densities of solid and fluid, c_s and c_f are the specific heats of solid and fluid respectively. h is the coefficient of solid-fluid interface heat transfer. According to the correlations for a porous bed particle established by Dixon & Cresswell (1979), $h = a_{fs} h^*_{int}$, where a_{fs} is specific surface area, h^* is a coefficient related with particle diameter, Nusselt number and heat conductivities. The determination of value h can be directly found by experiment (Grangeot et al. 1994; Polyaev 1996). The second terms both on the right hand in Equations (4.11) and (4.12) represent the integral heat transfer between solid and fluid phases.

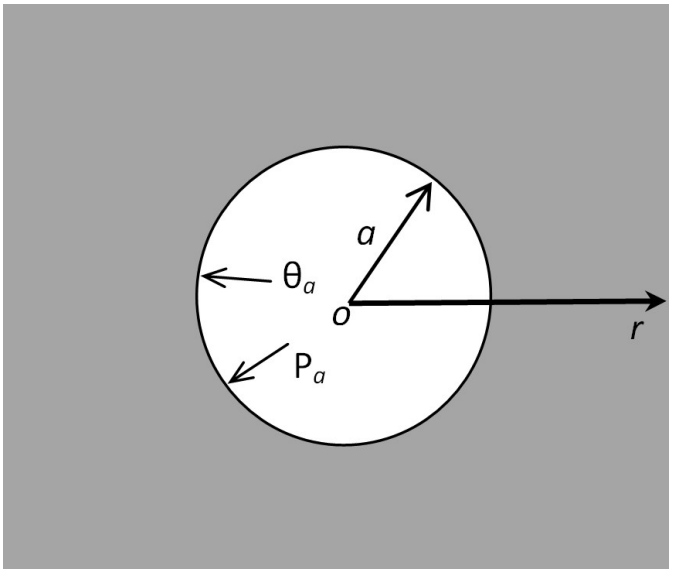

Figure 4.1: Cylindrical borehole in an infinite saturated poroelastic medium

4.3 Solutions for cylindrical borehole in an infinite saturated poroelastic medium

4.3.1 Mathematical model

In this section, an infinite homogeneous, isotropic thermal poroelastic medium with a cylindrical hole subjected to axisymmetric boundary pressure and temperature, as shown in Figure 4.1, is considered. Analytical solutions of temperature, pore pressure, stress, displacement and fluid flux are derived in Laplace transform space. The LTNE effects are also discussed in detail. In order to solve the problem, the inner boundary of the cylindrical hole is assumed to be permeable and subjected to impact thermal and mechanical loadings.

4.3.2 Boundary conditions

The boundary conditions for this model are

$$\theta_s(r,t)|_{r=a} = \theta_f(r,t)|_{r=a} = \theta_0 H(t),$$

$$p(r,t)|_{r=a} = p_0 H(t),$$
$$\frac{\partial \theta_s(r,t)}{\partial t}|_{r\to\infty} = \frac{\partial \theta_f(r,t)}{\partial t}|_{r\to\infty} = 0, \tag{4.13}$$

$$\frac{\partial p(r,t)}{\partial t}|_{r\to\infty} = \frac{\partial \sigma_r(r,t)}{\partial t}|_{r\to\infty} = 0$$

where θ_0 and p_0 are constant, $H(t)$ is the Heaviside step function.

4.3.3 Initial conditions

The initial conditions can be expressed as

$$\begin{gathered}\theta_s(r,t)|_{t=0} = \theta_f(r,t)|_{t=0} = 0,\\ p(r,t)|_{t=0} = 0, \sigma_r(r,t)|_{t=0} = 0,\\ u(r,t)|_{t=0} = 0\end{gathered} \tag{4.14}$$

4.3.4 Analytical solutions

The Laplace transform can be utilized, which is defined by

$$\begin{aligned}\hat{f}(s) &= \int_0^{\infty} e^{-st} f(t) dt\\ f(t) &= \int_{c-i\infty}^{c+\infty} e^{st} \hat{f}(s) ds\end{aligned} \tag{4.15}$$

where $\hat{f}(s)$ is called the transform of the original function $f(t)$, s is a complex variable with real part c, e^{-st} is called the kernel of the transformation. A sufficient condition for the existence of the integral is that $f(t)$ is integrable on $[0, +\infty]$ and that $f(t)$ is of exponential order. The second formula in Equation (4.15) defines the inverse transform.

Application of Laplace transform to Equations (4.4), (4.10), (4.11) and (4.12) with initial conditions (4.14) results in

$$2G\frac{1-\nu}{1-2\nu}\nabla\hat{\varepsilon}_{kk} - \xi\nabla\hat{p} - K\alpha\nabla\hat{\theta}_s = 0 \tag{4.16}$$

$$k_h\nabla^2\hat{p} + S_w\nabla^2\hat{\theta}_f = \xi s\hat{\varepsilon}_{kk} - f_1 s\hat{\theta}_f - f_2 s\hat{\theta}_s + f_3 s\hat{p} \tag{4.17}$$

$$(1-\phi)\rho_s c_s s\hat{\theta}_s = (1-\phi)k_s\nabla^2\hat{\theta}_s + h(\hat{\theta}_f - \hat{\theta}_s) \tag{4.18}$$

$$\phi\rho_f c_f s\hat{\theta}_f = \phi k_f\nabla^2\hat{\theta}_f - h(\hat{\theta}_f - \hat{\theta}_s) \tag{4.19}$$

The transformed temperatures can be derived by Equations (4.18) and (4.19) as follows

$$\hat{\theta}_s(r,s) = A_1(s)\frac{K_0(r\sqrt{\lambda_1})}{K_0(a\sqrt{\lambda_1})} - A_2(s)\frac{K_0(r\sqrt{\lambda_2})}{K_0(a\sqrt{\lambda_2})} \tag{4.20}$$

$$\hat{\theta}_f(r,s) = A_3(s)\frac{K_0(r\sqrt{\lambda_1})}{K_0(a\sqrt{\lambda_1})} - A_4(s)\frac{K_0(r\sqrt{\lambda_2})}{K_0(a\sqrt{\lambda_2})} \tag{4.21}$$

where $K_i()(i \in R)$is the second kind modified Bessel function of i-th order or MacDonald function, and

$$\lambda_{1,2} = [b_1 s + b_2 \pm \sqrt{b_3 s^2 + b_4 s + b_2^2}]/\kappa_s,$$

$$A_1(s) = \frac{\theta_0(s-\kappa_s\lambda_2)}{s\kappa_s(\lambda_1-\lambda_2)}, A_2(s) = \frac{\theta_0(s-\kappa_s\lambda_1)}{s\kappa_s(\lambda_1-\lambda_2)},$$

$$A_3(s) = \frac{\theta_0(a_1 s/a_2-\kappa_s\lambda_2)}{s\kappa_s(\lambda_1-\lambda_2)}, A_4(s) = \frac{\theta_0(a_1 s/a_2-\kappa_s\lambda_1)}{s\kappa_s(\lambda_1-\lambda_2)}$$

in which

$$b_1 = \frac{1}{2}(1+\frac{a_1}{a_2}), b_2 = \frac{h}{2}(1+\frac{1}{a_2}), b_3 = \frac{1}{4}(1-\frac{a_1}{a_2})^2, b_4 = \frac{h}{2}(1-\frac{1}{a_2})(1-\frac{a_1}{a_2}),$$

$$\kappa_s = \frac{k_s}{\rho_s c_s}, h = \frac{h}{(1-\phi)\rho_s c_s}, a_1 = \frac{\phi\rho_f c_f}{(1-\phi)\rho_s c_s}, a_2 = \frac{\phi k_f}{(1-\phi)k_s}$$

where κ_s and the latter κ_f are the thermal diffusivities of solid and fluid phases.

Integrating Equation (4.16) yields

$$\hat{\varepsilon}_{kk} = \frac{1}{2G}\frac{1-2\nu}{1-\nu}(\xi\hat{p} + K\alpha\hat{\theta}_s + d_1 lnr + d_2) \tag{4.22}$$

where d_1 and d_2 are integral constants and can be determined by boundary conditions.

Substituting Equation (4.22) into Equation (4.17) results in

$$\nabla^2\hat{p} - g_1 s\hat{p} = -g_2\nabla^2\hat{\theta}_f - g_3 s\hat{\theta}_f + g_4 s\hat{\theta}_s + g_5 s(d_1 Inr + d_2) \tag{4.23}$$

where

$$g_1 = (\frac{1}{2G}\frac{1-2\nu}{1-\nu}\xi^2 + f_3)/k_h, g_2 = \frac{S_w}{k_h}, g_3 = \frac{f_1}{k_h},$$

$$g_4 = (\frac{1}{2G}\frac{1-2\nu}{1-\nu}K\alpha\xi - f_2)/k_h, g_5 = \frac{1}{2G}\frac{1-2\nu}{1-\nu}\frac{\xi}{k_h}$$

Using Equations (4.20), (4.21) and boundary conditions (4.13) gives the transformed pore pressure

$$\hat{p}(r,s) = B_1(s)\frac{K_0(r\sqrt{g_1 s})}{K_0(a\sqrt{g_1 s})} + B_2(s)\frac{K_0(r\sqrt{\lambda_1})}{K_0(a\sqrt{\lambda_1})} + B_3(s)\frac{K_0(r\sqrt{\lambda_2})}{K_0(a\sqrt{\lambda_2})} \tag{4.24}$$

where

$$B_1(s) = -B_2(s) - B_3(s),$$
$$B_2(s) = -[g_2 A_3(s)\lambda_1 + g_3 A_3(s)s - g_4 A_1(s)s]/(\lambda_1 - g_1 s),$$
$$B_3(s) = [g_2 A_4(s)\lambda_2 + g_3 A_4(s)s - g_4 A_2(s)s]/(\lambda_2 - g_1 s)$$

The transformed bulk strain can be obtained by substituting Equations (4.24), (4.20) and (4.21) into Equation (4.22) as follows

$$\begin{aligned}\hat{\varepsilon}_{kk}(r,s) =& \frac{1}{2G}\frac{1-2\nu}{1-\nu}\{\xi B_1(s)\frac{K_0(r\sqrt{g_1 s})}{K_0(a\sqrt{g_1 s})} + [\xi B_2(s) + K\alpha A_1(s)]\frac{K_0(r\sqrt{\lambda_1})}{K_0(a\sqrt{\lambda_1})} \\ &+ [\xi B_3(s) - K\alpha A_2(s)]\frac{K_0(r\sqrt{\lambda_2})}{K_0(a\sqrt{\lambda_2})}\}\end{aligned} \tag{4.25}$$

Here a potential function $\psi(r,s)$ is introduced which satisfies

$$\hat{u}_r(r,s) = \frac{\partial \psi(r,s)}{\partial r} \tag{4.26}$$

So we can get the following equation

$$\hat{\varepsilon}_{kk}(r,s) = \frac{\partial \hat{u}}{\partial r} + \frac{\hat{u}}{r} = \frac{\partial^2 \psi}{\partial r^2} + \frac{\partial \psi}{r \partial r} = \nabla^2 \psi \tag{4.27}$$

and dealing with the ordinary differential Equation (4.27) can get the variable $\psi(r,s)$, then substitute $\psi(r,s)$ into Equation (4.26). The transformed radial displacement can thus be obtained as

$$\begin{aligned}\hat{u}_r(r,s) =& -\frac{1}{2G}\frac{1-2\nu}{1-\nu}\{\frac{\xi B_1(s)}{\sqrt{g_1 s}}\frac{K_1(r\sqrt{g_1 s}) - (a/r)K_1(a\sqrt{g_1 s})}{K_0(a\sqrt{g_1 s})} \\ &+ \frac{\xi B_2(s) + K\alpha A_1(s)}{\sqrt{\lambda_1}}\frac{K_1(r\sqrt{\lambda_1}) - (a/r)K_1(a\sqrt{\lambda_1})}{K_0(a\sqrt{\lambda_1})} \\ &+ \frac{\xi B_3(s) - K\alpha A_2(s)}{\sqrt{\lambda_2}}\frac{K_1(r\sqrt{\lambda_2}) - (a/r)K_1(a\sqrt{\lambda_2})}{K_0(a\sqrt{\lambda_2})}\} + \frac{1}{2G}\frac{a^2}{r}\frac{p_0}{s}\end{aligned} \tag{4.28}$$

The transformed radial stress and fluid flux can also be obtained by Equations (4.1), (4.9), and (4.20), (4.21), (4.24) and (4.28) as follows:

$$\hat{\sigma}_r(r,s) = -\frac{2G}{r}\hat{u}_r(r,s) \tag{4.29}$$

$$\begin{aligned}\hat{q}_f(r,s) =& k_h B_1(s)\sqrt{g_1 s}\frac{K_1(r\sqrt{g_1 s})}{K_0(a\sqrt{g_1 s})} + [k_h B_2(s) + S_w A_3(s)]\sqrt{\lambda_1}\frac{K_1(r\sqrt{\lambda_1})}{K_0(a\sqrt{\lambda_1})} \\ &+ [k_h B_3(s) - S_w A_4(s)]\sqrt{\lambda_2}\frac{K_1(r\sqrt{\lambda_2})}{K_0(a\sqrt{\lambda_2})}\end{aligned} \tag{4.30}$$

Based on the LTE transfer theory which assumes that $\theta_s = \theta_f = \theta$, the transformed temperature can be expressed as

$$\hat{\theta}(r,s) = \frac{\theta_0}{s}\frac{K_0(r\sqrt{s/\kappa})}{K_0(a\sqrt{s/\kappa})} \tag{4.31}$$

where $\kappa = k/\rho c$ and $k = (1-\phi)k_s + \phi k_f$, $\rho c = (1-\phi)\rho_s c_s + \phi\rho_f c_f$. The above solution can also be derived by combining Equations (4.11) and (4.12). Compared with Equations (4.20) and (4.21), the above temperature can be approximately regarded as an average temperature or a limit case. If h tends to infinity, the interface heat transfer between the two phases is sufficient enough to make the two temperatures almost equivalent. However the value h can not be so large in reality, and even very small under some circumstances, e.g., transfer in heat insulation materials. Its value is usually in the range $10 - 1000W/(m^3K)$ (Nield & Bejan 2006). Furthermore, the assumption $\theta_s = \theta_f$ will deduce $a_1 = a_2$ or $\kappa_s = \kappa_f$, that implies the LTE transfer theory can be adopted if the two thermal diffusivity parameters of solid and fluid phases are identical. With Equation (4.31) we can get the relevant analytical solutions of pore pressure, bulk strain, radial displacement, radial stress and fluid flux by Laplace transform as follows

$$\hat{p}_e(r,s) = B_0(s)[\frac{K_0(r\sqrt{g_1 s})}{K_0(a\sqrt{g_1 s})} - \frac{K_0(r\sqrt{s/\kappa})}{K_0(a\sqrt{s/\kappa})}] \tag{4.32}$$

$$\begin{aligned}\hat{u}_{er}(r,s) = &-\frac{1}{2G}\frac{1-2\nu}{1-\nu}\{\frac{\xi B_0(s)}{\sqrt{g_1 s}}\frac{K_1(r\sqrt{g_1 s}) - (a/r)K_1(a\sqrt{g_1 s})}{K_0(a\sqrt{g_1 s})} \\ &+ \frac{-\xi B_0(s) + K\alpha\theta_0/s}{\sqrt{s/\kappa}}\frac{K_1(r\sqrt{s/\kappa}) - (a/r)K_1(a\sqrt{s/\kappa})}{K_0(a\sqrt{s/\kappa})}\} \\ &+ \frac{1}{2G}\frac{a^2}{r}\frac{p_0}{s}\end{aligned} \tag{4.33}$$

$$\hat{\sigma}_{er}(r,s) = -\frac{2G}{r}\hat{u}_{er}(r,s) \tag{4.34}$$

$$\begin{aligned}\hat{q}_{ef}(r,s) =& k_h B_0(s)\sqrt{g_1 s}\frac{K_1(r\sqrt{g_1 s})}{K_0(a\sqrt{g_1 s})} \\ &+ [-k_h B_0(s) + S_w\theta_0/s]\sqrt{s/\kappa}\frac{K_1(r\sqrt{\lambda_1})}{K_0(a\sqrt{\lambda_1})}\end{aligned} \tag{4.35}$$

where $\hat{f}_e(r,s)$ represents the solution fulfilling LTE condition, $B_0(s) = \frac{g_2+\kappa g_3-\kappa g_4}{1-\kappa g_1}\frac{\theta_0}{s}$.

4.4 Parameter study

Because of the difficulty of Laplace transform inversion towards complex analytical solutions, numerous methods have been utilized for the numerical evaluation. In this section,

a numerical inversion method based on a Fourier series expansion presented by Durbin (1974) and developed by Honig & Hirdes (1984) is adopted to obtain the approximate solutions of Equations (4.20), (4.21), (4.24), (4.25), (4.28)- (4.30) and (4.32) - (4.35). Durbin's formula can be written as follows:

$$f(t) = \frac{2e^{st}}{t_0}[-\frac{1}{2}Re\{\hat{f}(s)\} + \sum_{n=0}^{N}(\Re\{f(s+in\frac{2\pi}{t_0})\}\cos n\frac{2\pi}{t_0}t - \Im\{f(s+in\frac{2\pi}{t_0})\}\sin n\frac{2\pi}{t_0}t)] \tag{4.36}$$

where t_0 is a parameter, the numerical results are valid only for $t \leq t_0/2$. The error is essentially bounded by e^{-st_0}, so suitable choice of st_0 is important for the accuracy of the results. It is reported (Durbin 1974) that, $st_0 = 5$ to 10 and N ranging from 50 to 5000 gave good results. The parameters in Equation (4.36) are defined as $t_0 = 20$, $s = 0.25$ and $N = 500$ in this paper.

Table 4.1 lists the material properties of a typical clay (He & Jin 2011). The radius of the cylindrical cavity is taken as $a = 0.5m$, initial temperature is $\theta_a = 20^0C$. For the purpose to investigate the influence of temperature fields on the thermo-poroelastic response, the boundary is assumed to be drained and stress free, subjected to an impact thermal loading by taking $\theta_0 = 50^0C$ and $p_0 = 0$. In addition, all variables are normalized by $p_a(= 100kPa)$, a, k_h and θ_0, respectively.

In parameter study, thermo-osmosis effects on pore pressure, radial stress, displacement and fluid flux, are investigated. LTNE effect is also studied by comparing the results fulfilling LTNE condition with those fulfilling LTE condition.

Figure 4.2a shows the thermally induced pore pressures (normalized by p_a)along radius (normalized by a) at time $t = 20$ hour. Here positive sign means compressive pressure. Due to heating, both solid skeleton and pore fluid will expand. But the expansion value of fluid is much larger than that of solid because the volumetric thermal expansion coefficient $\alpha_f(= 3\times10^{-4}/^0C)$ of fluid is larger than $\alpha_s(= 3\times10^{-6}/^0C)$. This makes the pore pressure initially generates near the inner boundary and increases along radius. In addition the pore pressure at $r/a = 1$ is equal to zero because it is permeable on the inner boundary. As time progresses, the process of drainage occurs and then leads to the dissipation of pore pressure gradually as shown in Figure 4.2b. However, the dissipation procedure will last longer and the peak value of pore pressure will be larger due to lower permeability or thermo-osmosis effect. Comparisons with the two curves in each figure indicate that, thermo-osmosis has substantial influence on pore pressure. The results with this effect are always larger than these without this effect, especially on the peak value. That's because the permeability coefficient for the typical clay is relatively small compared with

Table 4.1: Material parameters (He & Jin 2011)

Parameter	Value	Parameter	Value
ϕ: [-]	0.375	α: $1/^0C$	3×10^{-6}
G: P_a	1.2×10^6	α_s: $1/^0C$	3×10^{-6}
ν: [-]	0.2	α_f : $1/^0C$	3×10^{-4}
K: P_a	1.6×10^6	k_s: W/m^0C	3.29
ρ_s: kg/m^3	2610	k_f: W/m^0C	0.582
ρ_f: kg/m^3	1000	h_{int}: $W/m^{20}C$	10
K_f: m/s	5×10^{-10}	c_s: J/kg^0C	937
S_w: m^2/s^0C	2.7×10^{-10}	c_f: $1/^0C$	4180
ξ: [-]	1.0		

the ratio $g_2 = S_w/K_f$. The terms $B_2(s)$, $B_3(s)$ related with the ratio in Equation (4.24) will significantly influence the result of pore pressure in some extent. Furthermore, for many other materials with large permeability coefficient, the influence of thermo-osmosis on pore pressure is slight due to small ratio g_2, thus the thermo-osmosis effect can be neglected in this case.

Figures 4.3a and 4.3b show the thermally induced displacements (normalized by $a \times 10^{-3}$) along radius at time $t = 20$ hour, and with time at $r/a = 1.5$, respectively. The phenomenon that, displacements increase first along radius and then decrease, indicates that clay expands due to heating at the inner boundary. As time progresses, it will gradually shrink. Because as the process of drainage continues, pore pressure will decrease, the loss of pore fluid will result in the decrease of expansion. Due to the existence of thermo-osmosis effect, the bulk strain expressed by Equation (4.25) becomes larger. In the same way, displacements with thermo-osmosis effect expressed by Equation (4.28) are also larger than those without this effect. If the permeability coefficient is even smaller, the ratio $g_2 = S_w/K_f$ should be consequently much larger, thermo-osmosis effect could be more intensive, these will make the differences of bulk strain and displacement even more obvious.

Figure 4.4a shows the thermally induced radial stresses (normalized by $p_a \times 10^{-2}$)along radius at time $t = 20$ hour. Minus sign denotes compressive stress. The radial stress has a close relationship with displacement from Equation (4.29), it first grows up to peak value

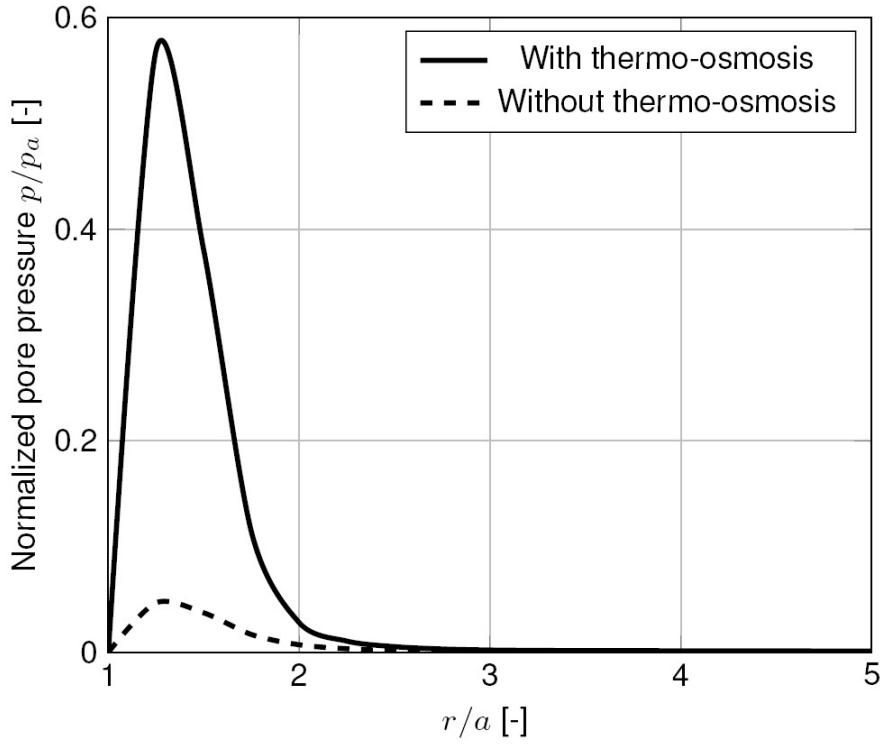

(a)

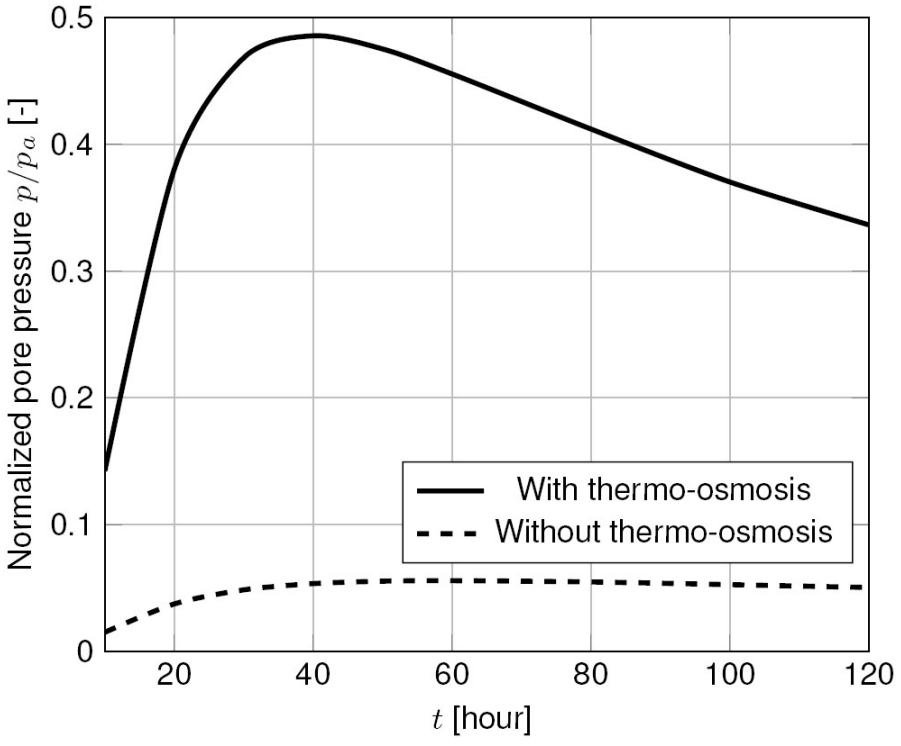

(b)

Figure 4.2: Pore pressure (a) along radius at time $t = 20$ hour (b) with time at $r/a = 1.5$

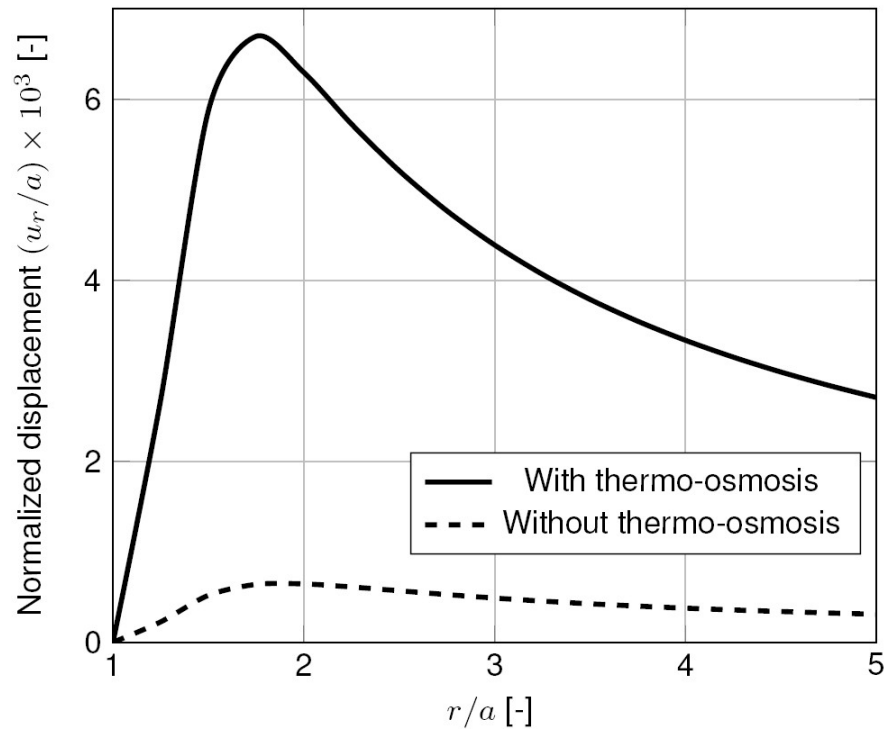

(a)

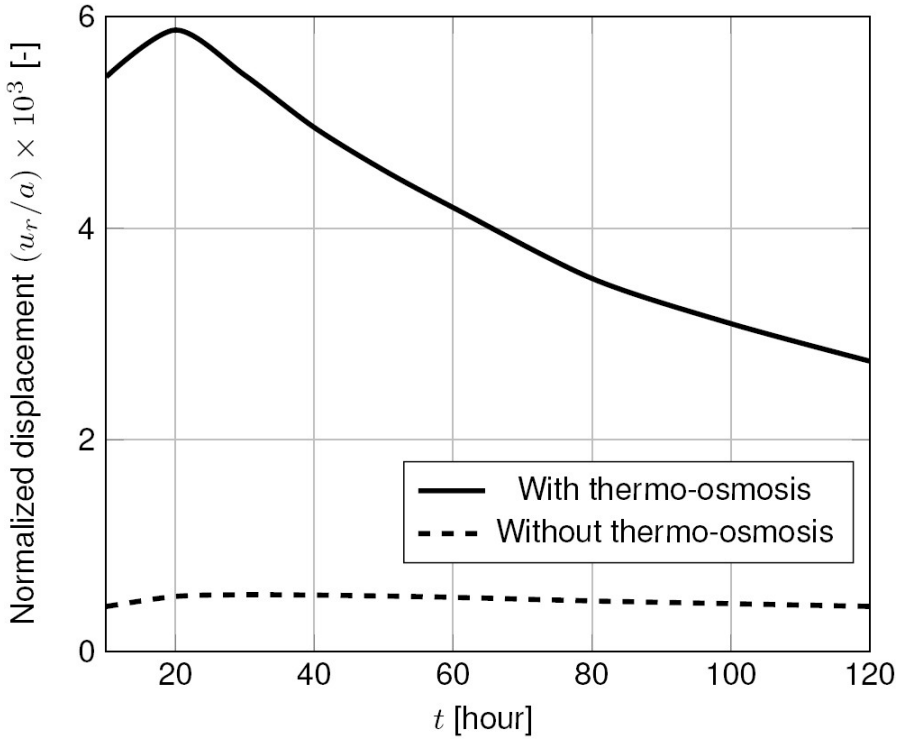

(b)

Figure 4.3: Displacement (a) along radius at time $t = 20$ hour (b) with time at $r/a = 1.5$

with the growth of displacement, and then declines with increasing r/a. When the ratio r/a continues increasing, the displacement tends to steady state shown in Figure 4.3a, but radial stresses tend to zero due to increasing radius r. At an observation point $r/a = 1.5$ as shown in Figure 4.4b, the compressive radial stresses will first increase and then dissipate gradually as time progresses, while the magnitude with thermo-osmosis effect is larger than the one without this effect.

Figures 4.5a and 4.5b show the distributions of thermally induced fluid flux (normalized by K_f). The fluid flux with thermo-osmosis effect is significantly greater than Darcy flux, i.e., without such effect. The difference of the two peak values is as great as two orders of magnitudes for this group of parameters in this study. Darcy flux is related with the gradient of pore pressure, its value should be minus with positive gradient of pore pressure within the domain $0 < r/a < 1.3$. in this region very close to the inner boundary, the pore water will expand under heating and thus flow out from the permeable boundary, so it results in the minus value for fluid flux. Fluid flux then tends to zero near $r/a = 1.3$ where the gradient of pore pressure equals to zero too. After this point, the value of fluid flux will gradually evolve from positive to zero with the increase of the negative gradient of pore pressure. If we take thermo-osmosis effect into consideration, the fluid flux is not only related with the gradient of pore pressure but also with the gradient of temperature based on Equation (4.9). And the gradient of temperature is always minus from Figure 6a which leads to the second term $-S_w \nabla \theta_f$ on the right hand of Equation (4.9) is always positive. For the clay, the permeability coefficient K_f is very low, that makes the ratio S_w/K_f relatively large, so the second term on the right hand of Equation (4.9) plays a dominant role in the distribution of fluid flux. That's why fluid flux with thermo-osmosis effect is always positive and greatly larger than Darcy flux.

Concluding up to now, the phenomenon of thermo-osmosis is significant in this type of materials, e.g., clay, limestone and granite, whose permeability coefficients are really very low. But in gravel, sand, loess and many other soils and rocks with large values of permeability, this phenomena is slight and can be neglected both in experimental and theoretical works.

Different heat transfer theories will result in different temperature fields, which will significantly affect thermally induced stress, pore pressure and so on. Temperatures generated from LTNE heat transfer and LTE heat transfer theories (normalized by θ_0) are plotted in Figures 4.6a and 4.6b. Their distributions are similar, i.e., all decrease gradually from the inner boundary to zero along radial direction. The similarity can be explained through Equations (4.20), (4.21) and (4.31) because they all observe the similar mathematical

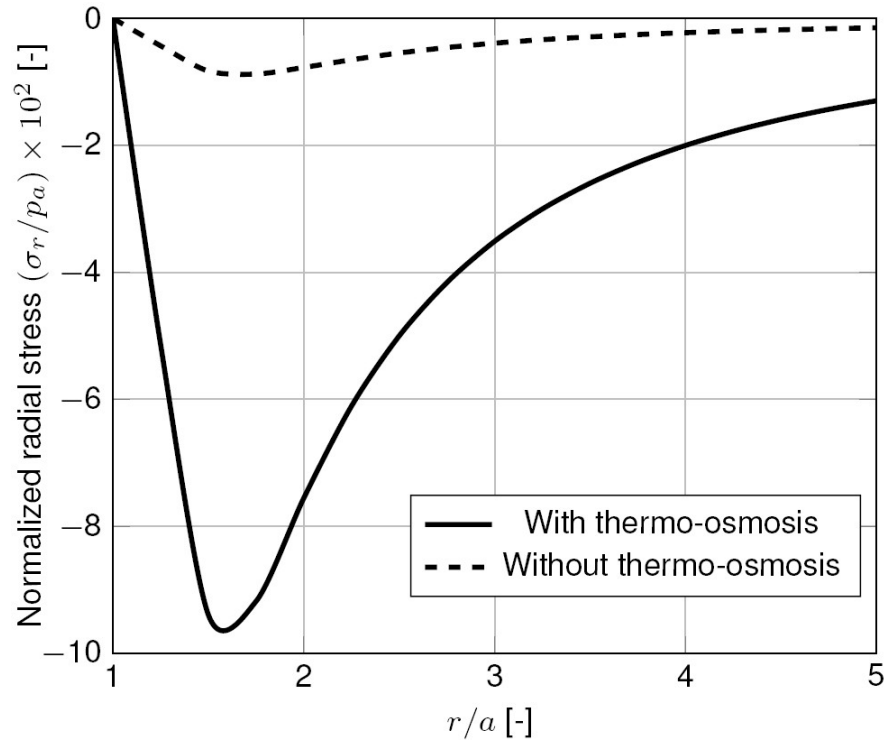

(a)

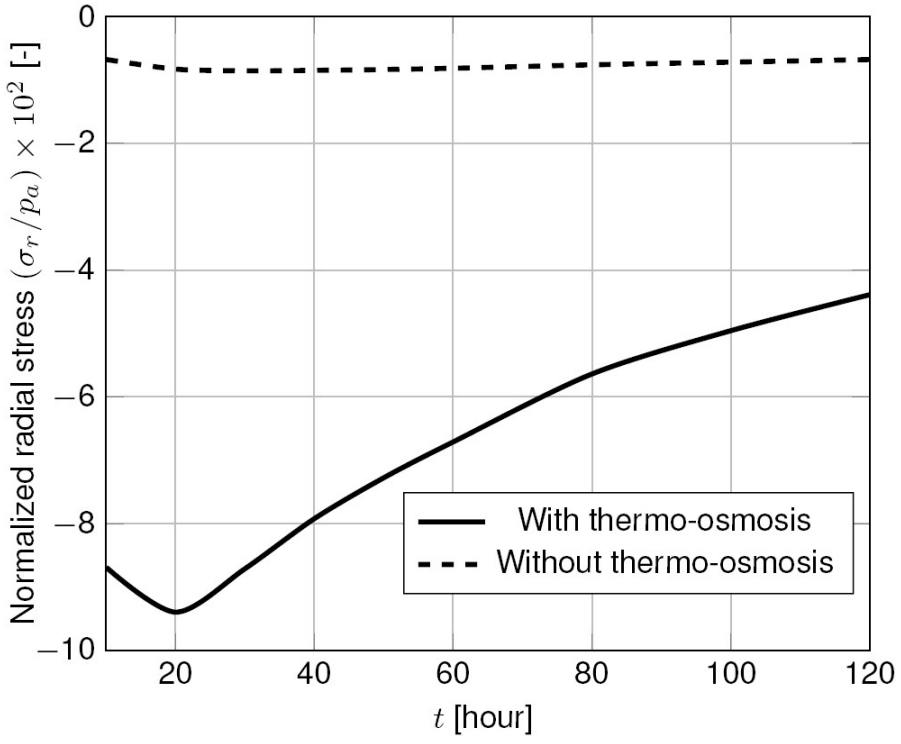

(b)

Figure 4.4: Radial stress (a) along radius at time $t = 20$ hour (b) with time at $r/a = 1.5$

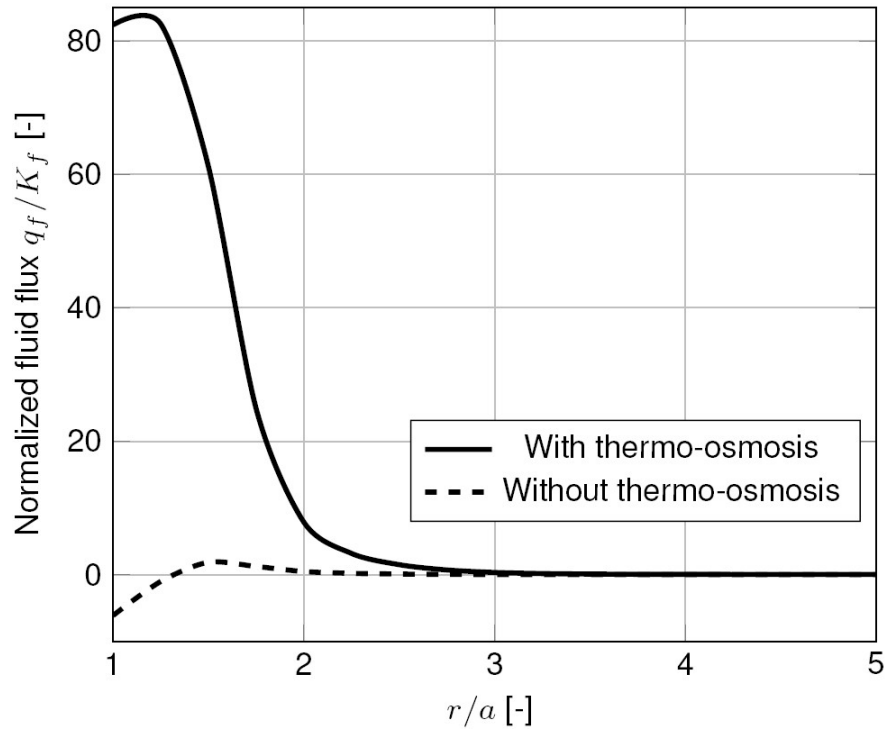

(a)

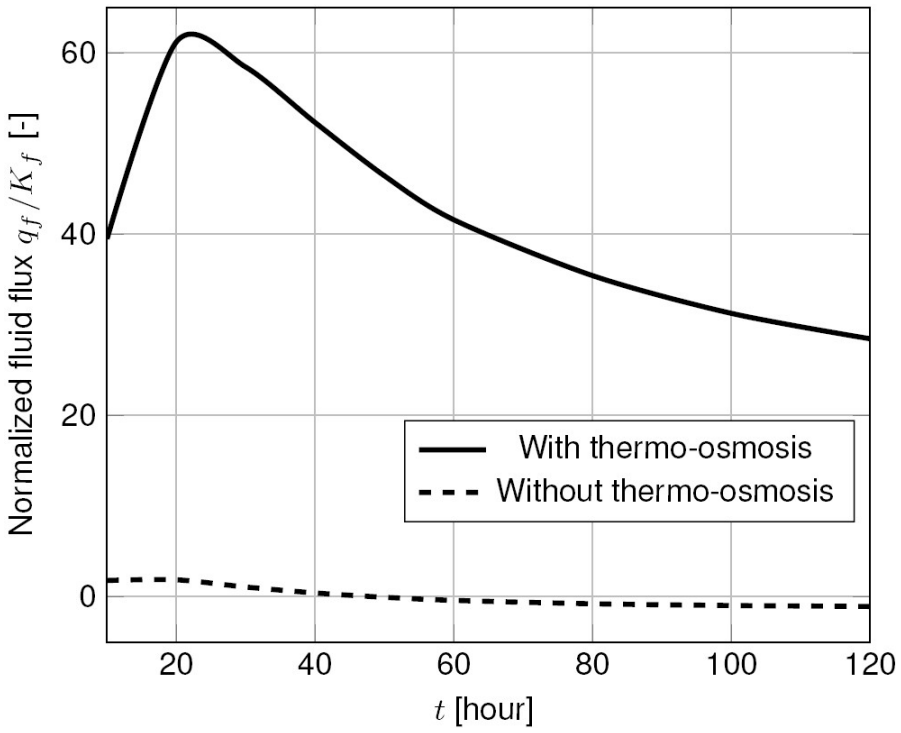

(b)

Figure 4.5: Fluid flux (a) along radius at time $t = 20$ hour (b) with time at $r/a = 1.5$

forms which relate with MacDonald function. As time progresses, all the temperatures will rise up due to heat transfer. In general, heat conductivity $k_s > k_f$ from Table 4.1, and the mixture heat conductivity k can be regarded as an average heat conductivity of the two phases expressed under Equation (4.31), that's why clay temperature is larger than fluid temperature, and the equilibrium temperature always lies between solid and fluid temperatures.

Take thermo-osmosis effect into consideration, the magnitudes of LTNE pore pressure, radial stress and displacement are larger than the corresponding LTE ones as shown in Figures 4.7–4.9, especially at the peak values. The peak value of LTNE fluid flux is also larger than that of LTE fluid flux as shown in Figure 4.10. Furthermore, if the coefficient of solid-fluid interface heat transfer h in Equation (4.11) and (4.12) is even more smaller the difference with temperatures is more obvious especially at initial time, and this difference could result in more significant differences in pore pressure, stress, displacement and fluid flux.

4.5 Conclusions

Thermo-poroelastic theory fulfilling LTNE is employed to investigate the quasi static response of temperatures, pore pressure, stress, displacement and fluid flux around a cylindrical borehole subjected to impact thermal and mechanical loadings in an infinite saturated porous medium. Analytical solutions are derived in Laplace transform space. A group of parameters for a typical clay used in nuclear waste storage are adopted in parameter study. Results fulfilling LTNE show that, with thermo-osmosis effect , the magnitudes of thermally induced pore pressure, stress, displacement and fluid flux are larger than those without this effect especially in the vicinity of the borehole. The difference of fluid flux is as greater as two to three orders of magnitudes in this study. Temperatures derived from LTNE heat transfer theory are different from that derived from LTE heat transfer theory. It is shown both from the analytical solutions and the parameter results that the LTE is a limit case of LTNE. These differences will result in differences in pore pressure, stress, displacement and fluid flux, especially when the coefficient of solid-fluid interface heat transfer is very small.

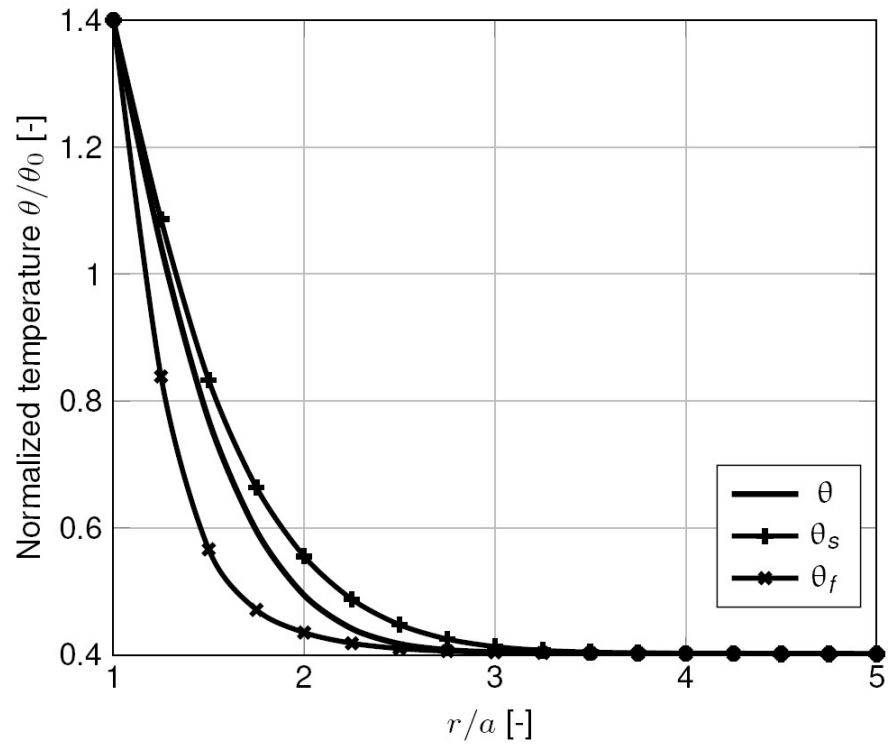

(a)

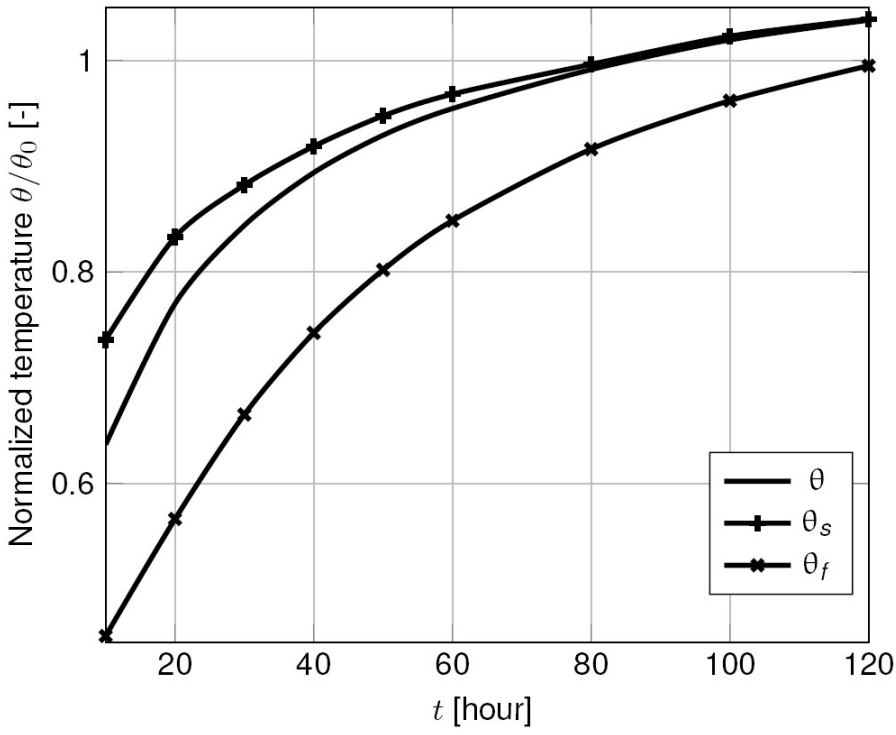

(b)

Figure 4.6: Temperature (a) along radius at time $t = 20$ hour (b) with time at $r/a = 1.5$

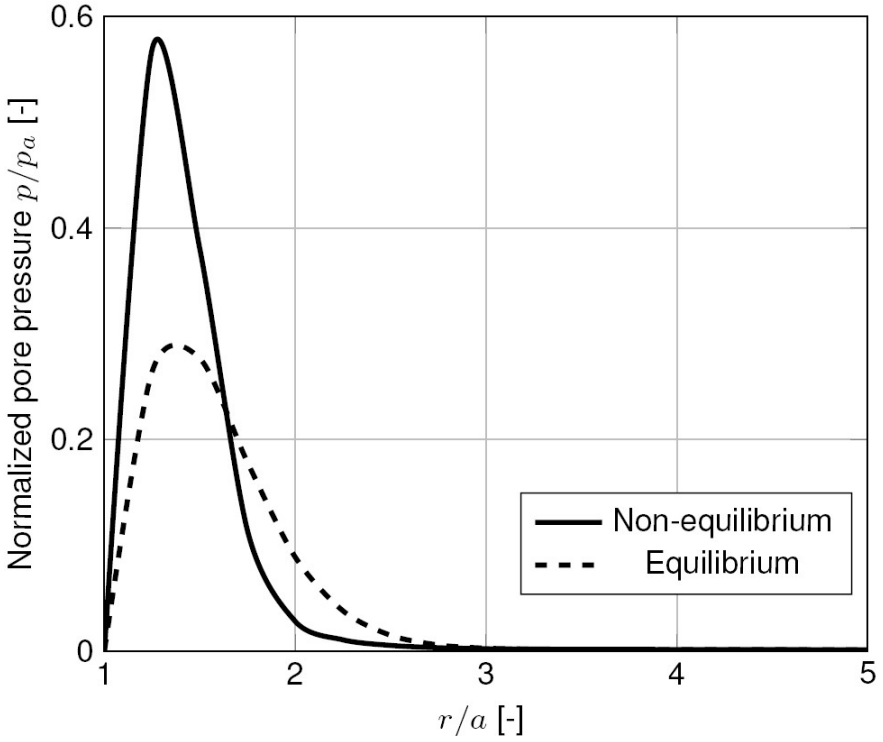

Figure 4.7: Pore pressure along radius at time $t = 20$ hour

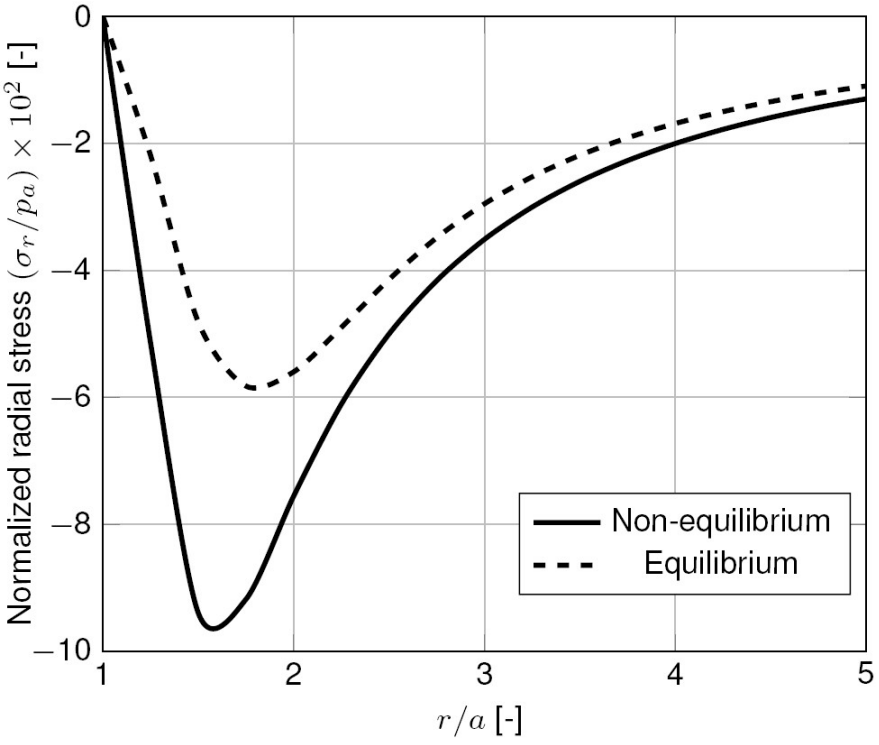

Figure 4.8: Displacement along radius at time $t = 20$ hour

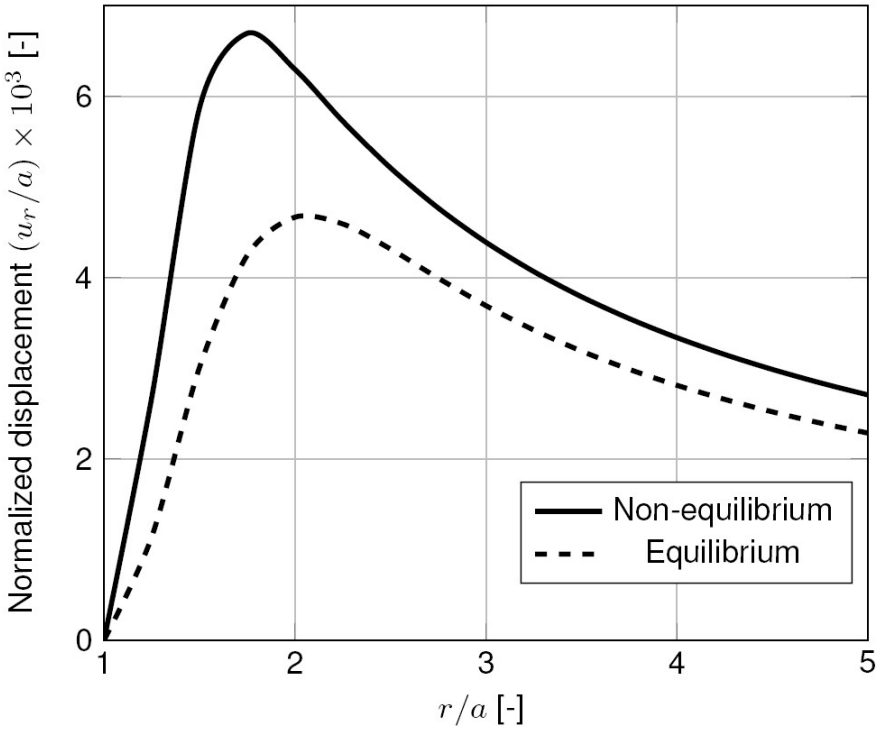

Figure 4.9: Stress along radius at time $t = 20$ hour

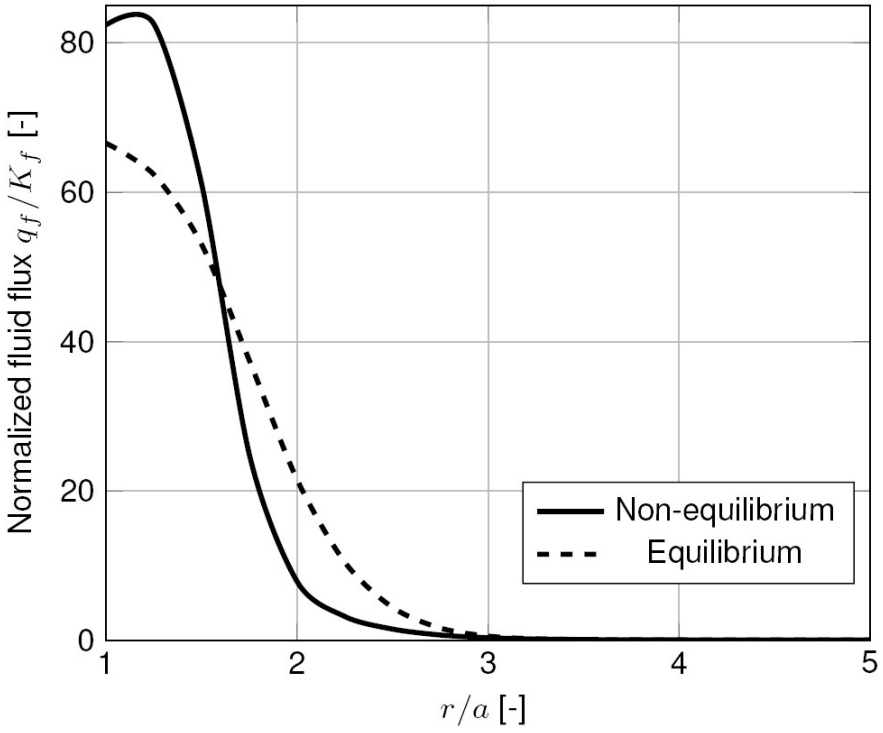

Figure 4.10: Fluid flux along radius at time $t = 20$ hour

5 Analysis of Multilayered Thermoelastic Media

5.1 Introduction

Multilayered structures widely exist in nature and are relevant to different engineering problems. For instance, the geological structure may be considered for simplicity as multilayered half space (Kennett 2009). There are also various manmade materials or structures that can be regarded as multilayered structures for modelling applications.

More often the multilayered structure is assumed to be composed of homogeneous parallel layers. Several approaches exist to solve the static and dynamic problems for multilayered structures. The most common numerical methods are FEM and BEM. As an alternative one can consider the finite layer method (FLM) (Small & Booker 1984, 1986*a*) and the analytical layer-element method (ALEM) (Ai et al. 2015*b*; Ai & Wang 2015; Ai et al. 2015*a*). However, both methods require an assembling of a stiffness matrix whose size is proportional to the number of layers N and thus the methods are becoming inefficient if the number N is large (Pan 1989*b*, 1997). One of the best methods to treat problems is the propagator matrix method (PMM) (Singh 1970).

In this chapter, we will adopt the generalized propagator matrix method to analyze of temperature-induced deformations in multilayered thermoelastic media. First will be presented the governing equations for a 3D formulation of the problem for the response of multilayered thermoelastic media subjected to surface loads and containing a heat sources. Second, a set of vector surface harmonics (Kennett 2009) will be introduced, followed by application of PMM with the aid of continuity conditions to derive the general solution for temperature, displacements and stress. Moreover, the numerical instability problem in the conventional PMM algorithm will be discussed and resolved in a special generalization technique. Next, a numerical strategy of high-order adaptive Gaussian quadrature method with continued fraction expansions (Chave 1983) will be employed to approximate the

integral–form solution expressed in terms of semi-infinite Hankel-type integrals. Finally, the solution will be firstly applied to treat the problem of repository for heat-emitting high-level nuclear waste (HLW) in a geological formation. The temperature-induced deformations, stresses and the temperature distribution are investigated and compared with relevant previous results. The influence of source shape on the thermoelastic responses is also discussed.

5.2 Governing equations

5.2.1 Governing equations for homogeneous thermoelastic media

In this study we consider the temperature distribution in a deformable body and therefore the corresponding model evokes solution of a coupled thermo-mechanical problem. To simplify the problem we assume that the thermal solution is independent of the mechanical solution, although the thermoelastic coupling effect actually exists (Rundle 1982). In case the material is homogeneous and isotropic and the heat flow obeys Fourier's law the relation between the heat flux and the gradient of the excess temperature reads:

$$\mathbf{q}_H = -k\nabla\theta \tag{5.1}$$

where θ is the excess temperature, $\mathbf{q}_H$ is the heat flux, k is heat conductivity. Combining Equation (5.1) with the conservation of energy equation leads to:

$$\rho c\dot{\theta} = k\nabla^2\theta + q \tag{5.2}$$

where ρ is density of the material, c is the specific heat capacity, q denotes the heat generated by the heat source per time and volume. The Duhamel-Neumann relations establish the relationships between the states of stress, strain and temperature, and can be written as follows:

$$\boldsymbol{\sigma} = 2G\boldsymbol{\varepsilon} + \lambda\varepsilon_v\,\mathbf{I} - 3K\alpha\theta\mathbf{I} \tag{5.3}$$

where $\boldsymbol{\sigma}$ and $\boldsymbol{\varepsilon}$ are stress and strain tensors, respectively, ε_v is the volumetric strain, G and λ are Lame coefficients, $K = (3\lambda + 2G)/3$ is the bulk modulus, α is the linear thermal expansion coefficient, and $\mathbf{I}$ denotes the second order identity tensor. The strain-displacement relations are:

$$\boldsymbol{\varepsilon} = [\nabla\mathbf{u} + (\nabla\mathbf{u})^T]/2 \tag{5.4}$$

where $\mathbf{u}$ is displacement vector and the superscript $()^T$ represents transpose vector or matrix. The static equilibrium, with the body force being neglected, is given by

$$\nabla \cdot \boldsymbol{\sigma} = 0 \tag{5.5}$$

Suppose that at the surface of the model domain ($z = 0$) a traction vector $\mathbf{T}_0^{\mathbf{e}_z}$ and temperature θ_0 are applied, that means

$$\sigma_{zj}\boldsymbol{e}_j|_{z=0} = \mathbf{T}_0^{\mathbf{e}_z}, \quad \theta|_{z=0} = \theta_0 \tag{5.6}$$

where $\boldsymbol{e}_j, \quad j = 1, 2, 3$ or $j = z, \varphi, r$ are the three orthogonal unit vectors in Cartesian or cylindrical coordinate systems. If the medium fills the half space, infinite boundary conditions can be written as

$$\lim_{z\to\infty}(\mathbf{u}, \theta) \to 0 \tag{5.7}$$

If the medium is placed in a finite in z–direction domain and the bottom is considered to be fixed, e.g. at z_n, the boundary conditions are:

$$\mathbf{u}|_{z=z_n} = 0, \quad \frac{\partial\theta}{\partial z}|_{z=z_n} = 0 \tag{5.8}$$

Furthermore, if a multilayered structure is considered, the boundary conditions at the welded contact interface are the continuity of displacement and temperature conditions that hold at each interface z_i:

$$\mathbf{u}|_{z=z_i+} = \mathbf{u}|_{z=z_i-} \qquad \theta|_{z=z_i+} = \theta|_{z=z_i-} \tag{5.9}$$

5.2.2 Vector surface harmonics

Now we introduce a set of vector surface harmonics in 3D cylindrical coordinate system, defined as (Kennett 2009):

$$\mathbf{L}_\xi^m(r, \varphi) = S_\xi^m \mathbf{e}_z \tag{5.10}$$

$$\mathbf{M}_\xi^m(r, \varphi) = \frac{\partial S_\xi^m}{\partial r}\mathbf{e}_r + \frac{\partial S_\xi^m}{r\partial\varphi}\mathbf{e}_\varphi \tag{5.11}$$

$$\mathbf{N}_\xi^m(r, \varphi) = \frac{\partial S_\xi^m}{r\partial\varphi}\mathbf{e}_r - \frac{\partial S_\xi^m}{\partial r}\mathbf{e}_\varphi \tag{5.12}$$

where $(\mathbf{e}_r, \mathbf{e}_\varphi, \mathbf{e}_z)$ are orthogonal unit vectors in cylindrical coordinate system, and the scalar functions S_ξ^m are defined as:

$$S_\xi^m(r, \varphi) = J_m(\xi r)e^{im\varphi}/\sqrt{2\pi} \quad m = 0, \pm1, \pm2, ... \tag{5.13}$$

These functions satisfy the Helmholtz equation:

$$\nabla^2 S_\xi^m + \eta^2 S_\xi^m = 0 \tag{5.14}$$

where η is the wavenumber, and $J_m(\xi r)$ denotes the m-th order Bessel function of the first kind. The vector surface harmonics in cylindrical coordinate system form an orthogonal and complete space and any integrable scalar and vector function can be expressed in terms of the vector surface harmonics. Thus, the displacement vector, traction vector at the surface, temperature and the heat flux in z-direction $q_{Hz} = \theta_{,z}$ can be expanded in the following way:

$$\hat{\mathbf{u}}(r,\varphi,z,s) = \hat{u}_r\mathbf{e}_r + \hat{u}_\varphi\mathbf{e}_\varphi + \hat{u}_z\mathbf{e}_z = \sum_m \int_0^\infty [\hat{U}_{\xi L}^m(z,s)\mathbf{L}_\xi^m + \hat{U}_{\xi M}^m(z,s)\mathbf{M}_\xi^m + \hat{U}_{\xi N}^m(z,s)\mathbf{N}_\xi^m]\xi \mathrm{d}\xi \tag{5.15}$$

$$\hat{\mathbf{T}}^{\mathbf{e}_z}(r,\varphi,z,s) = \hat{\sigma}_{rz}\mathbf{e}_r + \hat{\sigma}_{\varphi z}\mathbf{e}_\varphi + \hat{\sigma}_z\mathbf{e}_z = \sum_m \int_0^\infty [\hat{T}_{\xi L}^m(z,s)\mathbf{L}_\xi^m + \hat{T}_{\xi M}^m(z,s)\mathbf{M}_\xi^m + \hat{T}_{\xi N}^m(z,s)\mathbf{N}_\xi^m]\xi \mathrm{d}\xi \tag{5.16}$$

$$\hat{\theta}(r,\varphi,z,s) = \sum_m \int_0^\infty \hat{\Theta}_\xi^m(z,s) S_\xi^m \xi \mathrm{d}\xi \tag{5.17}$$

$$\hat{q}_{Hz}(r,\varphi,z,s) = \sum_m \int_0^\infty \hat{Q}_{\xi H}^m(z,s) S_\xi^m \xi \mathrm{d}\xi \tag{5.18}$$

Furthermore, $\hat{q}$, $\hat{\mathbf{T}}_0^{\mathbf{e}_z}(r,\varphi,s)$ and $\hat{\theta}_0(r,\varphi,s)$ are given as:

$$\hat{q}(r,\varphi,z,s) = \sum_m \int_0^\infty \hat{\mathcal{Q}}_\xi^m(z,s) S_\xi^m \xi \mathrm{d}\xi \tag{5.19}$$

$$\hat{\mathbf{T}}_0^{\mathbf{e}_z}(r,\varphi,s) = \sum_m \int_0^\infty [\hat{T}_{\xi L0}^m(s)\mathbf{L}_\xi^m + \hat{T}_{\xi M0}^m(s)\mathbf{M}_\xi^m + \hat{T}_{\xi N0}^m(s)\mathbf{N}_\xi^m]\xi \mathrm{d}\xi \tag{5.20}$$

$$\hat{\theta}_0(r,\varphi,s) = \sum_m \int_0^\infty \hat{\Theta}_{\xi 0}^m(s) S_\xi^m \xi \mathrm{d}\xi \tag{5.21}$$

where the functions with hat are defined as:

$$\hat{f}(r,\varphi,z,s) = \int_0^\infty e^{-st} f(r,\varphi,z,t)\mathrm{d}t \tag{5.22}$$

The complex variable s implies that Laplace transform method is employed to suppress the time factor t.

Substituting Equations (5.15)–(5.18) into Equations (5.1)–(5.5), after considerable algebraic manipulation, we can obtain the following systems of ordinary differential equations

for the expansion coefficients in Equations (5.15)–(5.18):

$$\frac{\mathrm{d}}{\mathrm{d}z}\begin{bmatrix}\hat{U}^m_{\xi L}\\ \hat{U}^m_{\xi M}\\ \hat{T}^m_{\xi L}\\ \hat{T}^m_{\xi M}\\ \hat{\Theta}^m_{\xi}\\ \hat{Q}^m_{\xi H}\end{bmatrix} = \begin{bmatrix}0 & \frac{\lambda}{M}\eta^2 & \frac{1}{M} & 0 & \frac{\alpha_0}{M} & 0\\ -1 & 0 & 0 & \frac{1}{\mu} & 0 & 0\\ 0 & 0 & 0 & \eta^2 & 0 & 0\\ 0 & (M-\frac{\lambda^2}{M})\eta^2 & -\frac{\lambda}{M} & 0 & \alpha_0(1-\frac{\lambda}{M}) & 0\\ 0 & 0 & 0 & 0 & 0 & -\frac{1}{k}\\ 0 & 0 & 0 & 0 & -k(\frac{s}{\kappa}+\eta^2) & 0\end{bmatrix}\begin{bmatrix}\hat{U}^m_{\xi L}\\ \hat{U}^m_{\xi M}\\ \hat{T}^m_{\xi L}\\ \hat{T}^m_{\xi M}\\ \hat{\Theta}^m_{\xi}\\ \hat{Q}^m_{\xi H}\end{bmatrix} \tag{5.23}$$

In a compact form it reads:

$$\frac{\mathrm{d}}{\mathrm{d}z}\mathbf{f} = \mathbf{M}_1\mathbf{f} \tag{5.24}$$

where $M = \lambda + 2G$, $\alpha_0 = K\alpha$, $\kappa = k/(\rho c)$ is the heat diffusivity. The vector f is defined as:

$$\mathbf{f} = [\hat{U}^m_{\xi L}, \hat{U}^m_{\xi M}, \hat{T}^m_{\xi L}, \hat{T}^m_{\xi M}, \hat{\Theta}^m_{\xi}, \hat{Q}^m_{\xi H}]^T \tag{5.25}$$

Finally, $\mathbf{M}_1$ is the notation for the corresponding matrix in Equation (5.23).

5.2.3 Propagator matrix method

In a homogeneous media, the general solution of Equation (5.24) is

$$\mathbf{f}(z) = e^{\mathbf{M}_1(z-z^\star)}\mathbf{f}(z^\star) = \mathbf{P}^z_{z^\star}\mathbf{f}(z^\star) \tag{5.26}$$

where the matrix $\mathbf{P}^z_{z^\star} = e^{\mathbf{M}_1(z-z^\star)}$ is called propagator because it propagates the solutions at $z^\star$ to z. The matrix $\mathbf{M}_1$ should be diagonalized by a similarity transformation in order to get the propagator matrix:

$$\mathbf{P}^z_{z^\star} = \mathbf{E}e^{\mathcal{M}_1(z-z^\star)}\mathbf{E}^{-1} \tag{5.27}$$

where $\mathcal{M}_1$ is the diagonal matrix composed of the eigenvalues of $\mathbf{M}_1$, $\mathbf{E}$ is the matrix containing the corresponding eigenvectors. Equation (5.26) can also be written as

$$\mathbf{f}(z) = \mathbf{G}^z_{z^\star}\mathbf{V}_1(z^\star)\ , \tag{5.28}$$

where $\mathbf{G}^z_{z^\star} = \mathbf{E}e^{\mathcal{M}_1(z-z^\star)}$, $\mathbf{V}_1(z^\star) = \mathbf{E}^{-1}\mathbf{f}(z^\star)$. $\mathbf{f}(z^\star)$ and $\mathbf{V}_1(z^\star)$ are determined by the boundary conditions if all the variables at $z^\star$ are specified. In addition we have:

$$\mathbf{f}(z^\star) = e^{\mathbf{M}_1(z^\star-z)}\mathbf{f}(z) = \mathbf{P}^{z^\star}_z\mathbf{f}(z) \tag{5.29}$$

$$\mathbf{P}_{z^\star}^{z} = (\mathbf{P}_{z}^{z^\star})^{-1} \tag{5.30}$$

Equations (5.29) and (5.30) reveal that the solutions can also propagate in the converse direction with a suitable choice of the propagator matrix. An instructive approach is adopted here to obtain the propagator matrix. Note that $\mathbf{M}_1$ can be taken as a 6×6 triangular block matrix partitioned into 4×4 submatrix $\mathbf{A}$ for the purely elastic behavior, 2×2 submatrix $\mathbf{B}$ for the heat conduction behavior and a 4×2 submatrix $\mathbf{C}$ describing the coupled effect

$$\mathbf{M}_1 = \begin{bmatrix} \mathbf{A} & \mathbf{C} \\ 0 & \mathbf{B} \end{bmatrix} \tag{5.31}$$

Based on the properties of block matrix, the determinant of matrix $\mathbf{M}_1$ is equal to the multiplication of those of the submatrices on the main diagonal. The eigenvalues and corresponding eigenvectors are simply the combination of those of the submatrices. The procedure how to get the eigenvalues and eigenvectors $\mathbf{M}_1$ is shown in appendix A in details.

In the previous section we obtained the propagation relation for a homogeneous media. Hereafter we consider a semi-infinite thermoelastic medium consisting of n parallel homogeneous layers as depicted in Figure 5.1. The origin of the coordinate system is placed at the surface with the z-axis drawn down into the medium and $z_0 = 0$. The i-th layer is of thickness h_i, and bounded by the interface $z = z_{i-1}$ and $z = z_i$. $\mathbf{P}_{z_i}^{z_{i-1}}$ denotes the propagator matrix in the i-th homogeneous layer. Using Equations (5.29) and (5.9) successively, the global propagation relation can be written as:

$$\mathbf{f}(z_0) = \mathbf{P}_{z_n}^{z_0} \mathbf{f}(z_n) \tag{5.32}$$

where $\mathbf{P}_{z_n}^{z_0} = \mathbf{P}_{z_1}^{z_0} \cdot \mathbf{P}_{z_2}^{z_1} \cdots \mathbf{P}_{z_{n-1}}^{z_{n-2}} \cdot \mathbf{P}_{z_n}^{z_{n-1}}$ is the global propagator matrix which describes how solution propagates from $z = z_n$ through all the layers up to $z = z_0$.

5.2.4 Equivalent sources

The existence of a buried source will invoke discontinuity at the source level. Suppose that there are a traction $\hat{\mathbf{T}}^{\mathbf{e}_z}$ and a heat source $\hat{q}$ buried at depth $z = z_j$ which is just on the interface of j-th and $(j+1)$-th layers. $\hat{\mathbf{T}}^{\mathbf{e}_z}$ and $\hat{q}$ is expanded in vector surface harmonics:

$$\Delta\mathbf{f} = [\Delta\hat{U}_{\xi L}^m, \Delta\hat{U}_{\xi M}^m, \Delta\hat{T}_{\xi L}^m, \Delta\hat{T}_{\xi M}^m, \Delta\hat{\Theta}_{\xi}^m, \Delta\hat{Q}_{\xi H}^m]^T = \mathbf{f}(z_j+) - \mathbf{f}(z_j-) \tag{5.33}$$

together with the following two relations for the propagator:

$$\mathbf{f}(z_0) = \mathbf{P}_{z_j}^{z_0} \cdot \mathbf{f}(z_j-) \tag{5.34}$$

$$\mathbf{f}(z_j+) = \mathbf{P}_{z_n}^{z_j} \cdot \mathbf{f}(z_n) \tag{5.35}$$

By substituting Equations (5.33) and (5.35) into Equation (5.34), we have

$$\mathbf{f}(z_0) = \mathbf{P}_{z_n}^{z_0} \cdot \mathbf{f}(z_n) - \mathbf{P}_{z_j}^{z_0} \cdot \Delta\mathbf{f} \tag{5.36}$$

where $z_j\pm$ denote the depths above/below the source level. For the source type there are in literature examples for a point force (Kennett & Kerry 1979; Kennett 2009), fluid injection (Pan 1999; Zheng et al. 2013*a*) and displacement dislocation (Pan 1989*a*). The expressions for the expansion coefficients $\Delta\hat{U}_{\xi L}^m$, $\Delta\hat{U}_{\xi M}^m$, $\Delta\hat{T}_{\xi L}^m$ and $\Delta\hat{T}_{\xi M}^m$ can be found elsewhere, e.g. in the above cited papers. However, in our case the temperature field is taken into account, thus a source function for heat source defined in Equation (5.2) has to be defined. We consider a point heat source in cylindrical coordinate system as

$$\hat{q} = \hat{Q}(s) \cdot \frac{\delta(r)\delta(z - z_j)}{\pi r} \tag{5.37}$$

$\hat{Q}(s)$ represents a frequency dependent factor, δ denotes Dirac delta function. Expanding $\hat{q}$ in the vector surface harmonics as in Equation (5.19) and then substituting the expansion coefficients into Equations (5.2) and (5.1), we find

$$\hat{\mathcal{Q}}_\xi^m = \hat{Q}(s)\delta(z - z_j)/\sqrt{2\pi} \tag{5.38}$$

$$\Delta\hat{Q}_{\xi H}^m = \hat{Q}(s)/\sqrt{2\pi}, \quad \Delta\hat{\Theta}_\xi^m = 0 \tag{5.39}$$

In additional, if a circular-shaped heat source with the same $\hat{Q}(s)$ is taken into account, the corresponding equations are:

$$\hat{q} = \hat{Q}(s) \cdot \Pi_{r_0}(r)\delta(z - z_j) \tag{5.40}$$

$$\hat{\mathcal{Q}}_\xi^m = \sqrt{2\pi}\hat{Q}(s)\delta(z - z_j)r_0 J_1(r_0\xi)/\xi \tag{5.41}$$

$$\Delta\hat{Q}_{\xi H}^m = \sqrt{2\pi}\hat{Q}(s)r_0 J_1(r_0\xi)/\xi, \quad \Delta\hat{\Theta}_\xi^m = 0 \tag{5.42}$$

where $\Pi_{r_0}(r)$ is a rectangular function equal to 1 for $0 \leq r \leq r_0$ and 0 otherwise, r_0 is the radius of the source. Thus the propagation relations for a domain with a buried source are defined, however the unknown coefficients for $\mathbf{f}(z_0)$ and $\mathbf{f}(z_n)$ have to be determined by the boundary conditions.

5.3 Analytical solutions for fixed and infinite boundary conditions

We consider two cases for finding the general solution.

Case 1: the model consists of n parallel layers overlaying a homogeneous half space. In this case, Equation (5.36) can be rewritten as:

$$\mathbf{f}(z_0) = \mathbf{P}_{z_n}^{z_0} \cdot \mathbf{G}^{z_n}\mathbf{V}_1 - \mathbf{P}_{z_j}^{z_0} \cdot \Delta\mathbf{f} \tag{5.43}$$

where $\mathbf{V}_1 = [v_1, v_2, v_3, v_4, v_5, v_6]$ is the vector of unknowns. According to the conditions (5.7), $v_1 = v_3 = v_5 = 0$ because these members of $\mathbf{V}_1$ are related to the exponentially increasing terms Singh (1986). The left three coefficients v_2, v_4 and v_6 are determined by the boundary conditions (5.6) together with the expressions (5.20) and (5.21):

$$\hat{T}_{\xi L}^m(0) = \hat{T}_{\xi L0}^m = [\mathbf{P}_{z_n}^{z_0} \cdot \mathbf{G}^{z_n}]_{32} \cdot v_2 + [\mathbf{P}_{z_n}^{z_0} \cdot \mathbf{G}^{z_n}]_{34} \cdot v_4 + [\mathbf{P}_{z_n}^{z_0} \cdot \mathbf{G}^{z_n}]_{36} \cdot v_6 - [\mathbf{P}_{z_j}^{z_0} \cdot \Delta\mathbf{f}]_{31} \tag{5.44}$$

$$\hat{T}_{\xi M}^m(0) = \hat{T}_{\xi M0}^m = [\mathbf{P}_{z_n}^{z_0} \cdot \mathbf{G}^{z_n}]_{42} \cdot v_2 + [\mathbf{P}_{z_n}^{z_0} \cdot \mathbf{G}^{z_n}]_{44} \cdot v_4 + [\mathbf{P}_{z_n}^{z_0} \cdot \mathbf{G}^{z_n}]_{46} \cdot v_6 - [\mathbf{P}_{z_j}^{z_0} \cdot \Delta\mathbf{f}]_{41} \tag{5.45}$$

$$\hat{\Theta}_{\xi}^m(0) = \hat{\Theta}_{\xi 0}^m = [\mathbf{P}_{z_n}^{z_0} \cdot \mathbf{G}^{z_n}]_{52} \cdot v_2 + [\mathbf{P}_{z_n}^{z_0} \cdot \mathbf{G}^{z_n}]_{54} \cdot v_4 + [\mathbf{P}_{z_n}^{z_0} \cdot \mathbf{G}^{z_n}]_{56} \cdot v_6 - [\mathbf{P}_{z_j}^{z_0} \cdot \Delta\mathbf{f}]_{51} \tag{5.46}$$

Case 2: the model comprises of n parallel layers and is finite in z direction. Based on the boundary Equations (5.6) and (5.8), the three unknown coefficients $\hat{T}_{\xi R}^m$, $\hat{T}_{\xi S}^m$ and $\hat{\Theta}_{\xi}^m$ in $\mathbf{f}(z_n)$ are determined by the following three equations:

$$\hat{T}_{\xi L}^m(0) = \hat{T}_{\xi L0}^m = [\mathbf{P}_{z_n}^{z_0}]_{33} \cdot \hat{T}_{\xi L}^m(z_n) + [\mathbf{P}_{z_n}^{z_0}]_{34} \cdot \hat{T}_{\xi M}^m(z_n) + [\mathbf{P}_{z_n}^{z_0}]_{35} \cdot \hat{\Theta}_{\xi}^m(z_n) - [\mathbf{P}_{z_j}^{z_0} \cdot \Delta\mathbf{f}]_{31} \tag{5.47}$$

$$\hat{T}_{\xi M}^m(0) = \hat{T}_{\xi M0}^m = [\mathbf{P}_{z_n}^{z_0}]_{43} \cdot \hat{T}_{\xi L}^m(z_n) + [\mathbf{P}_{z_n}^{z_0}]_{44} \cdot \hat{T}_{\xi M}^m(z_n) + [\mathbf{P}_{z_n}^{z_0}]_{45} \cdot \hat{\Theta}_{\xi}^m(z_n) - [\mathbf{P}_{z_j}^{z_0} \cdot \Delta\mathbf{f}]_{41} \tag{5.48}$$

$$\hat{\Theta}_{\xi}^m(0) = \hat{\Theta}_{\xi 0}^m = [\mathbf{P}_{z_n}^{z_0}]_{53} \cdot \hat{T}_{\xi L}^m(z_n) + [\mathbf{P}_{z_n}^{z_0}]_{54} \cdot \hat{T}_{\xi M}^m(z_n) + [\mathbf{P}_{z_n}^{z_0}]_{55} \cdot \hat{\Theta}_{\xi}^m(z_n) - [\mathbf{P}_{z_j}^{z_0} \cdot \Delta\mathbf{f}]_{51} \tag{5.49}$$

After determination of all the unknowns, we can write the expressions for the expansion coefficients. Thus, for case 1 we have

$$\mathbf{f}(z) = \mathbf{P}_{z_n}^{z} \cdot \mathbf{G}^{z_n}\mathbf{V}_1 - \mathbf{P}_{z_j}^{z} \cdot \Delta\mathbf{f} \quad z \leq z_j \tag{5.50}$$

$$\mathbf{f}(z) = \mathbf{P}_{z_n}^{z} \cdot \mathbf{G}^{z_n}\mathbf{V}_1 \quad z > z_j \tag{5.51}$$

While for for case 2 we obtain:

$$\mathbf{f}(z) = \mathbf{P}_{z_n}^{z} \cdot \mathbf{f}(z_n) - \mathbf{P}_{z_j}^{z} \cdot \Delta\mathbf{f} \quad z \leq z_j \tag{5.52}$$

$$\mathbf{f}(z) = \mathbf{P}_{z_n}^{z} \cdot \mathbf{f}(z_n) \quad z > z_j \tag{5.53}$$

Substituting Equations (5.50)- (5.53) into Equations (5.15)- (5.18), and applying Laplace inversion transform, we can get the solution in t–time domain for displacement vector, stress tensor, temperature and heat flux.

As mentioned earlier, the loss-of-precision problem will arise if the number and thickness of the layers are large. Let us consider as an example case 1. It is clear that each element in the propagator matrix $\mathbf{P}_{z_i}^{z_{i-1}}$ is proportional to $e^{(\zeta_1+\zeta_5)h_i}$ that increases exponentially. We factor out $e^{(\zeta_1+\zeta_5)h_i}$ from the matrix $\mathbf{P}_{z_i}^{z_{i-1}}$, thus a new matrix $\mathbf{P}_{z_i}^{z_{i-1}\star}$ is obtained:

$$\mathbf{P}_{z_i}^{z_{i-1}} = e^{(\zeta_1+\zeta_5)h_i}\mathbf{P}_{z_i}^{z_{i-1}*} \tag{5.54}$$

Equations (5.50) and (5.51) can be rewritten, respectively, as

$$\mathbf{f}(z) = e^{-(z-z_n)}\mathbf{P}_{z_n}^{z*}\cdot\mathbf{G}^{z_n}\mathbf{V}_1 - e^{-(z-z_j)}\mathbf{P}_{z_j}^{z*}\cdot\Delta\mathbf{f} \quad z \le z_j \tag{5.55}$$

$$\mathbf{f}(z) = e^{-(z-z_n)}\mathbf{P}_{z_n}^{z*}\cdot\mathbf{G}^{z_n}\mathbf{V}_1 \quad z > z_j \tag{5.56}$$

It is to point out that because all the matrices in the above equation are exponentially decaying, this fact together with the normalization technique will efficiently prevent the occurring of the loss-of-precision.

5.4 Parameter study

The explicit solution is expressed in terms of semi-infinite Hankel integrals in the form:

$$\hat{f}_m(r,z,s) = \int_0^\infty \hat{\mathcal{F}}_m(\xi,z,s)J_m(r\xi)\xi\mathrm{d}\xi \tag{5.57}$$

Chave (1983) developed a method that comprises of a high order adaptive algorithm of quadratures and continued fraction expansion to accurately evaluate the Hankel transform in Equation (5.57). This algorithm applies numerical quadrature to the evaluation of a sequence of partial integration terms as follows:

$$\int_0^\infty \hat{\mathcal{F}}_m(\xi,z,s)J_m(r\xi)\mathrm{d}\xi = \sum_{i=0}^{I}\int_{\xi_i}^{\xi_{i+1}} \hat{\mathcal{F}}_m(\xi,z,s)J_m(r\xi)\mathrm{d}\xi \tag{5.58}$$

where $\xi_0 = 0$, $\xi_i\,(i = 1,2,3,...I)$ is the i-th zero of $J_m(r\xi)$. For each partial integration term, the N-node Gaussian quadrature algorithm is applied to approximate the value of the integral:

$$\int_{\xi_i}^{\xi_{i+1}} \hat{\mathcal{F}}_m(\xi,z,s)J_m(r\xi)\mathrm{d}\xi = \frac{\xi_{i+1}-\xi_i}{2}\sum_{j=1}^{J} w_j\hat{\mathcal{F}}_m(\bar{\Xi}_j,z,s)J_m(r\bar{\Xi}_j) \tag{5.59}$$

where $\bar{\Xi}_j = \frac{\xi_{i+1}-\xi_i}{2}\Xi_j + \frac{\xi_{i+1}+\xi_i}{2}$, Ξ_j and w_j are Gaussian node and corresponding weight, respectively. The method applied to the numerical inverse Laplace transform is the Crump method (Crump 1976), and it gives as a result the solution in time domain:

$$\begin{aligned} f_m(r,z,t) =& \frac{2e^{s_0 t}}{t_0}\{-\frac{1}{2}\Re(\hat{f}_m(r,z,s_0)) + \sum_{k_0=0}^{K_0}(\Re(\hat{f}_m(r,z,s_0+in\frac{2\pi}{t_0}))\cos k_0\frac{2\pi}{t_0}t \\ & - \Im(\hat{f}_m(r,z,s_0+in\frac{2\pi}{t_0}))\sin k_0\frac{2\pi}{t_0}t)\} \end{aligned} \tag{5.60}$$

where t_0 and s_0 are parameters and $t_0 s_0 = 5$ to 10 gives good results, $\Re$ and $\Im$ denote the real and imaginary parts of $\hat{f}_m$. The numerical results are valid only for $t \leq t_0/2$.

5.5 Application to heat emitting HLW repository

5.5.1 Description of the problem

The numerical example presented in this section is applicable to modelling the processes that take place in repository for heat-emitting HLW. Figure 5.2 shows the problem for simulating a repository facility for heat-emitting HLW. According to the project report of the Belgian Nuclear Research Centre in Mol and the information given in Picard (1994), the HLW is assumed to be a decaying point heat source situated at 230 m depth from the ground surface of a Boom clay layer. For the point heat source we have Small & Booker (1986*a*):

$$q = Q_0 e^{-\omega t} \cdot \frac{\delta(r)\delta(z-z_j)}{\pi r} \tag{5.61}$$

where Q_0 is the initial strength of the source, $\omega = \ln 2/t_{0.5}$ is decay constant, $t_{0.5}$ is half life of the HLW. The particular values used here are Q_0 =2 KW/m^3 and ω =0.024. The layer of Boom clay with a thickness of about 100 m is the buffer which overlays a half space. We divide this layer into two sublayers at the heat source level z =180 m. Thus, the model can be regarded as an axisymmetric four-layered thermoelastic half space with a point heat source at z_j =230 m and r =0.

5.5.2 Numerical results and discussions

For an axisymmetric model, the index m in the vector surface harmonics is zero (Pan 1997). The analytical solutions are presented in appendix B. We select the first 15 integral intervals, i.e. $I = 15$ in Equation (5.58), and adopt 20-node quadrature rule ($J = 20$)

Table 5.1: Material parameters for multilayered structures

Parameter	Unit	L 1	L 2 and 3	L 4
depth z	m	180	50	$+\infty$
μ	MPa	70	60	70
K	MPa	166	100	166
α	$1/^{\circ}C$	1×10^{-5}	1×10^{-5}	1×10^{-6}
ρ	kg/m^3	2×10^3	2.61×10^3	2×10^3
c	J/(kg°C)	937	937	937
k	W/(m°C)	2.21	2.21	2.75

for the first 5 intervals, 10-node quadrature rule ($J = 10$) for the last 10 intervals in Equation (5.59). In Equation (5.60), we define $t_0 = 20$, $s_0 = 0.25$ and $K_0 = 100$. The material parameters are listed in Table 5.1. In the following a group of normalized parameters is introduced:

$$z^\star = \frac{z}{L} \quad r^\star = \frac{r}{L} \quad t^\star = \frac{\kappa}{L^2} t \tag{5.62}$$

where L is a characteristic scale length and set to be 280 m which is equal to the width (total depth) of the nonhomogeneous layers.

First of all, we compare our results with those reported in Small & Booker (1986a) as verification. Figure 5.3 shows the variation of temperature with time at mid-depth. It is clear that the temperature distribution obtained using the approach in this study perfectly matches the results in the literature, which confirm the accuracy and applicability of the proposed here method for solving thermoelastic problems. The definitions and values of all the parameters can be found in Small & Booker (1986a).

Figures 5.4a and 5.4b show, respectively, the variation of temperature along depth $z^\star$ after 50 years and with time for three different depths. The temperature increases along depth and reaches its peak of about 95^0C near the source, and tends to zero as $z^\star \to \infty$. After about 50 years, temperature reaches its peak. After 200 years of HLW repository operating the released temperature from the HLW will be 10% of the peak value.

The heat source will invoke deformations and stresses in the ground. Figures 5.5- 5.8 show the thermal induced vertical and radial displacements along depth after 50 years and the evolution with time of the displacements at three different depths, respectively. It is well known that there is a singularity at the source level. The direction of vertical deformation beneath/above the source is positive/negative. The surface deformation, as shown in

Figure 5.5b, first increases with time and then tends to be zero gradually. The maximum deformation at the surface is less than 2mm. The radial displacement along depth is presented in Figure 5.6a. It is evident that the maximum of the radial displacement along depth first increases with increasing of $r^\star$ and after, at least for $r^\star > 0.268$ it starts to decrease. It is clearly seen from Figure 5.6b that, the tendency of time history of radial displacement is similar to the time history of the temperature evolution. After about 50 years, the radial displacement at $r^\star = 0.035$ attains the maximum value 3.04 mm. The radial displacement value sharply drops down after 100 years and be only 6% of the maximum value at 200 years.

Figures 5.7a and 5.7b depict, respectively, the variations of thermal induced vertical stress along depth after 50 years and versus time at three different depths. The maximum vertical stress is about 56 kPa near the source level, however, it is equal to zero at the surface. Far from the center line, the vertical stress declines gradually and its value at $r^\star = 0.36$ is about 10% of the peak value. Corresponding to the time history of temperature, the vertical stress also increases first and attains peak value after about 50 years, then it decreases gradually in the course of time. After 100 years the value of the vertical stress decrease sharply and will be nearly zero after 500 years. The thermal induced radial stress, as shown in Figures 5.8a and 5.8b, has similar distribution with the thermal induced vertical stress. However, the peak value at center line is about 38 kPa which is slightly below the corresponding value of the vertical stress.

In order to study the influence of heat source shape on temperature, displacements and stresses distributions, a circular-shaped heat source with the same strength and decay constant as defined in Equation (5.40) is selected for analysis. Figure 5.9 shows the impact of source shape on the distributions of temperature in 100 years. The temperature increases when the radius of the source increases and be always larger than that caused by point heat source. The maximum temperature at radius $r_0 = 1.5m$ is about 90^0C which is 1.6 times larger than the relative value caused be point source. The source shape will also affects the variations of vertical and radial displacements as depicted in Figures 5.10 and 5.11. They indicate that the absolute values of displacements will increase with source's radius and are always larger than the relative values caused by point source. The similar conclusions can also be obtained from Figures 5.12 and 5.13 which depict the effects of source shape on the vertical and radial stresses.

In this study, the heat emission of the HLW after 100 years is only 9% of the initial value which can be obtained from Equation (5.61). The temperature has a strong effect on the static response in the ground in the first 200 years. However, temperature will tend

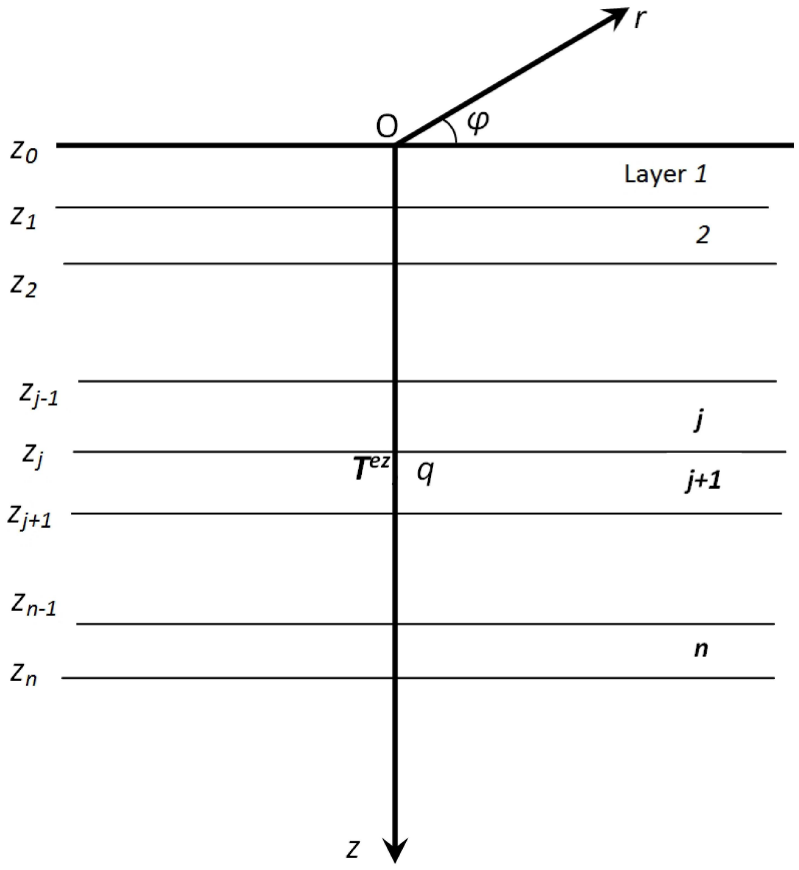

Figure 5.1: 3D multilayered structure with surface loads and internal heat sources

to zero after 500 years, and all the variables, like the thermal induced deformations and stresses, will also tend to zero. The magnitudes of temperature, deformations and stresses are consistent that reported in the previous works (Small & Booker 1986*a*; Picard 1994). Through the numerical simulations in this study, it indicates that the HLW significantly influences the surrounding ground at the first 500 years, especially at the first 200 years.

5.6 Conclusions

In this article, a comprehensive analytical solutions for the axisymmetric analyses of multilayered thermoelastic media with surface loads and containing heat source are presented. The governing equations together with boundary and initial conditions for a 3D formulation of the problem for the response of multilayered thermoelastic media subjected to surface loads and containing a heat source are first presented. A set of vector harmonics

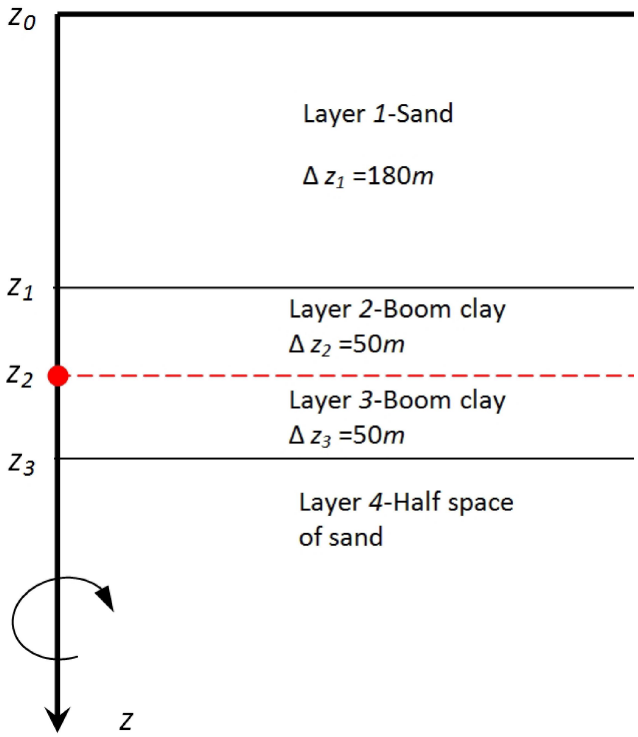

Figure 5.2: 3D axisymmetric multilayered structure with internal heat source

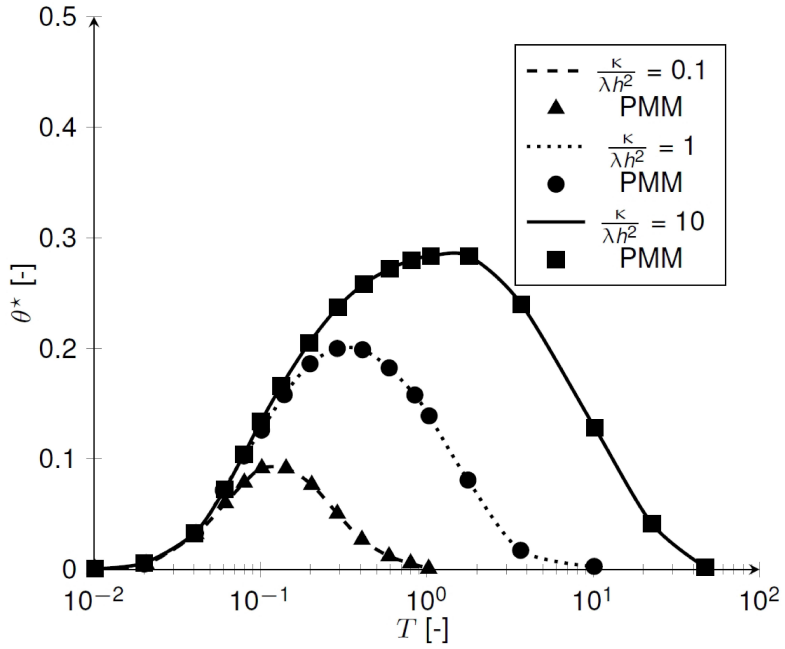

Figure 5.3: Comparisons of temperature distributions with time at mid-depth $z = 0.5h$ to Small & Booker Small & Booker (1986*a*)(lines)

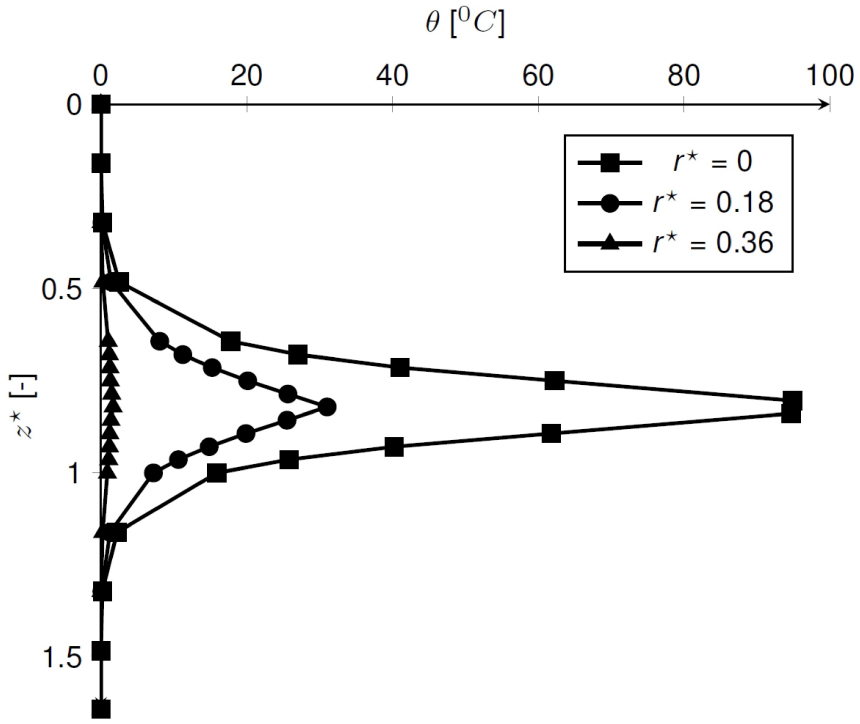

(a)

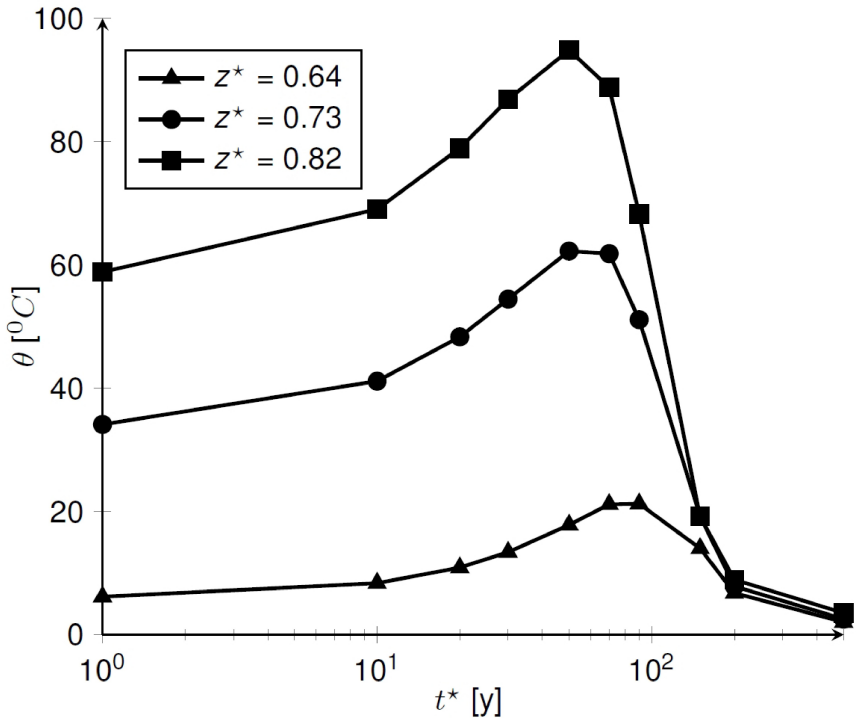

(b)

Figure 5.4: Variations of temperatures (a) along depth $z^\star$ in 50 years (b) with time $t^\star$ at $r^\star = 0$

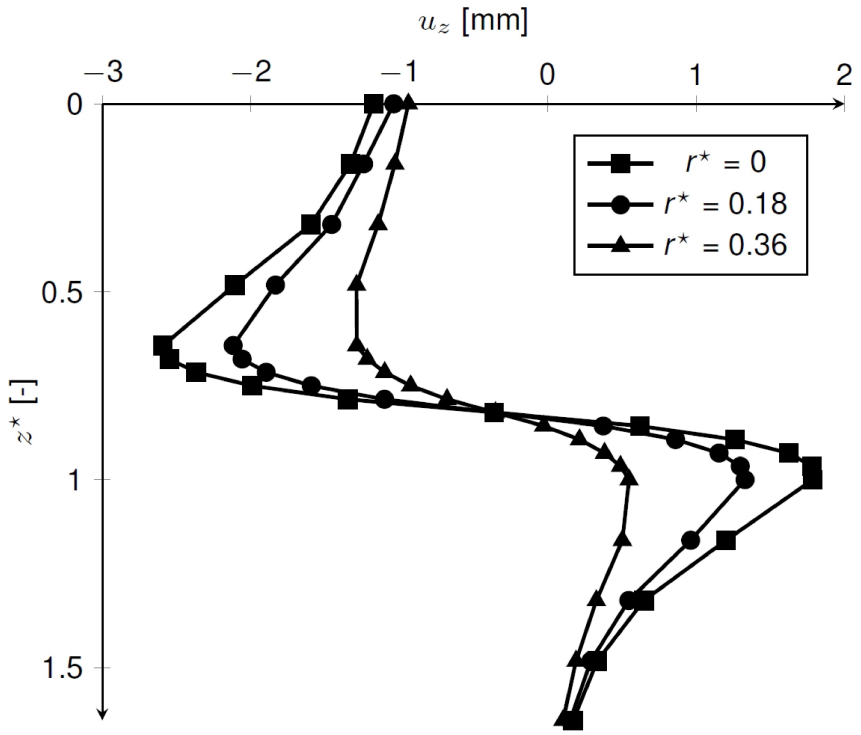

(a)

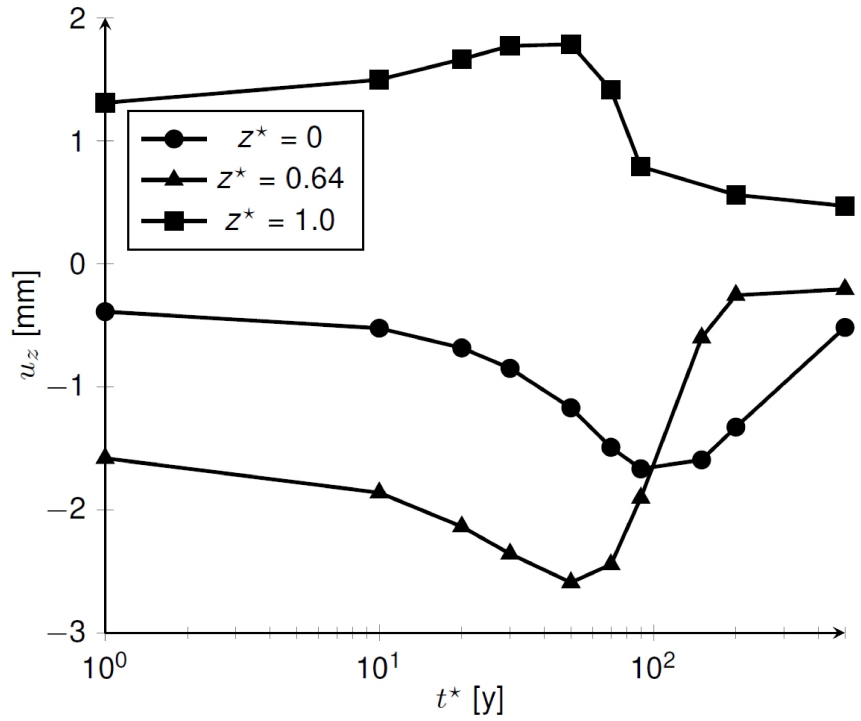

(b)

Figure 5.5: Variations of the vertical displacements (a) along depth $z^\star$ in 50 years (b) with time $t^\star$ at $r^\star = 0$

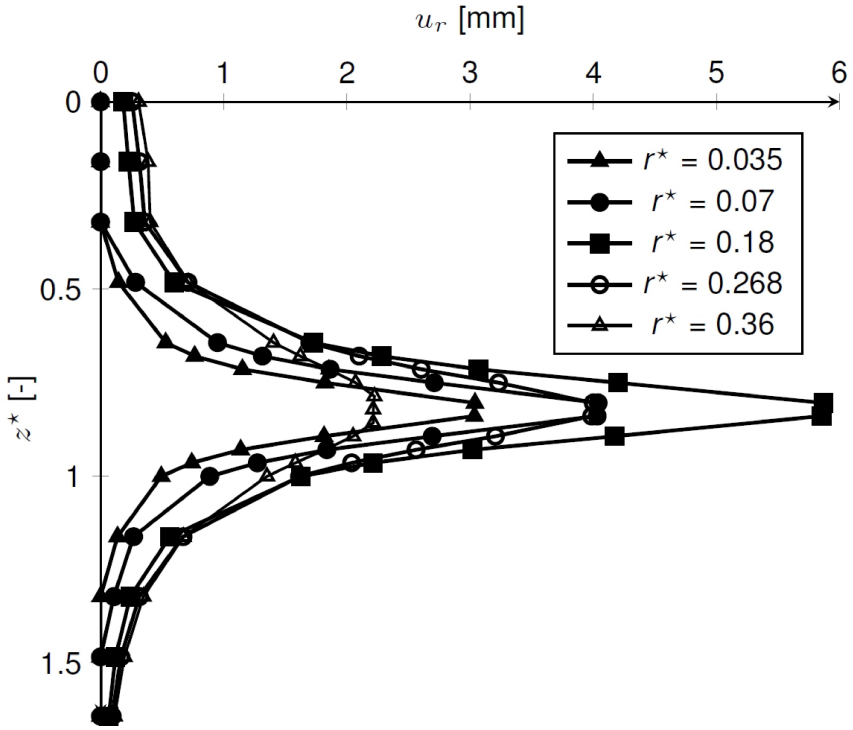

(a)

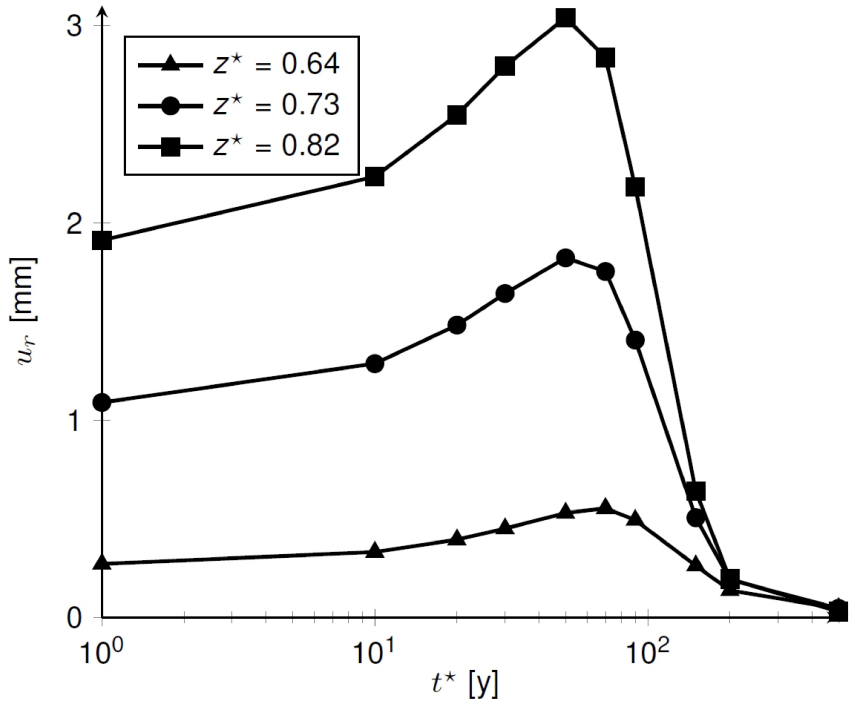

(b)

Figure 5.6: Variations of thermal induced radial displacements (a) along depth $z^\star$ in 50 years (b) with time $t^\star$ at $r^\star = 0.035$

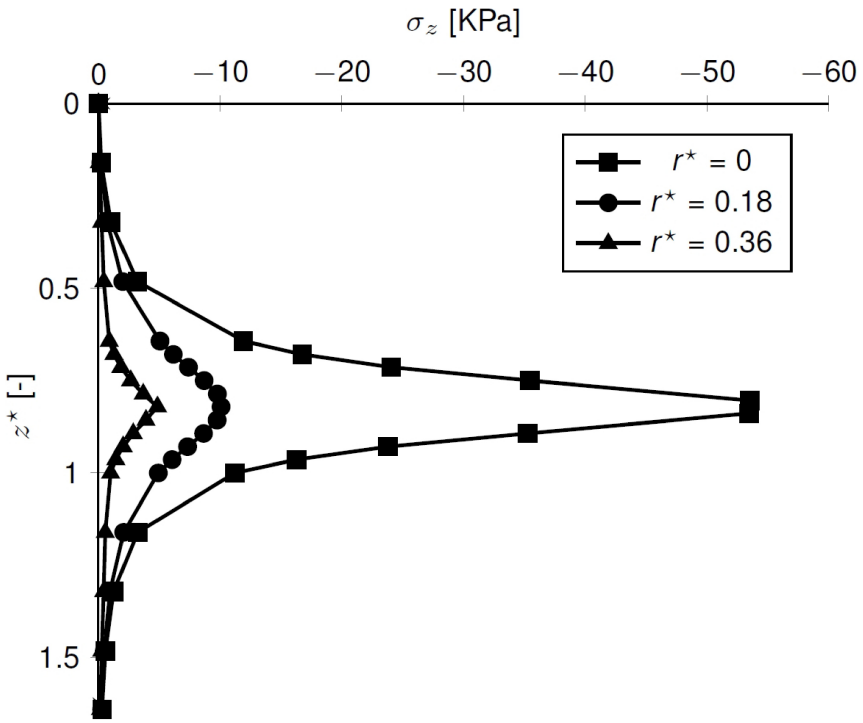

(a)

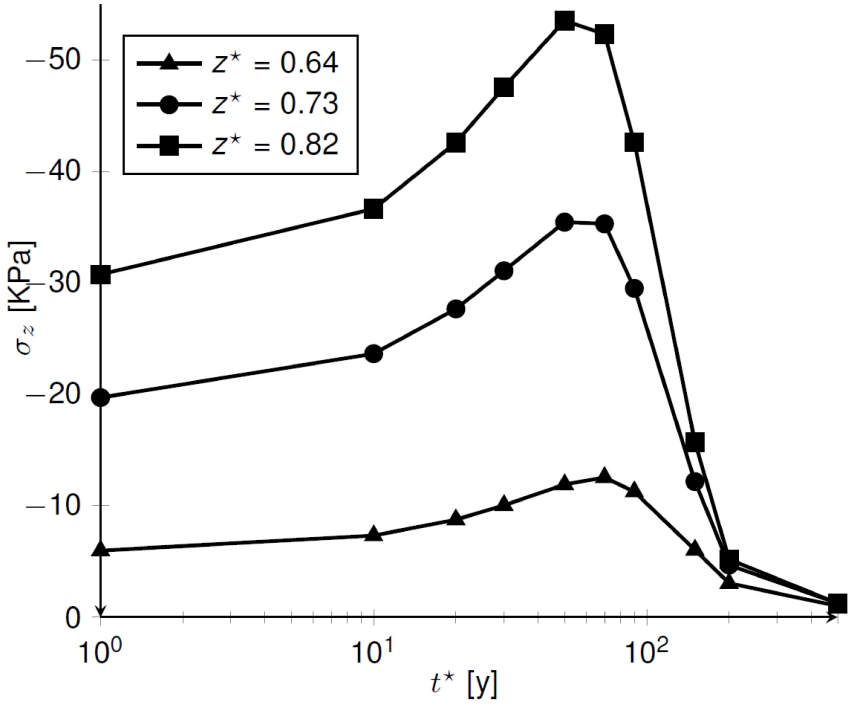

(b)

Figure 5.7: Variations of thermal induced vertical stresses (a) along depth $z^\star$ in 50 years (b) with time $t^\star$ at $r^\star = 0$

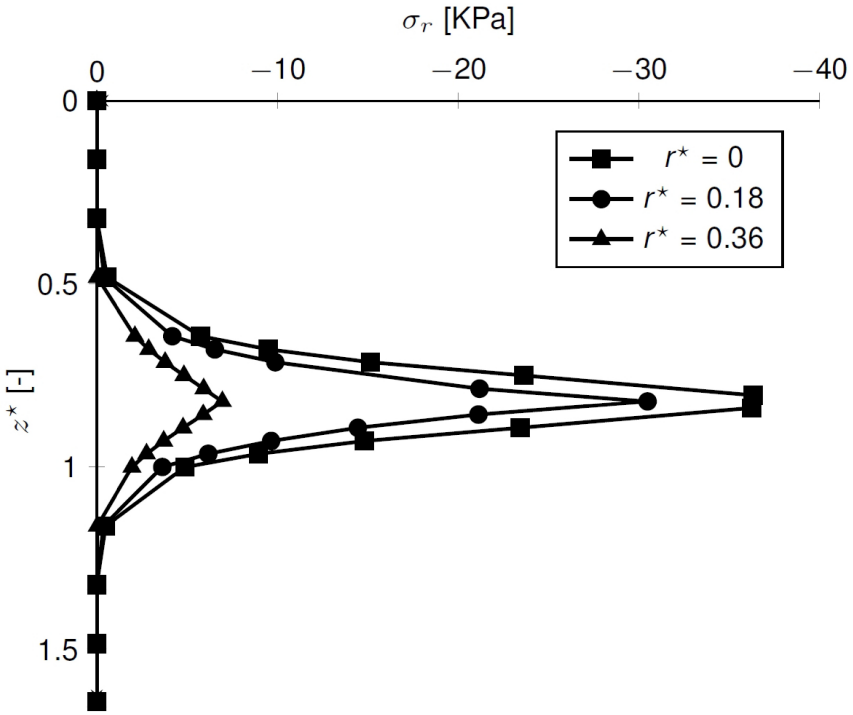

(a)

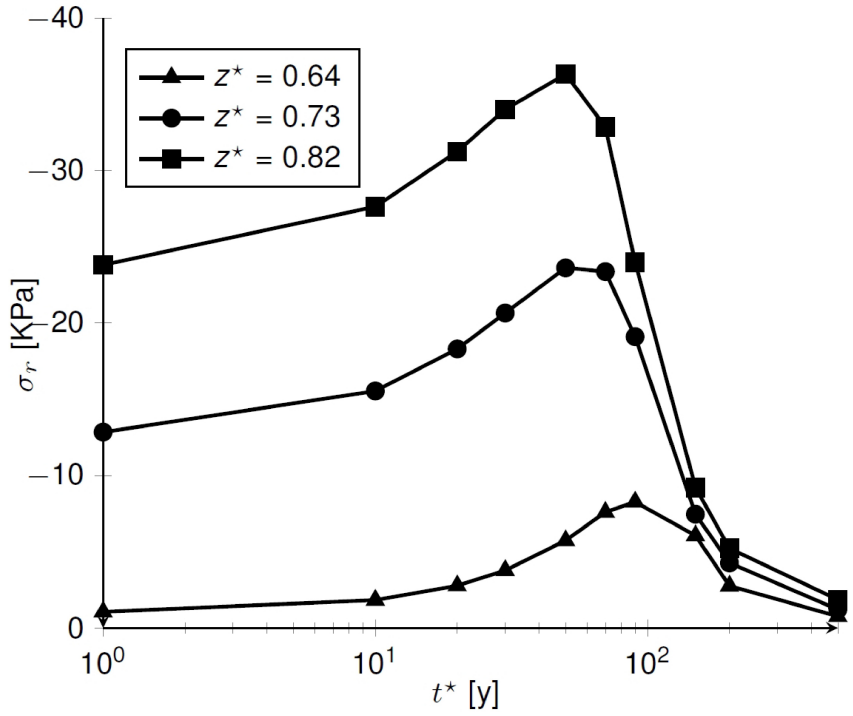

(b)

Figure 5.8: Variations of thermal induced radial stresses (a) along depth $z^\star$ in 50 years (b) with time $t^\star$ at $r^\star = 0$

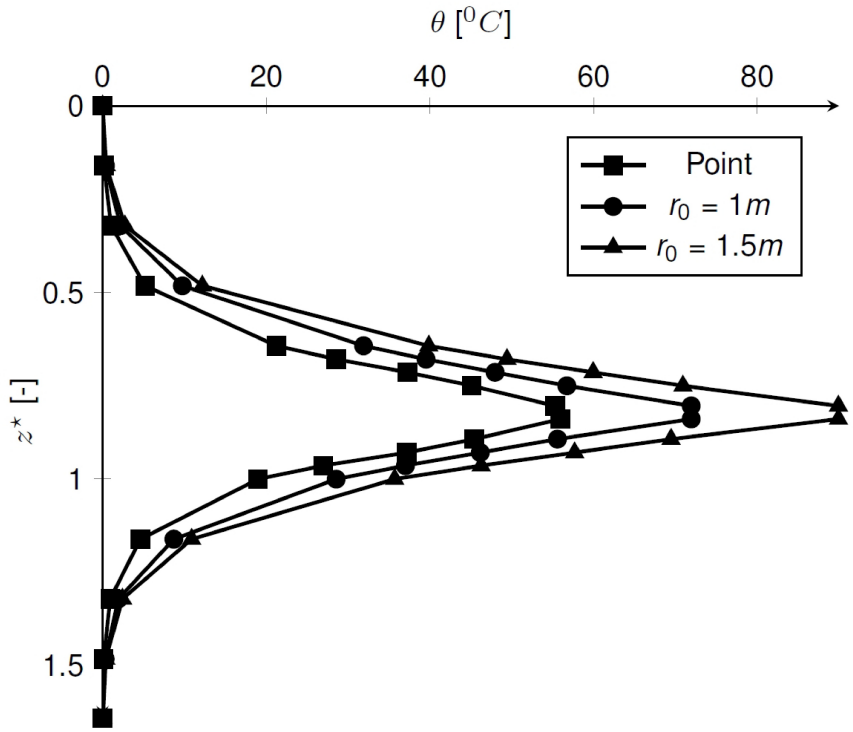

Figure 5.9: Effect of source's shape on temperature in 100 years

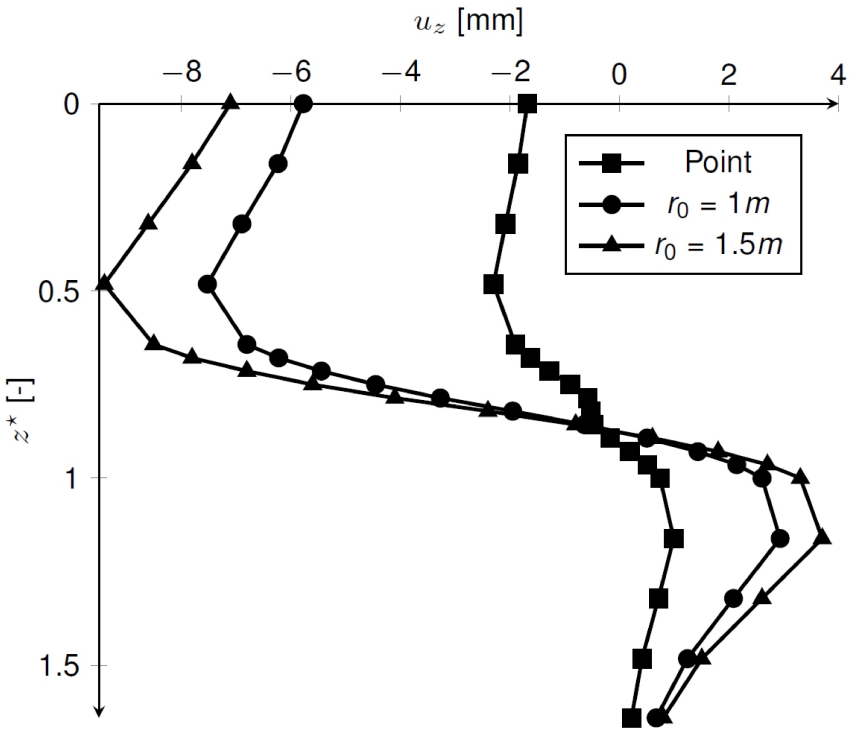

Figure 5.10: Effect of source's shape on vertical displacement in 100 years

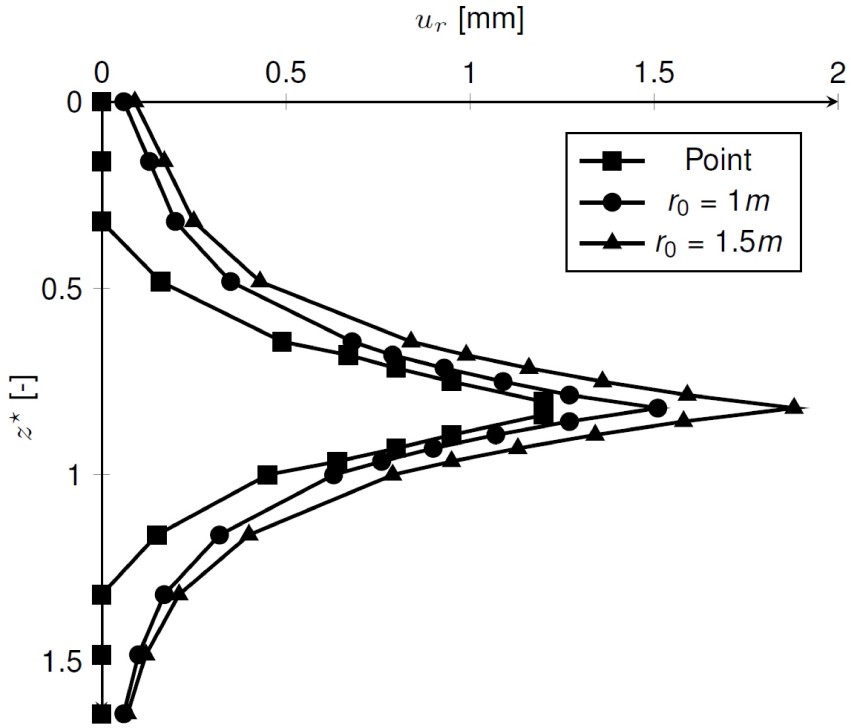

Figure 5.11: Effect of source's shape on radial displacement in 100 years

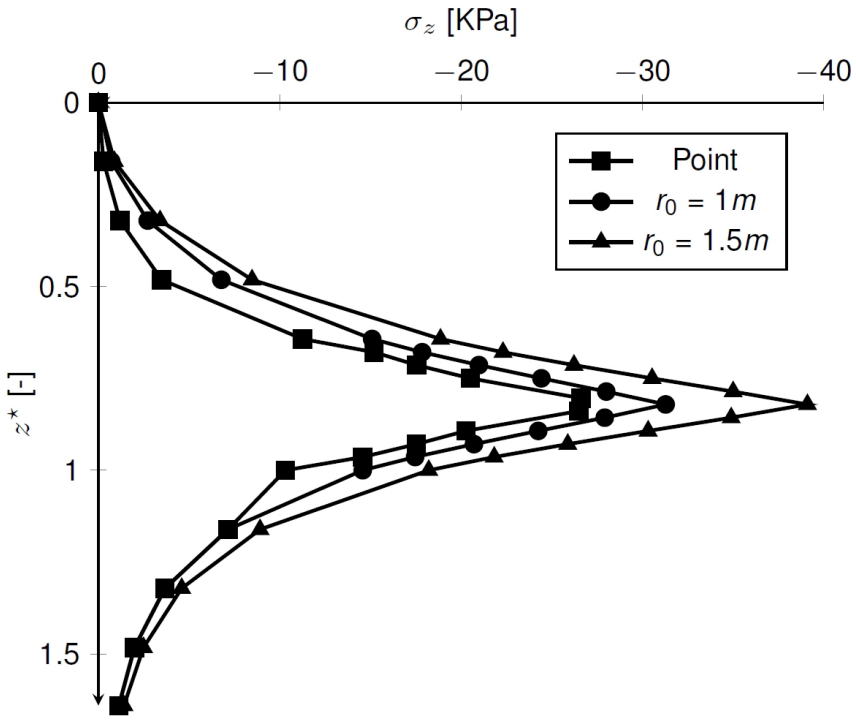

Figure 5.12: Effect of source's shape on vertical stress in 100 years

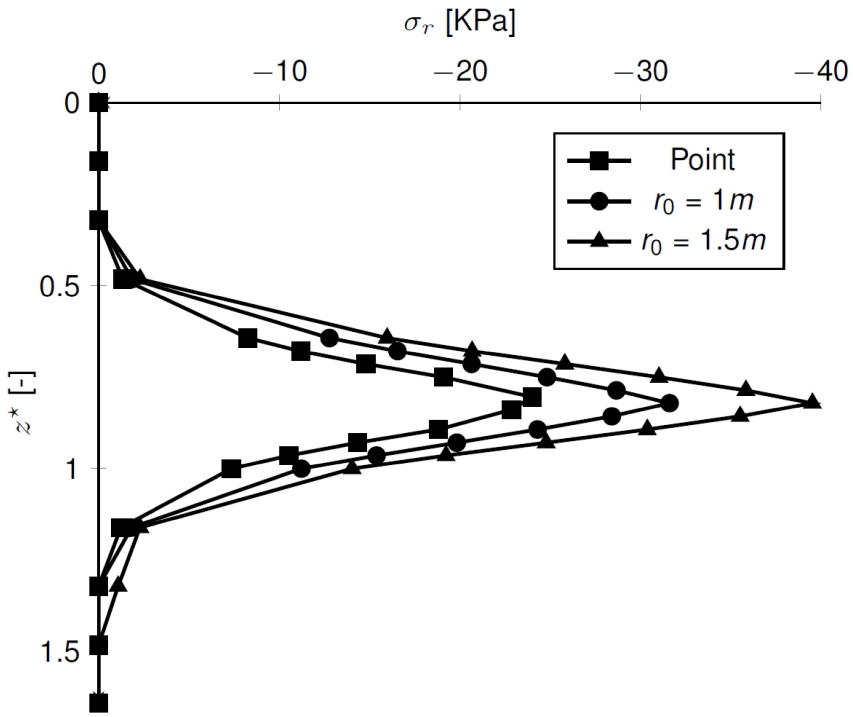

Figure 5.13: Effect of source's shape on radial stress in 100 years

is introduced, and then propagator matrix method is employed, with the aid of source functions, to derive the general solutions of static response. The numerical instability problem in the conventional algorithm is discussed and resolved by introduction of normalization technique and a improved new propagator matrix. Next, a numerical scheme of high-order adaptive Gaussian quadrature method with continued fraction expansions, and Crump's method for Laplace inversion are employed to approximate the integral solutions expressed in terms of semi-infinite Hankel-type integrals. Finally, the solutions are applied to solve the problem of repository for heat-emitting HLW in which the geological structure is treated as a four-layered half space and the HLW as a decaying with time point heat source. The variations of temperatures and the temperature-induced displacements and stresses are investigated with a kind of Boom clay which is used as the buffer in repository for heat-emitting HLW. The influences of source shape on the thermoelastic responses are also discussed. The numerical results agree well with the previous works and provide a verification to the propagator matrix method which can effectively solve the problem of static response in 3D multilayered thermoelastic media.

6 Heat Transfer in a Geothermal Heat-Pump System

6.1 Introduction

Geothermal heat is a type of energy produced mainly through radioactive decay in the core of the earth, about 6000 km below the surface. Geothermal heat-pump systems utilize the ground as a heat source. The system, which works by supplying heat to the ground during the summer and extracting heat during the winter, is more efficient than electric or gas/oil heating systems. A geothermal heat-pump system can reduce energy consumption by up to 44% compared with an air-source heat-pump system and up to 72% compared with conventional electrical heating and air conditioning (Omer 2008). Another important advantage of geothermal heat-pump systems is that they are less damaging to the environment.

A typical geothermal heat-pump system consists of a heat pump and a vertical heat exchanger system installed into the ground at depths ranging from 40 to 200 m. A heat-pump system model that involves two working modes, passive and active, is considered in this paper. In the heating mode, a certain amount of fluid is injected into the borehole and is then pumped out through a pipe after being heated or cooled to the required temperature. Many different factors influence geothermal heat-pump system performance, including the ground temperature distribution, possible freezing and thawing of the soil, thermal resistance of the pipe and of the grouting material, etc. Suitable modelling and an analytical solution of the problem describing geothermal heat-pump system response are thus necessary to better predict performance and improve the design of such systems.

6.2 Formulation of the problem and the governing equation

6.2.1 Modelling of a vertical U-tube ground heat exchanger

In practice, U-tube heat exchanger systems are the most often investigated and applied geothermal heat exchangers. The first analytical theory of heat transfer in a geothermal heat-pump system was proposed by Ingersoll & Plass (1948), and this served as a basis for the development of many later design programmes. A schematic illustration of a single U-tube vertical heat exchanger used in simulations is depicted in Figure 6.1. Because the depth of the borehole is much larger than its diameter, the heat transfer process near the borehole is often formulated by line-source theory (i.e. Kelvin's infinite line source) or the cylindrical-source theory proposed by Carslaw & Jaeger (1947). However, both these theories neglect axial heat flow along the depth and are only adequate for short time applications of durations from hours to months.

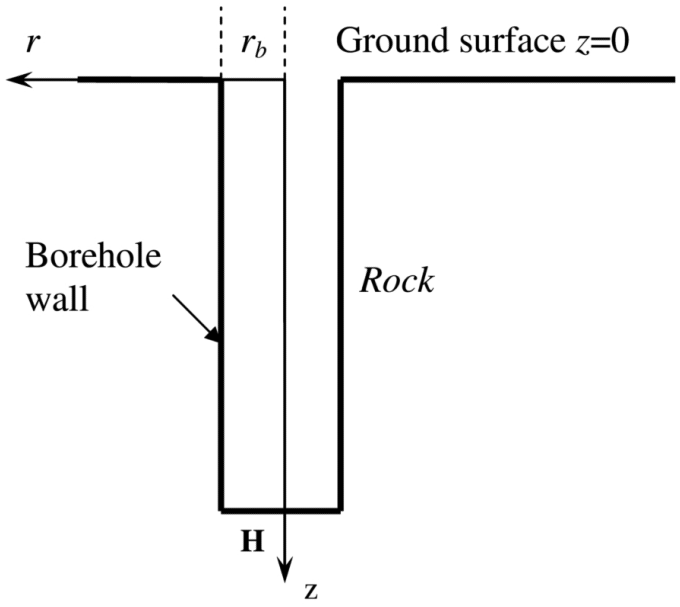

Figure 6.1: Vertical borehole in geothermal heat-pump system (U-tube model)

In practice, U-tube heat exchanger systems are the most often investigated and applied geothermal heat exchangers. The first analytical theory of heat transfer in a geothermal heat-pump system was proposed by Ingersoll & Plass (1948), and this served as a basis for the development of many later design programmes. A schematic illustration of a single

U-tube vertical heat exchanger used in simulations is depicted in Fig. 1. Because the depth of the borehole is much larger than its diameter, the heat transfer process near the borehole is often formulated by line-source theory (i.e. Kelvin's infinite line source) or the cylindrical-source theory proposed by Carslaw & Jaeger (1947). However, both these theories neglect axial heat flow along the depth and are only adequate for short time applications of durations from hours to months.

A finite line-source theory was developed by Eskilson (1987) and improved by Zeng et al. (2002), taking the axial heat flow condition into consideration. Bandos et al. (2009) investigated a three-dimensional finite line-source model for a borehole heat exchanger. Based on this theory, in the domain $r_b \leq r$, $0 \leq z \leq H$, $0 \leq t$ the distribution of the ground temperature θ is governed by the heat conduction equation

$$\frac{1}{a}\frac{\partial\theta(r,z,t)}{\partial t} = \frac{\partial^2\theta(r,z,t)}{\partial r^2} + \frac{1}{r}\frac{\partial\theta(r,z,t)}{\partial r} + \frac{\partial^2\theta(r,z,t)}{\partial z^2} \tag{6.1}$$

Considering the geothermal gradient implies that the initial ground temperature increases linearly with depth, such that

$$\theta(r,z,t)|_{t=0} = \theta_0 + \frac{q_{geo}}{k}z \tag{6.2}$$

The ground temperature at the surface is assumed to be constant and equal to the ambient temperature

$$\theta(r,z,t)|_{z=0} = \theta_0 \tag{6.3}$$

The borehole can be regarded as a line source, so the boundary condition at the borehole wall is

$$-k\frac{\partial\theta(r,z,t)}{\partial r}\Big|_{r=r_b} = \frac{q_b}{2\pi r_b} \tag{6.4}$$

In the above equations a is the ground thermal diffusivity, k is the ground thermal conductivity, q_b is the heating rate per unit length, q_{geo} is the geothermal heat flux and r_b is the radius of the borehole. Compared with the models of Eskilson (1987) and Zeng et al. (2002), in the case considered here the initial temperature is not uniform but linearly increases with depth. This augment is much higher near tectonic plate boundaries where the earth's crust is thinner.

In order to derive an analytical solution to the problem defined by Equations (6.1)–(6.4) there are some necessary assumptions to be accepted Zeng et al. (2002).

- The ground is regarded as a homogeneous semi-infinite media with constant thermal properties.

- Ground surface temperature is constant and it may be considered to be equal to the annual average ambient temperature.
- The cylindrical borehole is approximated by a finite line source and this may be assumed because the borehole radius is much smaller than the length of the borehole.
- The heating rate per unit line-source length is constant.

Solution of the boundary and initial value problem defined by Equations (6.1)–(6.4) is

$$\begin{aligned}\theta(r,z,t) &= \theta_1(r,z,t) + \theta_2(r,z,t) \\ &= \frac{q_b}{4\pi k}\int_0^H \left\{ \frac{erfc\left(\left[r^2+(z-h)^2\right]^{1/2}/2(at)^{1/2}\right)}{\left[r^2+(z-h)^2\right]^{1/2}} \right. \\ &\quad \left. - \frac{erfc\left(\left[r^2+(z+h)^2\right]^{1/2}/2(at)^{1/2}\right)}{\left[r^2+(z+h)^2\right]^{1/2}} \right\} \mathrm{d}h + \theta_0 + \frac{q_{geo}}{k} z\end{aligned} \tag{6.5}$$

where the first term on the right-hand side denotes the solution for constant initial conditions. The solution given by Equation (6.5) may be considered equivalent to the solution proposed by Bandos et al. (2009). Of most interest is the temperature excess of the borehole wall, especially the temperature at the midpoint of the line source $\theta_b = \theta(r_b, 0.5H, t)$, which is often adopted as representative of the borehole temperature.

6.2.2 Two-stage open heat exchange system

The heat exchanger system whose mathematical modelling is proposed in this paper employs the concept of a two-stage open heat exchange system - the passive step is shown schematically in Figure 6.2, and Figure 6.3 illustrates the active step. In the following, the basic assumptions are introduced, the mathematical model describing each step is formulated and the corresponding analytical solutions are obtained and discussed. Based on the corresponding analytical solutions, the performance of the two-stage heat exchange system is then compared with that of the U-tube heat exchanger. In addition, a parameter study is performed and the outcome is reported.

6.2.3 The passive step of the two-stage model

At the initial state the borehole is filled with fluid with a uniformly distributed initial temperature (i.e. constant). This fluid serves as the heat exchange medium. The fluid will be heated over time by the surrounding rock mass.During this procedure the temperature

at the top remains constant and equal to the ground surface temperature. Because the fluid is supposed not to move during this stage, this step of the modelling process is defined here as the 'passive step'. Figure 6.2 depicts the implementation of the above approach to the first phase (passive step) of the considered mathematical model.

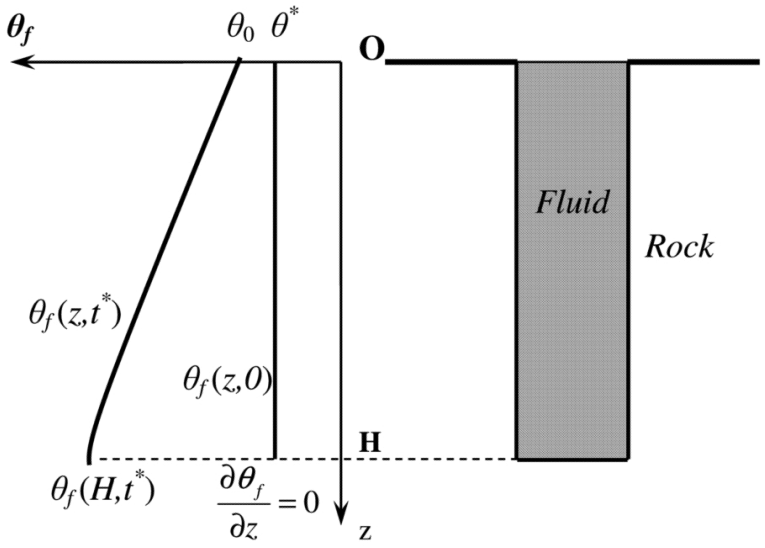

Figure 6.2: Fluid temperature distribution inside borehole during the passive step

The radius of the borehole is much smaller than its depth and the temperature distribution in the fluid may be considered to vary only with depth. In this case the temperature is constant at a cross-section of the borehole, so that radial heat flow is minor. In the domain $0 \leq z \leq H$, $0 \leq t \leq t^*$ the fluid temperature $\theta_f(z,t)$ during the passive step is governed by the heat conduction equation with a heat source term as

$$\frac{1}{a_f}\frac{\partial \theta_f}{\partial t} = \frac{\partial^2 \theta_f}{\partial z^2} + \frac{q_f}{k_f} \tag{6.6}$$

At the start, the filling fluid has a uniform temperature, so the initial condition is

$$\theta_f(z,0) = \theta^* \tag{6.7}$$

The temperature of the fluid at the top surface is assumed to be equal to the ambient temperature, so the boundary condition at $z = 0$ reads

$$\theta_f(0,t) = \theta_0 + (\theta^* - \theta_0)h(-t) \tag{6.8}$$

The bottom of the borehole is considered to be insulated and therefore there we have the following boundary condition for the fluid temperature

$$\frac{\partial \theta_f(z,t)}{\partial z}\Big|_{z=H} = 0 \tag{6.9}$$

In these equations, a_f is the fluid thermal diffusivity, k_f is the fluid thermal conductivity, q_f is the heating rate, H is the depth of the borehole, $h(-t)$ is the Heaviside step function and θ_0 and θ^* are constants.

In order to derive the analytical solution, the heating rate q_f along the z-axis is assumed to be constant. The analytical solution of the boundary and initial value problem for the fluid temperature evolution defined via Equations (6.6)–(6.9) is

$$\theta_f(z,t) = -\frac{q_f}{2k_f}z^2 + \frac{q_f}{k_f}Hz + \theta_0 + \sum_{n=1}^{\infty} a_n sin\frac{(2n+1)\pi z}{2H} exp\left(-\frac{a_f(2n+1)^2\pi^2 t}{4H^2}\right) \quad (6.10)$$

where

$$a_n = \frac{4}{(2n+1)\pi}\left(\theta^* - \theta_0 - \frac{q_f H^2}{k_f}\frac{4}{(2n+1)^2\pi^2}\right) \quad (6.11)$$

It can be observed that, as time t tends to infinity, the terms in the infinite series in Equation (6.10) will tend to zero and the fluid temperature will step into a steady-state quite quickly. This property of the model may be considered as proof of its physical consistence.

6.2.4 The active step of the two-stage model

After the passive step, it is assumed that the fluid will start to be pumped out through a pipe during $t^* < t \leq 2t^*$ as shown in Figure 6.3. This step is called hereafter the 'active step'. In general, the temperature variation inside the pipe can be considered to be slow, so it is common practice to model the heat transfer as a steady-state process (Eskilson & Claesson 1988; Zeng et al. 2002). Therefore, the boundary value problem for the fluid temperature distribution can be formulated as

$$\rho_f c_f V_p \frac{\partial \theta_f(z)}{\partial z} = \frac{\theta_f(z) - \theta_b}{R} \quad (6.12)$$

$$\theta_f(z)|_{z=H} = \theta_H \quad (6.13)$$

where ρ_f is the fluid density, c_f is the fluid specific heat, V_p is the pumping rate, θ_b is the borehole wall temperature (which is regarded as constant in order to make the problem manageable), R is the thermal resistance between the pumped fluid and the borehole wall and θ_H is constant and can be calculated using Equation (6.10) (i.e. $\theta_H = \theta_f(H, t^*)$).

In order to make a comparison with the U-tube model, which is a closed-loop system, the retention time t^* is introduced, which can be calculated using the formula $t^* = \pi r_p^2 H/V_p$ in which r_p denotes the radius of the pumping pipe. In the U-tube model, fluid is injected

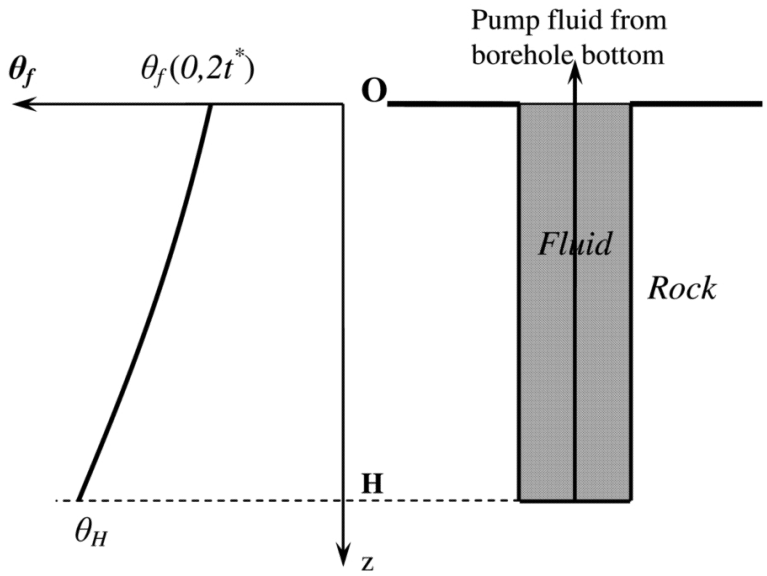

Figure 6.3: Schematic illustration of the heat exchange process during the active step

into the inlet pipe and then flows continuously out of the outlet pipe, so the flowing period is $2t^*$. However, in approach the presented here the fluid remains in a static state during the time period $0 < t \leq t^*$ and after that, pump outs for time $t^* < t \leq 2t^*$. The purpose of the following discussion is to compare the fluid temperature distributions under the two different working conditions with the same pumping period $2t^*$ and pumping rate V_p.

By introducing the dimensionless parameter

$$\bar{\Theta}_f(Z) = \frac{\theta_f(Z) - \theta_b}{\theta^* - \theta_b} \tag{6.14}$$

in which $Z = z/H$, solution of Equation (6.12) with the boundary condition given in Equation (6.13) gives the value of the outflow fluid temperature at time $2t^*$ as

$$\bar{\Theta}_f(HZ) = \bar{\Theta}_f(H)\left(cosh\frac{H}{\rho_f c_f V_p R} - sinh\frac{H}{\rho_f c_f V_p R}\right) \times \left(cosh\frac{HZ}{\rho_f c_f V_p R} + sinh\frac{HZ}{\rho_f c_f V_p R}\right) \tag{6.15}$$

It is obvious from the solution that the thermal resistance R plays an important role in the outflow temperature.

6.3 Parameter study

For the parameter study, a group of parameters characterising the type of rock and the fluid was adopted as shown in Table 6.1.

parameters	values	parameters	values
a	$1.15 \times 10^{-6} m^2/s$	n_{max}	2000
a_f	$1.56 \times 10^{-7} m^2/s$	R	$0.1 mK/W$
c_f	$3795 J/kg/K$	r_b	$50 - 100 mm$
H	$100 m$	r_p	$16 m$
k	$1.5 W/m/K$	V_p	$0.0004 m^3/s$
k_f	$0.6 W/m/K$	θ_0	$10^0 C$
q_b	$30 W/m$	θ^*	$10^0 C$
q_{geo}	$0.1 W/m^2$	ρ_f	$1000 kg/m^3$

Table 6.1: Model parameters (Eskilson & Claesson 1988; Zeng et al. 2003)

The simulation results are presented in terms of the dimensionless variables

- $Z = z/H$
- $\bar{r} = r/H$
- $T = at/H^2$
- $\Theta(\bar{r}, Z, T) = (4\pi k/q_b)\theta(\bar{r}, Z, T)$
- $\Theta_f(Z, T) = (4\pi k/q_b)\theta_f(Z, T)$

During the passive step, the fluid inside the borehole is heated by the surrounding rock mass; the evolution of the fluid temperature at different locations is given in Figure 6.4. The results shown in Figure 6.4 were obtained using Equation (6.10). It is evident that the temperature increases and seems to have the tendency to reach a steady state with time. The distribution of the fluid temperature along the borehole length is shown in Figure 6.5. At the free surface, the temperature remains constant due to the restriction defined in Equation (6.8) and it continuously increases with depth. This temperature distribution in the passive step is of course different from that in the U-tube model where the fluid is flowing through the inlet pipe.

The active step begins when the fluid temperature reaches $\theta_f(z, t^*)$, during the passive step. In the active step, pumping of the fluid out through the pipe is simulated with the same pumping rate as in the U-tube model. The upper and middle curves in Figure 6.6 are from the work of Diao et al. (2004), in which a single U-tube model was considered. Equation (6.6) represents the dimensionless temperature distribution in the inlet and outlet pipes under a certain pumping rate. The solutions for fluid temperature in the

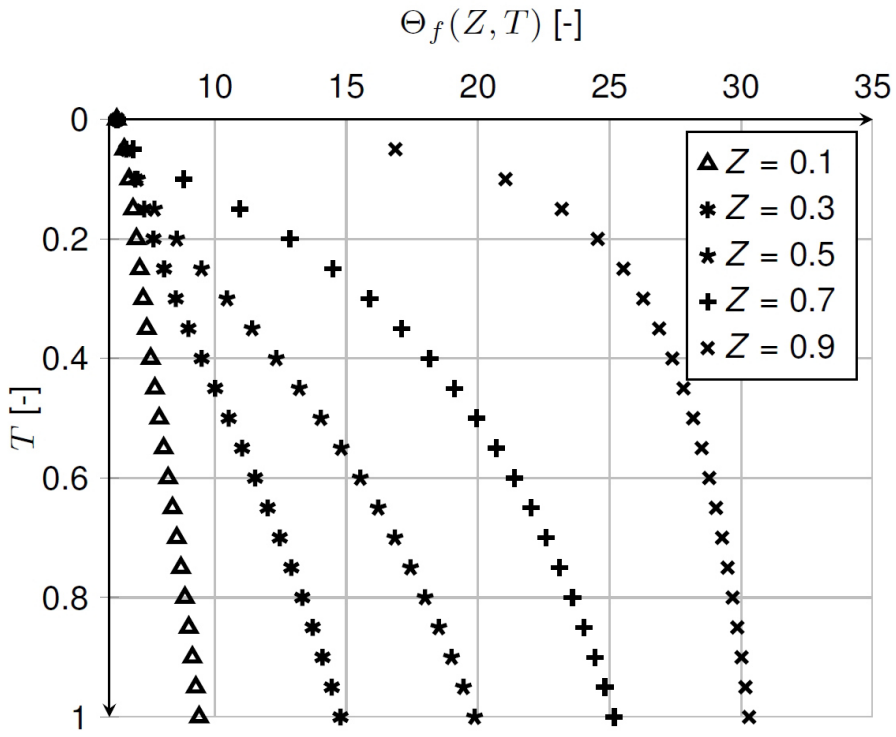

Figure 6.4: Fluid temperature change with time during the passive step

inlet and outlet pipes presented by Diao et al. (2004) for the U-tube model are

$$\begin{aligned}\bar{\Theta}_{fin}(Z) = cosh(\beta Z) - \frac{R_{11}}{(R_{11}^2 - R_{12}^2)^{1/2}} \\ \times \left[1 - \frac{R_{12}}{R_{11}} \frac{cosh\beta - [(R_{11}-R_{12})/(R_{11}+R_{12})]^{1/2} sinh\beta}{cosh\beta + [(R_{11}-R_{12})/(R_{11}+R_{12})]^{1/2} sinh\beta}\right] sinh(\beta Z)\end{aligned} \tag{6.16}$$

$$\begin{aligned}\bar{\Theta}_{fout}(Z) = \frac{cosh\beta - [(R_{11}-R_{12})/(R_{11}+R_{12})]^{1/2} sinh\beta}{cosh\beta + [(R_{11}-R_{12})/(R_{11}+R_{12})]^{1/2} sinh\beta} cosh(\beta Z) \\ + \frac{R_{11}}{(R_{11}^2 - R_{12}^2)^{1/2}} \left[\frac{cosh\beta - [(R_{11}-R_{12})/(R_{11}+R_{12})]^{1/2} sinh\beta}{cosh\beta + [(R_{11}-R_{12})/(R_{11}+R_{12})]^{1/2} sinh\beta} - \frac{R_{12}}{R_{11}}\right] sinh(\beta Z)\end{aligned} \tag{6.17}$$

where

$$\beta = \frac{H}{\rho_f c_f V_p \left[(R_{11}+R_{12})(R_{11}-R_{12})\right]^{1/2}} \tag{6.18}$$

and R_{11} and R_{12} are coefficients of thermal resistance between pipes and between the pipe and borehole wall, respectively.

The lower curve in Figure 6.6, computed according to Equation (6.14), represents the fluid temperature distribution during the active step of the open loop and the same pumping

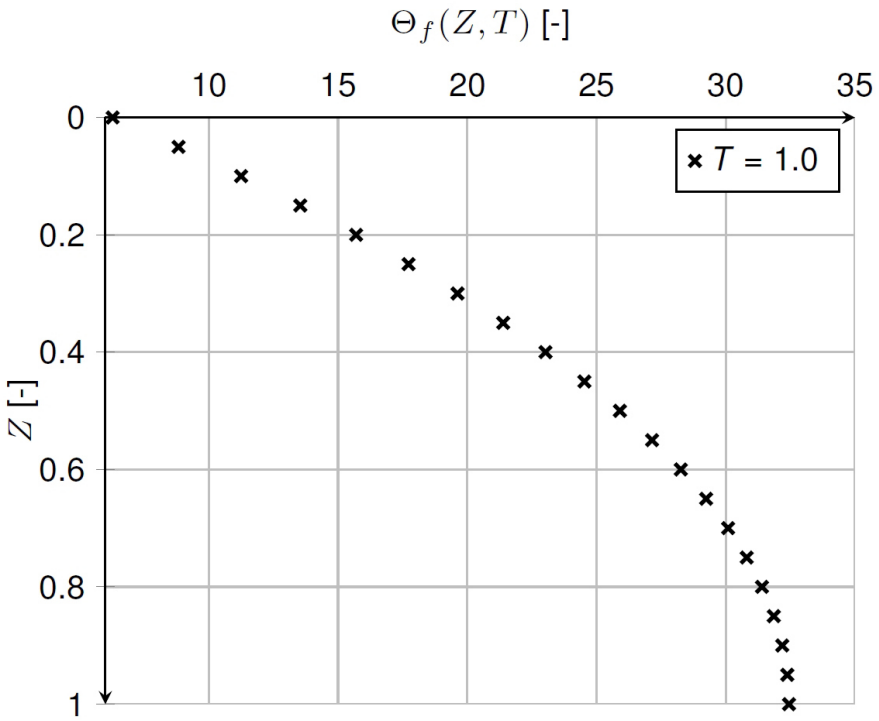

Figure 6.5: Fluid temperature distribution along the depth during the passive step

rate as the curves in the closed-loop model. Notably, the initial value is $\theta_f(H, t^*)$. Comparison of the results in Figure 6.6 indicates that the fluid in the passive step accumulates much more energy from the surrounding rock mass. Therefore, the heat exchange model in this study increases the borehole efficiency to some extent.

Figure 6.7 shows the temperature evolution with time at the mid-height of the borehole wall and employs the solution given in Equation (6.5). The temperature at the considered location increases rapidly at the beginning of the heat exchange system operation and reaches steady state after approximately $T = 0.3$. The influence of the borehole radius is also obvious from Figure 6.7 - the smaller the borehole radius, the larger the value of dimensionless temperature at the steady state.

Figure 6.8 shows the distribution of the borehole wall temperature with depth at steady state (i.e. $t \to \infty$) and using Equation (6.5). The borehole wall temperature increases rapidly from the ground surface, changes slightly in the region $0.2H$ to $0.8H$ and finally drops rapidly in the last portion of the borehole depth. It can also be seen that smaller values of borehole radius contribute to a higher temperature along the borehole length. It is therefore to be concluded that the size of the borehole radius is an important factor and has to be accounted for in the design of a geothermal heat-pump system.

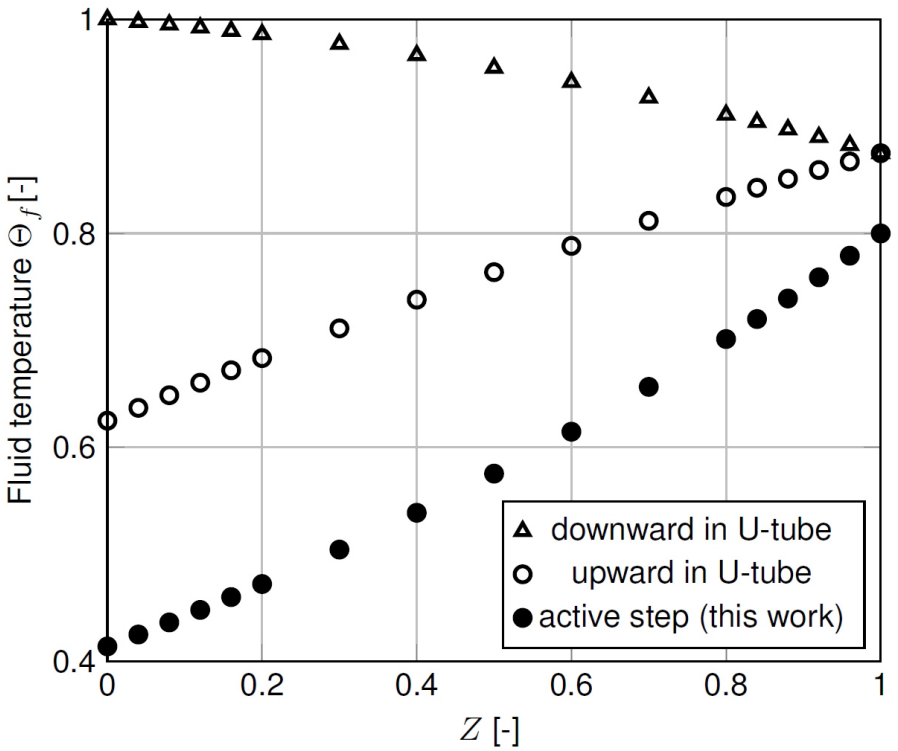

Figure 6.6: Fluid temperature distribution plotted against depth for open-loop and closed-loop (U-tube) models

Due to the geothermal gradient, the ground has a nonuniform initial temperature and this is accounted for by a linearly increasing initial temperature as explained by Equation (6.2). This difference in initial temperature will result in a shifted temperature distribution outside the borehole if compared with the results of Zeng et al. (2002). This difference is significant near tectonic plate boundaries where a relatively high geothermal heat flow exists.

6.4 Conclusions

A concept for a geothermal heat-pump system with a single vertical borehole and having two working modes has been presented and the corresponding initial and boundary value problem formulated. Furthermore, an analytical solution for a semi-infinite ground model with a finite line source functioning in a two-mode regime was derived and the temperature distribution of the fluid filling the borehole was obtained. The simplifications and assumptions used in order to be able to find the analytical solution were explained and

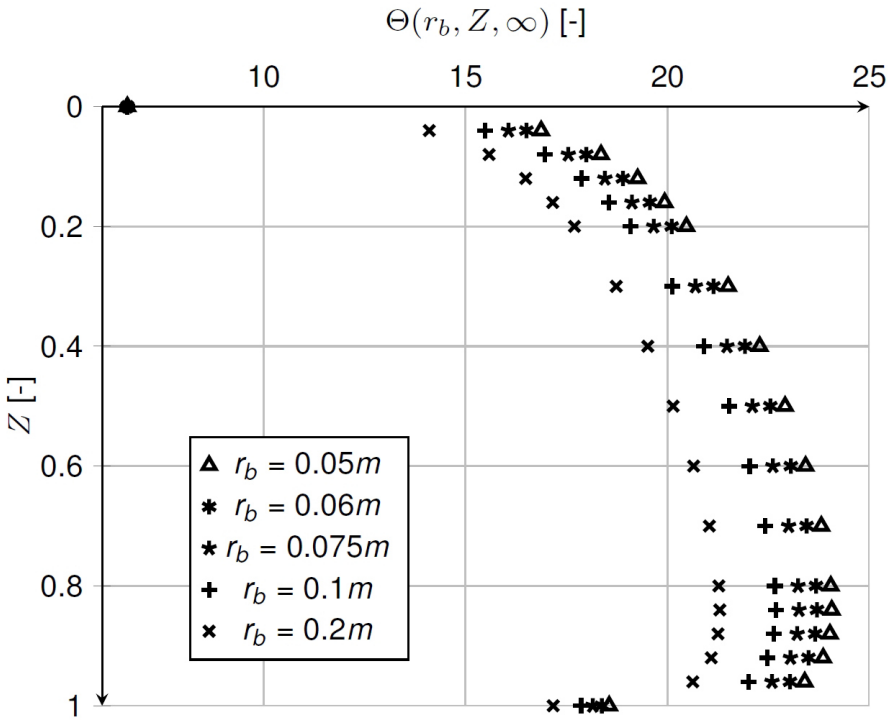

Figure 6.7: Mid-borehole wall temperature distribution plotted against time for different borehole radii

discussed. The obtained solution was compared with the well-accepted and investigated U-tube model (closed-loop model). The following important conclusions can be drawn based on the results of the performed parameter study.

- The temperature of the borehole wall increases with the Fourier number T and, for $T > 0.3$, reaches the steady state.
- The temperature of the borehole wall at steady state increases with depth rapidly at first, quickly reaches saturation and becomes almost constant along the larger portion of the borehole depth ($0.2H$ to $0.8H$), then drops rapidly drops near the bottom of the borehole.
- The size of the borehole radius is an important factor in the efficiency of a heat exchange system because a smaller borehole radius contributes to relatively higher temperature along the system. This has to be accounted in the design of geothermal heat-pump systems.
- The outflow temperature for the heat exchange system proposed in this study is higher than that in the U-tube model. This indicates that the passive plus active

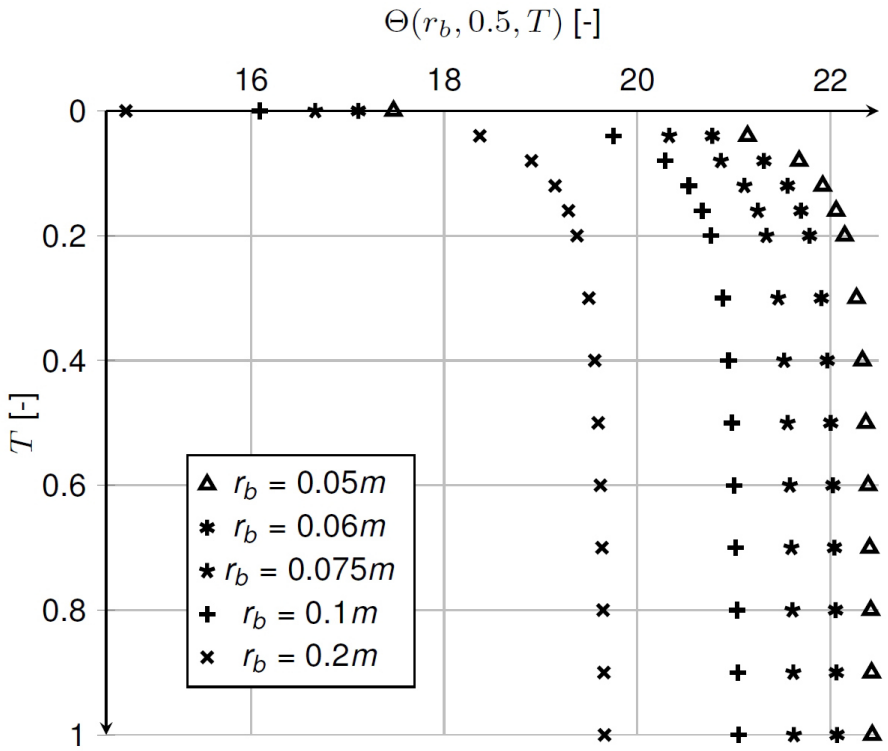

Figure 6.8: Steady-state borehole wall temperature along depth for different borehole radii

operation can obtain more energy from the hot rock mass and thus improve the efficiency of the system.

Even though the assumptions and simplifications considered here may be restrictive in representing the real functioning of a geothermal heat-pump system, the derived analytical solution promises to be useful in assessing some important features of this type of heat exchange system. Furthermore, the results obtained may be used to validate more complex models that allow only approximate numerical solutions.

7 Conclusions and recommendations

7.1 Conclusions

In this contribution, three problems which are closely related with heat transfer and temperature-induced behaviours in Geoscience are theoretically and numerically investigated. The three problems are heat transfer in geothermal heat-pump system, thermo-osmosis effect in saturated porous media in which a THM coupled model is introduced and the analysis of multilayered thermoelastic media with application to a repository for heat-emitting high-level nuclear waste in a Geological Formation , respectively. The mathematical-physical models for these problems are established first, the analytical solutions are obtained and then the numerical simulations are implemented to investigate the distributions of temperature response and the relevant temperature-induced behaviours. The main derived conclusions are categorized as follows.

Coupled THM behaviour in saturated porous medium

The thermo-poroelastic theory fulfilling LTNE is employed to investigate the quasi-static response of temperatures, pore pressure, stress, displacement and fluid flux around a cylindrical borehole subjected to impact thermal and mechanical loadings in a semi-infinite saturated porous medium. Analytical solutions are derived in Laplace transform space. A group of parameters for a typical clay used in nuclear waste storage are adopted in parameter study. Results fulfilling LTNE condition show that, with thermo-osmosis effect , the magnitudes of thermally induced pore pressure, stress, displacement and fluid are larger than those without this effect especially in the vicinity of the borehole. The difference of fluid flux is as greater as two to three orders of magnitudes in this study. Temperatures derived from LTNE heat transfer theory are different from that derived from LTE heat transfer theory. It is shown both from the analytical solutions and the parameter results that the LTE is a special case of LTNE. These differences will result

in differences in pore pressure, stress, displacement and fluid flux, especially when the coefficient of solid-fluid interface heat transfer is very small.

Multilayered thermoelastic media

A comprehensive analytical solutions for the axisymmetric analyses of multilayered thermoelastic media with surface loads and containing heat source are presented. The governing equations together with boundary and initial conditions for a 3D formulation of the problem for the response of multilayered thermoelastic media subjected to surface loads and containing a heat source are first presented. A set of vector harmonics is introduced, and then propagator matrix method is employed, with the aid of source functions, to derive the general solutions of static response. The numerical instability problem in the conventional algorithm is discussed and resolved by introduction of normalization technique and a improved new propagator matrix. Next, a numerical scheme of high order adaptive Gaussian quadrature method with continued fraction expansions, and Crump method for Laplace inversion are employed to approximate the integral solutions expressed in terms of semi-infinite Hankel-type integrals. Finally, the solutions are applied to solve the problem of repository for heat-emitting HLW in which the geological structure is treated as a four-layered half space and the HLW as a decaying with time point heat source. The variations of temperatures and the temperature-induced displacements and stresses are investigated with a kind of Boom clay which is used as the buffer in repository for heat-emitting HLW. The influences of source shape on the thermoelastic responses are also discussed. The numerical results agree well with the previous works and provide a verification to the propagator matrix method which can effectively solve the problem of static response in 3D multilayered thermoelastic media.

Heat transfer in geotechnics

A concept to model a geothermal energy heat-pump system with a single vertical borehole is presented and the corresponding initial and boundary value problem is formulated. Furthermore, the analytical solution for semi-infinite ground model with finite line source is derived and the temperature distribution in the borehole wall and in the fluid filling the borehole is obtained. The accepted simplifications and assumptions in order to be able to find the analytical solution are explained and discussed. Several important conclusions can be drawn based on the results of the performed parametric study of the analytical solution:

- The temperature of the borehole wall increases with the Fourier number T and reaches the steady state for $T > 0.3$;
- The temperature of the borehole wall at steady state increases with depth first rapidly, fast reaches saturation and is almost constant along the larger portion of the borehole depth $(0.2H - 0.8H)$, then near the bottom rapidly drops;
- The size of the borehole radius r_b is an important factor for the efficiency of the heat exchange system because smaller borehole radii contribute to relatively higher temperature along the system. This has to be accounted in the design of the geothermal heat pump system;
- Outflow temperature increases when accelerating the pumping velocity.

Even the assumptions and simplifications considered here may be restrictive for the model to represent the real functioning of a geothermal heat-pump system, the derived analytical solution is very useful to assess some important features of this type of heating exchange systems. The results obtained here may be further used to validate more complex models which allow only approximated numerical solutions.

7.2 Works in the next step

This thesis focuses on the heat transfer mechanism and the temperature-induced behaviours in Geotechnics and could be developed in the future. The very interesting and constructive development could state as follows:

- The coupled THM model can be further developed to study the dynamic response with the consideration of thermo-osmosis effect. The body force should be taken into account. For a more complete energy balance equation, the heat convective process in the fluid phase is also worthy of attention.
- The coupled THM model in saturated porous media can be improved to analyze the static and dynamic responses in unsaturated porous media. To achieve it, the governing equations for three phases (solid, fluid and gas phases) and four constituents (solid, fluid, vapor and air) should be presented.
- The multilayered thermoelastic structure can be improved to the more complete multilayered thermoporoelastic structure with the introduction of pore pressure and fluid velocity in the governing equations. Thus the scale of the relevant propagator matrix will be enlarged from 6×6 to 8×8. The developed theoretical work can be

applied to investigate the thermoporoelastic behaviours in the heat-emitting high level nuclear waste repository in geological formation.

Bibliography

Ai, Z. Y. & Wang, L. J. (2015), 'Axisymmetric thermal consolidation of multilayered porous thermoelastic media due to a heat source', *Int. J. Numer. Anal. Meth. Geomech.* **39**, 1912–1931.

Ai, Z. Y., Wang, L. J. & Zeng, K. (2015*a*), 'Analytical layer-element method for 3d thermoelastic problem of layered medium around a heat source', *Meccanica* **50**, 49–59.

Ai, Z. Y., Wang, L. J. & Zeng, K. (2015*b*), 'Time-dependent analysis of 3d thermo-mechanical behavior of a layered half-space with anisotropic thermal diffusivity', *Int. J. Numer. Anal. Meth. Geomech.* **39**, 1912–1931.

Ai, Z. Y., Wu, Q. L. & Wang, L. J. (2016), 'Extended precise integration method for axisymmetric thermo-elastic problem in transversely isotropic material', *Int. J. Numer. Anal. Meth. Geomech.* **40**, 297–312.

Ai, Z. Y., Yue, Z. Q., Tham, L. & Yang, M. (2002), 'Extended sneddon and muki solutions for multilayered elastic materials', *International Journal of Engineering Science* **40**, 1453–1483.

Al-Khoury, R., Koelbel, T. & Schramedei, R. (2010), 'Efficient numerical modeling of borehole heat exchangers', *Computers and Geosciences* **36**, 1301–1315.

Alonso, E. E., Alcoverro, J., Coste, F. & L. Malinsky, e. a. (2005), 'The febex benchmark test: case definition and comparison of modelling approaches', *International Journal of Rock Mechanics and Mining Sciences* **42**, 611–638.

Bai, M. & Abousleiman, Y. (1997), 'Thermoporoelastic coupling with application to consolidation', *International Journal for Numerical and Analytical Methods in Geomechanics* **21**, 121–132.

Bandos, T. V., Montero, A., Fernandez, E., Santander, J. L. G., Isidro, J. M., Perez, J., de Cordoba, P. J. F. & Urchueguia, J. F. (2009), 'Finite line-source model for borehole heat exchangers: effect of vertical temperature variations', *Geothermics* **38**, 263–270.

Biot, M. (1955), 'Theory of elasticity and consolidation for a porous anisotropic solid', *J . Appl. Phys.* **26**, 182–185.

Biot, M. A. (1956), 'Theory of propagation of elastic waves in a fluid-saturated porous solid. i. low-frequency range', *J. Acoust. Soc. Am.* **28**(2), 168–178.

Biot, M. & Willis, D. G. (1957), 'The elastic coefficients of the theory of consolidation', *Journal of Applied Mechanics* **24**, 594–601.

Booker, J. R. & Small, J. C. (1985), 'Finite layer analysis of layered viscoelastic materials under three-dimensional loading conditions', *International Journal for Numerical Methods in Enginerring* **21**, 1709– 1727.

Booker, J. & Savvidou, C. (1985), 'Consolidation around a heat point source', *Int. J. Numer Anal. Methods Geomech.* **9**, 173–184.

Bose, J. E., Parker, J. D. & McQuiston, F. C. (1985), *Design/data manual for closed-loop ground coupled heat pump systems*, Oklahoma State Univ for ASHRAE.

Carnahan, C. (1983), Thermodynamic coupling of heat and matter flows in near-field regions of nuclear waste repositories, *in* 'Materials Research Society Annual Meeting'.

Carnahan, C. (1984), Thermodynamic coupling of heat and matter flows in near-field regions of nuclear waste repositories, *in* 'Scientific Basis for Nuclear Waste Management VII', McVay, North-Holland, pp. 1023–1030.

Carslaw, H. & Jaeger, J. (1947), *Conduction of Heat in Solids*, Oxford.

Chave, A. (1983), 'Numerical integration of related hankel transforms by quadrature and continued fraction expansion', *Geophysics* **48**, 1671–1686.

Chen, W. Z., Tan, X. J., Yu, H. D., Wu, G. J. & Jia, S. P. (2009), 'A fully coupled thermo-hydro-mechanical model for unsaturated porous media', *Journal of Rock Mechanics and Geotechnical Engineering* **1**(1), 31–40.

Chen, Y., Zhou, C. & Jing, L. (2009), 'Modeling coupled thm processes of geological porous media with multiphase flow: Theory and validation against laboratory and field scale experiments', *Computers and Geotechnics* **36**, 1308–1329.

Chung, M., Jung, P.-S. & Rangel, R. H. (1999), 'Semi-analytical solution for heat transfer from a buried pipe with convection on the exposed surface', *International Journal of Heat and Mass Transfer* **42**, 3771–3786.

Crump, K. S. (1976), 'Numerical inversion of laplace transform using a fourier series approximation', *ACM. Trans. Math. Soft.* **23**, 89–96.

Darcy, H. (1956), 'Les fontaines publiques de la ville de dijon'.

Degrande, G., de Roeck, G. & Broeck, P. V. D. (1998), 'Wave propagation in layered dry saturated and unsaturated poroelastic media', *Int. J. Solids Structures* **35**, 4753–4778.

Demir, H., Koyun, A. & Temir, G. (2009), 'Heat transfer of horizontal parallel pipe ground heat exchanger and experimental verification', *Applied Thermal Engineering* **29**, 224–233.

Derjaguin, B. & Sidorenkov, G. (1941), 'On thermo-osmosis of liquid in porous glass', *C.R. Acad. Sci. U.R.S.S.* **32**(9), 622–626.

Diao, N., Zeng, H. & Fang, Z. (2004), 'Improvement in modeling of heat transfer in vertical ground heat exchangers', *HVAC&R RESEARCH* **10**(4), 459–470.

Dixon, A. & Cresswell, D. (1979), 'Theoretical predictions of effective heat transfer mechanisms in regular shaped packed beds', *AIChE Journal* **25**, 663–676.

Dunkin, J. W. (1965), 'Computation of modal solution in layered, elastic media at high frequencies', *Bull. Seismol. Soc. Am.* **55**, 335–358.

Durbin, F. (1974), 'Numerical inversion of laplace transforms: An efficient improvement to dubner and abate's method', *Computer Journal* **17**, 371–376.

Ekbote, S. & Abousleiman, Y. (2005), 'Porochemothermoelastic solution for an inclined borehole in a transversly isotropic formation', *Journal of engineering mechanics* **131**, 522–533.

Esena, H., Inalli, M. & Esen, M. (2007), 'Numerical and experimental analysis of a horizontal ground-coupled heat pump system', *Building and Environment* **42**, 1126–1134.

Esena, H., Inalli, M., Esen, M. & Pihtili, K. (2007), 'Energy and exergy analysis of a ground-coupled heat pump system with two horizontal ground heat exchangers', *Building and Environment* **42**, 3606–3615.

Eskilson, P. (1987), Thermal analysis of heat extraction boreholes, PhD thesis, Department of mathematical Physics, University of Lund, Sweden.

Eskilson, P. & Claesson, J. (1988), 'Simulation model for thermally interacting heat extraction boreholes', *Numerical Heat Transfer* **2**, 149–165.

Fan, R., Jiang, Y., Yao, Y. & Ma, Z. (2008), 'Theoretical study on the performance of an integrated ground-source heat pump system in a whole year', *Energy* **33**, 1671–1679.

Fan, R., Jiang, Y., Yao, Y., Shiming, D. & Ma, Z. (2007), 'A study on the performance of a geothermal heat exchanger under coupled heat conduction and groundwater advection', *Energy* **33**, 2199–2209.

Francois, B., Laloui, L. & Laurent, C. (2009), 'Thermo-hydro-mechanical simulation of atlas in situ large scale test in boom clay', *Computers and Geotechnics* **36**, 626–640.

Gatmiri, B. & Jabbari, E. (2005*a*), 'Time-domain greenâs functions for unsaturated soils. part i: two-dimensional solution.', *International Journal of Solids and Structures* **42**, 5971–5990.

Gatmiri, B. & Jabbari, E. (2005*b*), 'Time-domain greenâs functions for unsaturated soils. part ii: three-dimensional solution', *International Journal of Solids and Structures* **42**, 5991–6002.

Gatmiri, B., Maghoul, P. & Duhamel, D. (2010), 'Two-dimensional transient thermo-hydro-mechanical fundamental solutions of multiphase porous media in frequency and time domains', *International Journal of Solids and Structures* **47**, 595–610.

Gawin, D. & Schrefler, B. A. (1996), 'Thermo-hydro-mechanical analysis of partially saturated porous materials', *Engineering Computations* **13**(7), 113–143.

Ghassemi, A. & Diek, A. (2002), 'Porothermoelasticity for swelling shales', *Journal of Petroleum Science and Engineering* **34**, 123–135.

Gilbert, F. & Backus, G. E. (1966), 'Propagator matrices in elastic wave and vibration problems', *Geophysics* **32**, 326–332.

Giraud, A. (1998), 'Thermoelastic and thermoplastic response of a double-layer porous space containing a decaying heat source', *International Journal for Numerical and Analytical Methods in Geomechanics* **22**, 133–149.

Giraud, A. & Rousset, G. (1995), 'Thermoelastic and thermoplastic response of a porous space submitted to a decaying heat source', *International Journal for Numerical and Analytical Methods in Geomechanics* **19**, 475–495.

Grangeot, G., Quintard, M. & Whitaker, S. (1994), 'Heat transfer in packed beds: interpretation of experiments in terms of one- and two-equation models', *Heat transfer* **5**, 291–296.

Haartsen, M. W. & Pride, S. R. (1997), 'Electroseismic waves from point sources in layered media', *J. Geophys. Res.* **102**, 24745–24769.

Haskell, A. (1953), 'The dispersion of surface waves on multilayered media', *Bul. Seis. Soc. Am.* **43**, 17–34.

He, L. & Jin, Z. (2011), 'Effects of local thermal non-equilibrium on the pore pressure and thermal stresses around a spherical cavity in a porous medium', *International Journal of Engineering Science* **49**, 240–252.

Honig, G. & Hirdes, U. (1984), 'A method for the numerical inversion of laplace transforms', *Journal of Computational and Applied Mathematics* **10**, 113–132.

Hueckel, T. & Pellegrini, R. (1992), 'Effective stress and water pressure in saturated clays during heating-cooling cycles', *Canadian Geotechnical Journal* **29**, 1095–1120.

Ingersoll, L. & Plass, H. (1948), 'Theory of the ground pipe source for the heat pump', *ASHVE Trans* **54**, 339–348.

Ingersoll, L., Zobel, O. & Ingersoll, A. (1954), *Heat conduction with engineering, geological, and other applications*, New York: McGraw-Hill.

Jabbari, E. & Gatmiri, B. (2007), 'Thermo-poro-elastostatic green functions for unsaturated soils', *International Journal of Computer Modelling in Engineering and Sciences* **18**, 31–43.

Jovanovich, D. B., Husseini, M. I. & Chinnery, M. A. (1974*a*), 'Elastic dislocations in a layered half-space-i. basic theory and numerical methods', *Geophys. J. R. astr. Soc* **39**, 205–217.

Jovanovich, D. B., Husseini, M. I. & Chinnery, M. A. (1974*b*), 'Elastic dislocations in a layered half-space-ii. the point source', *Geophys. J. R. astr. Soc* **39**, 219–239.

Julio Goncalves and, G. d. M. & Tremosa, J. (2012), 'Importance of thermo-osmosis for fluid flow and transport in clay formations hosting a nuclear waste repository', *Earth and Planetary Science Letters* **339-340**, 1–10.

Jussila, P. & Ruokolainen, J. (2007), 'Thermomechanics of porous media - ii: thermo-hydro-mechanical model for compacted bentonite', *Transp Porous Med* **67**, 275–296.

Kanj, M. & Abousleiman, Y. (2005), 'Porothermoelastic analyses of an anisotropic hollow cylinders with applications', *Int. J. Numer. Anal. Meth. Geomech.* **29**, 103–126.

Kennett, B. (1974), 'Reflections, rays, and reverberations', *Bulletin of the Seismological Society of America* **64**, 1685–1696.

Kennett, B. (2009), *Seismic Wave Propagation in Stratified Media*, AUN E Press, Australia.

Kennett, B. & Kerry, N. (1979), 'Seismic waves in a stratified half space', *Geophys. J. R. Astr. Soc* **57**, 557–583.

Kodashima, T. & Kurasbige, M. (2009), 'Active cooling and thermal stress reduction in a poroelastic hollow sphere', *Journal of Thermal Stresses* **20**(3), 389–405.

Kolditz, O., Bauer, S., Bilke, L., Boettcher, N., Delfs, J. O., Fischer, T., Goerke, U. J., Kalbacher, T., Kosakowski, G., McDermott, C. I., Park, C. H., Radu, F., Rink, K., Shao, H., Shao, H. B., Sun, F., Sun, Y. Y., Singh, A. K., Taron, J., Walther, M., Wang, W., Watanabe, N., Wu, Y., Xie, M., Xu, W. & Zehner, B. (2012), 'Opengeosys: an open-source initiative for numerical simulation of thermo-hydro-mechanical/chemical (thm/c) processes in porous media', *Environ Earth Sci* **67**, 589–599.

Kurashige, M. (1989), 'A thermoelastic theory of fluid-filled porous materials', *Int. J. Solids Structures* **25**(9), 1039–1052.

Lamarche, L. & Beauchamp, B. (2007), 'A new contribution to the finite line-source model for geothermal boreholes', *Energy and Buildings* **39**, 188–198.

Letey, J. & Kemper, W. (1969), 'Movement of water and salt through a clay-water system: experimental vertification of onsagerâs reciprocal relation', *Soil Sci. Soc. Am. Proc.* **33**, 22–29.

Liew, K. M., Yang, J. & Kitipornchai, S. (2003), 'Postbuckling of piezoelectric fgm plates subject to thermo-electro-mechanical loading', *International Journal of Solids and Structures* **40**, 3869–3892.

Liu, G. (2010), 'Mode of a spherical cavity's thermo-elastodynamic response in a saturated porous medium for non-torsional loads', *Computers and Geotechnics* **37**, 381–390.

Liu, G., Xie, K. & Ye, R. (2010), 'Mode of a spherical cavity's thermo-elastodynamic response in a saturated porous medium for non-torsional loads', *Computers and Geotechnics* **37**, 381–390.

Liu, G., Xie, K. & Zheng, R. (2009), 'Model of nonlinear coupled thermo-hydro-elastodynamics response for a saturated poroelastic medium', *Applied Mathematical Modelling* **52**(8), 2373–2383.

Liu, G., Xie, K. & Zheng, R. (2010), 'Thermo-elastodynamic response of a spherical cavity in saturated poroelastic medium', *Science in China Series E: Technological Sciences* **34**, 2203–2222.

Liu, T. & Zhao, C. (2013), 'Dynamic analyses of multilayered poroelastic media using the generalized transfer matrix method', *Soil Dynamics and Earthquake Engineering* **48**, 15–24.

Lu, J. F. & Hanyga, A. (2005), 'Fundamental solutions for a layered porous half space subject to a vertical point force or a point fluid source', *Comput. Mech.* **35**, 376–391.

Lund, J. W. & Boyd, T. L. (2015), Direct utilization of geothermal energy 2015 worldwide review, *in* 'Proceedings World Geothermal Congress 2015'.

Maghoul, P., Gatmiri, B. & Duhamel, D. (2010), 'Three-dimensional transient thermo-hydro-mechanical fundamental solutions of unsaturated soils', *Soil Dynamics and Earthquake Engineering* **34**, 297–329.

Maghoul, P., Gatmiri, B. & Duhamel, D. (2011), 'Boundary integral formulation and two-dimensional fundamental solutions for dynamic behavior analysis of unsaturated soils', *Int. J. Numer. Anal. Meth. Geomech.* **31**, 1480–1495.

McTigue, D. (1986), 'Thermoelastic response of fluid-saturated porous rock', *Journal of Geophysical Research* **91**(B9), 9533–9542.

McVay, D. (1984), *Scientific Basis for Nuclear Waste Management VII*, Elsevier Science Pub. Co, North-Holland, New York.

Nield, D. (1998), 'Effect of local thermal nonequilibrium in steady convection processes in saturated porous media: Forced convection in a channel', *Journal of Porous Media* **1**, 181–186.

Nield, D. & Bejan, A. (2006), *Convection in porous media (3rd ed)*, Berlin: Springer.

Nowacki, W. (1962), *Thermoelasticity*, Pergamon, Oxford.

Nowak, T., Kunz, H., Dixon, D., Wang, W., Goerke, U.-J. & Kolditz, O. (2011), 'Coupled 3-d thermo-hydro-mechanical analysis of geotechnological in situ tests', *International Journal of Rock Mechanics and Mining Sciences* **48**, 1–15.

Omer, A. M. (2008), 'Ground-source heat pumps systems and applications', *Renew. Sustain. Energy Rev.* **12**(2), 344–371.

Pan, E. (1989*a*), 'Static response of a transversely isotropic and layered half-space to general dislocation sources', *Physics of the Earth and Planetary Interiors* **58**, 103–117.

Pan, E. (1989*b*), 'Static response of a transversely isotropic and layered half-space to general surface loads', *Physics of the Earth and Planetary Interiors* **54**, 353–363.

Pan, E. (1990), 'Thermoelastic deformation of a transversely isotropic and layered half-space by surface loads and internal sources', *Physics of the Earth and Planetary Interiors* **60**, 254–264.

Pan, E. (1997), 'Static green's functions in multilayered half spaces', *Appl. Math. Modelling* **21**, 509–521.

Pan, E. (1999), 'Green's functions in layered poroelastic half-spaces', *International Journal for Numerical and Analytical Methods in Geomechanics* **23**, 1631–1653.

Picard, J. M. (1994), Ecrouissage thermique des argiles saturees: application au stockage des dechets radioactifs, PhD thesis, ENPC, Paris.

Piechowski, M. (1999), 'Heat and mass transfer model of a ground heat exchanger: Theoretical development', *International Journal of Energy Research* **23**, 571–588.

Polyaev, V. (1996), 'A study of internal heat transfer in nonuniform porous structures', *Expt. Therm. Fluid Sci.* **12**, 426–432.

Pulat, E., Coskun, S., Unlu, K. & Yamankaradeniz, N. (2009), 'Experimental study of horizontal ground source heat pump performance for mild climate in turkey', *Energy* **34**, 1284–1295.

Rajapakse, R. & Senjuntichai, T. (1995*a*), 'Dynamic-response of a multilayered poroelastic medium', *Earthquake Engineering & Structural Dynamics* **24**, 703–722.

Rajapakse & Senjuntichai (1995*b*), 'Exact stiffness method for quasi-static of a multilayered poroelastic medium', *International journal of solids and structures* **32**, 1535–1553.

Rastogi, Blokhra & Agarwal (1964), 'Cross-phenomenological coefficients. part 1-studies on thermo-osmosis', *Transactions of the Faraday Society* **60**.

Rice, J. & Cleary, M. (1976), 'Some basic stress diffusion ssolution for fluid-saturated elastic porous media with compressible constituents', *Reviews of Geophysics and Space Physics* **14**, 227–241.

Rundle, J. B. (1980), 'Static elastic-gravitational deformation of a layered half space by point couple sources', *J. Phys. Earth* **85**, 5355–5363.

Rundle, J. B. (1982), 'Some solutions for static and pseudo-static deformation in layered, nonisothermal, porous media', *Journal of Geophysical Research* **30**, 421–440.

Rutqvist, J., Boergesson, L., Chijimatsu, M., Kobayashi, A., Jing, L., Nguyen, T., Noorishad, J. & Tsang, C.-F. (2001), 'Thermohydromechanics of partially saturated geological media: governing equations and formulation of four finite element models', *International Journal of Rock Mechanics and Mining Sciences* **38**, 105–127.

Sanchez, M., Gens, A. & Olivella, S. (2012), 'Thm analysis of a large-scale heating test incorporating material fabric changes', *Int. J. Numer. Anal. Meth. Geomech.* **36**, 391–421.

Sanner, B., Karytsas, C., Mendrinos, D. & Rybach, L. (2003), 'Current status of ground source heat pumps and underground thermal energy storage in europe', *Int. J. Numer. Anal. Meth. Geomech.* **32**, 579–588.

Schrefler, B. A., Khoury, G. A., Gawin, D. & Majorana, C. E. (2002), 'Thermo-hydro-mechanical modelling of high performance concrete at high temperatures', *Engineering Computations* **19**(7), 787–819.

Senjuntichai, T. & Rajapakse, R. (1995), 'Exact stiffness method for quasi-statics of a multilayered poroelastic medium', *Int. J. Solids Structures* **32**, 1535–1553.

Singh, S. J. (1970), 'Static deformation of a multilayered half-space by internal sources', *Physics of the Earth and Planetary Interiors* **75**, 3257–3263.

Singh, S. J. (1986), 'Static deformation of a transversely isotropic multilayered half-space by surface loads', *J. Geophys. Res.* **42**, 263–273.

Singh, S. J. & Garg, N. R. (1985), 'On two-dimensional elastic dislocations in a multilayered half-space', *Physics of the Earth and Planetary Interiors* **40**, 135–145.

Small, J. C. & Booker, J. R. (1984), 'Finite layer analysis of layered elastic materials using a flexibility approach. part 1-strip loadings', *International Journal for Numerical Methods in Engineering* **20**, 1025–1037.

Small, J. C. & Booker, J. R. (1986*a*), 'The behaviour of layered soil or rock containing a decaying heat source', *International Journal for Numerical and Analytical Methods in Geomechanics* **10**, 501–519.

Small, J. C. & Booker, J. R. (1986*b*), 'Finite layer analysis of layered elastic materials using a flexibility approach. part 2-circular and rectangular loadings', *International Journal for Numerical Methods in Engineering* **23**, 959–978.

Srivastava, R. & Avasthi, P. (1975), 'Non-equilibrium thermodynamics of thermo-osmosis of water through kaolinite', *Journal of Hydrology* **24**, 111–120.

Thomas, H. & Cleall, P. (1999), 'Inclusion of expansive clay behaviour in coupled thermo hydraulic mechanical models', *Engineering Geology* **54**, 93–108.

Thomson, W. T. (1950), 'Transmission of elastic waves through a stratified soil medium', *J. Appl. Phys.* **21**, 89–93.

Vafai, K. & Alazmi, B. (2002), 'Constant wall heat flux boundary conditions in porous media under local thermal non-equilibrium conditions', *International Journal of Heat and Mass Transfer* **45**, 3071–3087.

Vafai, K. & Sheikh, A. H. (2004), 'Analysis of flow and heat transfer in porous media imbedded inside various-shaped ducts', *International Journal of Heat and Mass Transfer* **47**, 1889–1905.

Wang, J. & Fang, S. (2003), 'State space solution of non-axisymmetric biot consolidation problem for multilayered porous media', *Int. J. Eng. Sci.* **41**, 1799–1813.

Wang, L. J. & Ai, Z. Y. (2015), 'Plane strain and three-dimensional analyses for thermo-mechanical behavior of multilayered transversely isotropic materials', *International Journal of Mechanical Sciences* **103**, 199–211.

Wang, R. (1999), 'A simple orthonormalization method for stable and efficient computation of green's functions', *Bull. Seis. Soc. Am.* **89**, 733–741.

Wang, R. & Kuempel, H. J. (2003), 'Poroelasticity: Efficient modeling of strongly coupled, slow deformation processes in multilayered half-space', *Geophysics* **68**, 1–13.

Wu, W., Li, X., Charlier, R. & Collin, F. (2004), 'A thermo-hydro-mechanical constitutive model and its numerical modelling for unsaturated soils', *Computers and Geotechnics* **31**, 155–167.

Yang, Y., Datcheva, M., Koenig, D. & Schanz, T. (2014), 'Heat transfer in a geothermal heat-pump system-an analytical assessment', *Geotechnique Letters* **4**, 139–144.

Yang, Y., Datcheva, M. & Schanz, T. (2016), 'Axisymmetric analysis of multilayered thermoelastic media with application to a repository for heat-emitting high-level nuclear waste in a geological formation', *Geophysical Journal International* **206**, 1144–1161.

Yang, Y., Guerlebeck, K. & Schanz, T. (2014), 'Thermo-osmosis effect in saturated porous medium', *Transp Porous Med* **104**, 253–271.

Yavuzturk, C. & Spitler, J. D. (1999), 'A short time step response factor model for vertical ground loop heat exchangers', *ASHRAE Transactions* **2**, 475–485.

Yue, Z. (1995), 'On generalized kelvin solutions in multilayered elastic media', *Journal of Elasticity* **40**(1), 1–43.

Zeng, H., Diao, N. & Fang, Z. (2003), 'Heat transfer analysis of boreholes in vertical ground heat exchangers', *International Journal of Heat and Mass Transfer* **46**(23), 4467–4481.

Zeng, H. Y., Diao, N. R. & Fang, Z. H. (2002), 'A finite line-source model for boreholes in geothermal heat exchangers', *Heat Transf. Asian Res.* **7**, 558–567.

Zhang, H., Bai, M., Abousleiman, Y. & Roegiers, J. (1999), 'An elastoplastic analysis of non-isothermal consolidation', *Int. J. Numer Anal. Methods Geomech.* **23**, 1535–1557.

Zheng, P., Ding, B., Zhao, S. X. & Ding, D. (2013*a*), '3d dynamic green's functions in a multilayered poroelastic half-space', *Applied Mathematical Modelling* **37**, 10203–10219.

Zheng, P., Ding, B., Zhao, S. X. & Ding, D. (2013*b*), 'Dynamic response of a multilayered poroelastic half-space to harmonic surface tractions', *Transport in Porous Media* **99**, 229–249.

Zhong, Y. & Geng, L. (2009), 'Thermal stresses of asphalt pavement under dependence of material characteristics on reference temperature', *Mech Time-Depend Mater* **13**, 81–91.

Zhou, Y., Rajapakse, R. & Graham, J. (1998), 'A coupled thermoporoelastic model with thermo-osmosis and thermal-filtration', *Int. J. Solids Structures* **35**, 4659–4681.

Zhu, L. & Rivera, L. A. (2002), 'A note on the dynamic and static displacements from a point source in multilayered media', *Geophys. J. Int.* **148**, 619–627.

Appendix A

The characteristic equation for matrix $\mathbf{A}$ is given as:

$$\det(\mathbf{A}-\zeta\mathbf{I}) = \det\begin{bmatrix} -\zeta & \frac{\lambda}{M}\eta^2 & \frac{1}{M} & 0 \\ -1 & -\zeta & 0 & \frac{1}{\mu} \\ 0 & 0 & -\zeta & \eta^2 \\ 0 & (M-\frac{\lambda^2}{M})\eta^2 & -\frac{\lambda}{M} & -\zeta \end{bmatrix} \tag{A1}$$

The eigenvalues are $\zeta_1 = \zeta_2 = \eta, \zeta_3 = \zeta_4 = -\eta$. So we can get the diagonal matrix $\mathcal{A}$ and the expression $e^{\mathcal{A}z}$ as

$$e^{\mathcal{A}z} = \begin{bmatrix} e^{\zeta_1 z} & 0 & 0 & 0 \\ 0 & e^{-\zeta_1 z} & 0 & 0 \\ 0 & 0 & e^{\zeta_1 z} & 0 \\ 0 & 0 & 0 & e^{-\zeta_1 z} \end{bmatrix} \tag{A2}$$

The corresponding eigenvectors compose the matrix $\mathbf{E}_A$ and can be written as

$$\mathbf{E}_A = \begin{bmatrix} d_1(\zeta_1) & d_1(\zeta_1) & d_1'(\zeta_1)+zd_1(\zeta_1) & -d_1'(\zeta_1)+zd_1(\zeta_1) \\ d_2(\zeta_1) & -d_2(\zeta_1) & d_2'(\zeta_1)+zd_2(\zeta_1) & d_2'(\zeta_1)-zd_1(\zeta_1) \\ \frac{\eta^2}{\zeta_1} & -\frac{\eta^2}{\zeta_1} & -\frac{\eta^2}{\zeta_1^2}+z\frac{\eta^2}{\zeta_1} & -\frac{\eta^2}{\zeta_1^2}-z\frac{\eta^2}{\zeta_1} \\ 1 & 1 & z & z \end{bmatrix} \tag{A3}$$

where $d_1(\zeta_1) = \frac{\lambda\zeta_1^2+M\eta^2}{(M^2-\lambda^2)\zeta_1^2}$ $d_2(\zeta_1) = \frac{\lambda\eta^2+M\zeta_1^2}{(M^2-\lambda^2)\zeta_1\eta^2}$, the prime ' denotes the first derivative with respect to z. The propagator submatrix $\mathbf{P}_A$ can be obtained by

$$\mathbf{P}_A = \mathbf{E}_A e^{\mathcal{A}z}\mathbf{E}_A^{-1} = [a_{ij}] \tag{A4}$$

with the elements a_{ij} being

$$a_{11}=a_{33}=-\frac{M+\lambda}{2M}\eta z\sinh(\eta z)+\cosh(\eta z)\quad a_{12}=\frac{M-\lambda}{2M}\eta\sinh(\eta z)-\frac{M+\lambda}{2M}\eta^2 z\cosh(\eta z)$$
$$a_{13}=-(\frac{1}{2M}+\frac{1}{M-\lambda})\frac{1}{\eta}\sinh(\eta z)+\frac{1}{2M}\frac{M+\lambda}{M-\lambda}z\cosh(\eta z)\quad a_{14}=\frac{1}{2M}\frac{M+\lambda}{M-\lambda}\eta z\sinh(\eta z)$$
$$a_{21}=\frac{M-\lambda}{2M}\frac{1}{\eta}\sinh(\eta z)+\frac{M+\lambda}{2M}z\cosh(\eta z)\quad a_{22}=a_{44}=\frac{M+\lambda}{2M}\eta z\sinh(\eta z)+\cosh(\eta z)$$
$$a_{23}=-\frac{a_{14}}{\eta^2}\quad a_{24}=-(\frac{1}{2M}+\frac{1}{M-\lambda})\frac{1}{\eta}\sinh(\eta z)-\frac{1}{2M}\frac{M+\lambda}{M-\lambda}z\cosh(\eta z)$$
$$a_{31}=-\frac{M^2-\lambda^2}{2M}\eta(\sinh(\eta z)-\eta z\cosh(\eta z))\quad a_{32}=\frac{M^2-\lambda^2}{2M}\eta^3 z\sinh(\eta z)\quad a_{34}=-a_{21}\eta^2$$
$$a_{41}=-\frac{a_{32}}{\eta^2}\quad a_{42}=-\frac{M^2-\lambda^2}{2M}\eta(\sinh(\eta z)+\eta z\cosh(\eta z))\quad a_{43}=-\frac{a_{12}}{\eta^2}$$

and the submatrix $\mathbf{G}_A$ can also be obtained by

$$\mathbf{G}_A=\mathbf{E}_A e^{\mathcal{A}z}=\begin{bmatrix} d_1(\zeta_1)e^{\zeta_1 z} & d_1(\zeta_1)e^{-\zeta_1 z} & [d_1'(\zeta_1)+zd_1(\zeta_1)]e^{\zeta_1 z} & [-d_1'(\zeta_1)+zd_1(\zeta_1)]e^{-\zeta_1 z} \\ d_2(\zeta_1)e^{\zeta_1 z} & -d_2(\zeta_1)e^{-\zeta_1 z} & [d_2'(\zeta_1)+zd_2(\zeta_1)]e^{\zeta_1 z} & [d_2'(\zeta_1)-zd_2(\zeta_1)]e^{-\zeta_1 z} \\ \frac{\eta^2}{\zeta_1}e^{\zeta_1 z} & -\frac{\eta^2}{\zeta_1}e^{-\zeta_1 z} & (-\frac{\eta^2}{\zeta_1^2}+z\frac{\eta^2}{\zeta_1})e^{\zeta_1 z} & (-\frac{\eta^2}{\zeta_1^2}-z\frac{\eta^2}{\zeta_1})e^{-\zeta_1 z} \\ e^{\zeta_1 z} & e^{-\zeta_1 z} & ze^{\zeta_1 z} & ze^{-\zeta_1 z} \end{bmatrix} \tag{A5}$$

With the same methodology, we can get the eigenvalues of matrix $\boldsymbol{B}$ and the corresponding eigenvectors. Thus the matrix $\mathbf{E}_B$, propagator submatrix $\mathbf{P}_B$ and $\mathbf{G}_B$ can be consequently obtained as follows:

$$\zeta_5=\sqrt{\eta^2+s},\quad \zeta_6=-\sqrt{\eta^2+s} \tag{A6}$$

$$e^{\mathcal{B}z}=\begin{bmatrix} e^{\zeta_5 z} & 0 \\ 0 & e^{-\zeta_5 z} \end{bmatrix} \tag{A7}$$

$$\mathbf{E}_B=\begin{bmatrix} 1 & 1 \\ \frac{k}{L}\zeta_5 & -\frac{k}{L}\zeta_5 \end{bmatrix} \tag{A8}$$

$$\mathbf{P}_B=\mathbf{E}_B e^{\mathcal{B}z}\mathbf{E}_B^{-1}=[b_{ij}]=\begin{bmatrix} \cosh(\zeta_5 z) & -\frac{L}{k\zeta_5}\sinh(\zeta_5 z) \\ -\frac{k\zeta_5}{L}\sinh(\zeta_5 z) & \cosh(\zeta_5 z) \end{bmatrix} \tag{A9}$$

$$\mathbf{G}_B=\mathbf{E}_B e^{\mathcal{B}z}=\begin{bmatrix} e^{\zeta_5 z} & e^{-\zeta_5 z} \\ \frac{k\zeta_5}{L}e^{\zeta_5 z} & -\frac{k\zeta_5}{L}e^{-\zeta_5 z} \end{bmatrix} \tag{A10}$$

The expression of matrix $\mathbf{G}_C$ can be deduced directly from Equation (5.23) as

$$\mathbf{G}_C = \begin{bmatrix} \frac{\alpha_1}{\zeta_5} e^{\zeta_5 z} & -\frac{\alpha_1}{\zeta_5} e^{-\zeta_5 z} \\ 0 & 0 \\ 0 & 0 \\ \frac{\alpha_2}{\zeta_5} e^{\zeta_5 z} & -\frac{\alpha_2}{\zeta_5} e^{-\zeta_5 z} \end{bmatrix} \tag{A11}$$

and the propagator submatrix $\mathbf{P}_C$ can be derived based on the property of block matrix by

$$\mathbf{P}_C = -\mathbf{G}_A(0)\mathbf{G}_A^{-1}(z)\mathbf{G}_C(z)\mathbf{G}_B^{-1}(z) + \mathbf{G}_C(0)\mathbf{G}_B^{-1}(z) = [c_{ij}] \tag{A12}$$

with the none-zero elements being

$$c_{11} = -\frac{\alpha_1}{\zeta_5}\sinh(\zeta_5 z) \quad c_{12} = -\frac{zL}{\zeta_5^2 k}(\alpha_1 \frac{d_1}{d_2} - \alpha_2 \frac{d_1'}{d_2})\sinh(\zeta_1 z) + \frac{\alpha_1 L}{\zeta_5^2 k}(\cosh(\zeta_5 z) - \cosh(\zeta_1 z))$$

$$c_{22} = \frac{L}{\zeta_5^2 k}[((\alpha_1 - \alpha_2 d_1)\frac{d_2'}{d_1'} + \alpha_2 d_2)\sinh(\zeta_1 z) + (\alpha_1 - \alpha_2 d_1)\frac{d_2}{d_1'} z\cosh(\zeta_1 z)]$$

$$c_{32} = -\frac{\eta^2 L}{\zeta_1^2 \zeta_5^2 k}[((\alpha_1 - \alpha_2 d_1)\frac{1}{d_1'} - \alpha_2 \zeta_1)\sinh(\zeta_1 z) - (\alpha_1 - \alpha_2 d_1)\frac{\zeta_1}{d_1'} z\cosh(\zeta_1 z)]$$

$$c_{41} = -\frac{\alpha_2}{\zeta_5}\sinh(\zeta_5 z) \quad c_{42} = -\frac{zL}{\zeta_5^2 k}(\frac{\alpha_1}{d_1'} - \frac{\alpha_2 d_1}{d_1'})\sinh(\zeta_1 z) + \frac{\alpha_2 L}{\zeta_5^2 k}(\cosh(\zeta_5 z) - \cosh(\zeta_1 z))$$

It should be noted that, all the above mentioned matrices and elements are normalized by Equation (5.62) while the superscript * is omitted for brevity.

Appendix B

For the 3D axisymmetric problem as described in section 3, the analytical solutions for temperature θ, vertical displacement u_z, radial displacement u_r, vertical stress σ_z and radial stress σ_r in Laplace transform domain can be written as:

$$\theta = \int_0^\infty \hat{\Theta}_\xi^m S_\xi^m \xi \mathrm{d}\xi \tag{B1}$$

$$u_z = \int_0^\infty \hat{U}_{\xi L}^m S_\xi^m \xi \mathrm{d}\xi \tag{B2}$$

$$u_r = \int_0^\infty \hat{U}^m_{\xi M} \frac{\partial S^m_\xi}{\partial r} \xi \mathrm{d}\xi \tag{B3}$$

$$\sigma_z = \int_0^\infty \hat{T}^m_{\xi L} S^m_\xi \xi \mathrm{d}\xi \tag{B4}$$

$$\sigma_r = 2\mu \int_0^\infty \hat{U}^m_{\xi M} \frac{\partial^2 S^m_\xi}{\partial r^2} \xi \mathrm{d}\xi + M \int_0^\infty (-\xi^2 \hat{U}^m_{\xi M} + \frac{\partial \hat{U}^m_{\xi L}}{\partial z}) S^m_\xi \xi \mathrm{d}\xi - \alpha_0 \int_0^\infty \hat{\Theta}^m_\xi S^m_\xi \xi \mathrm{d}\xi \tag{B5}$$

The expressions for $\hat{U}^m_{\xi L}, \hat{U}^m_{\xi M}, \hat{T}^m_{\xi L}, \hat{T}^m_{\xi M}, \hat{\Theta}^m_\xi, \hat{Q}^m_{\xi H}$ can be found in Equations (5.50)- (5.53), and then the numerical results can be successfully obtained with the numerical strategy presented in section 3.

Appendix C

In this appendix we discuss the elements of the submatrix $[X(z)]_{4\times 2}$ as introduced in Pan (1990) for representing the effect of the temperature field to the displacements and stresses. We would like to underline that Pan (1990) is actually a fabulous paper on the topic, however, the non-zero elements of the submatrix $[X(z)]_{4\times 2}$ are given in Equation (16) incorrectly. The correct expressions for $[X(z)]_{4\times 2}$ read:

$$X_{11} = \frac{\beta_4}{x_3} e^{x_3 z}, \quad X_{12} = -\frac{\beta_4}{x_3} e^{-x_3 z}, \quad X_{41} = \frac{\beta_5}{x_3} e^{x_3 z}, \quad X_{42} = -\frac{\beta_5}{x_3} e^{-x_3 z} \tag{C1}$$

This correction to the expressions in Equation (16) from Pan Pan (1990) has to be taken in consideration in the following Equation (21) from the same paper. It has to be pointed, that the incorrect expressions for the submatrix $[X(z)]_{4\times 2}$ elements do not influence the quality of the Pan's paper and its essential contribution to the topic giving us the inspiration how to treat the effect of heating on the deformation of the lithosphere. In the context of this remark, equation (C1) may be regarded as an improving block to Pan's great building.

Schriftenreihe des Lehrstuhls für Grundbau, Boden- und Felsmechanik der Ruhr-Universität Bochum

Herausgeber: H.L. Jessberger

1 (1979) **Hans Ludwig Jessberger**
Grundbau und Bodenmechanik an der Ruhr-Universität Bochum

2 (1978) **Joachim Klein**
Nichtlineares Kriechen von künstlich gefrorenem Emschermergel

3 (1979) **Heinz-Joachim Gödecke**
Die Dynamische Intensivverdichtung wenig wasserdurchlässiger Böden

4 (1979) **Poul V. Lade**
Three Dimensional Stress-Strain Behaviour and Modeling of Soils

5 (1979) **Roland Pusch**
Creep of soils

6 (1979) **Norbert Diekmann**
Zeitabhängiges, nichtlineares Spannungs-Verformungsverhalten von gefrorenem Schluff unter triaxialer Belastung

7 (1979) **Rudolf Dörr**
Zeitabhängiges Setzungsverhalten von Gründungen in Schnee, Firn und Eis der Antarktis am Beispiel der deutschen Georg-von-Neumayer- und Filchner-Station

8 (1984) **Ulrich Güttler**
Beurteilung des Steifigkeits- und Nachverdichtungsverhaltens von ungebundenen Mineralstoffen

9 (1986) **Peter Jordan**
Einfluss der Belastungsfrequenz und der partiellen Entwässerungs-möglichkeiten auf die Verflüssigung von Feinsand

10 (1986) **Eugen Makowski**
Modellierung der künstlichen Bodenvereisung im grundwasserdurchströmten Untergrund mit der Methode der finiten Elemente

11 (1986) **Reinhard A. Beine**
Verdichtungswirkung der Fallmasse auf Lastausbreitung in nichtbindigem Boden bei der Dynamischen Intensivverdichtung

12 (1986) **Wolfgang Ebel**
Einfluss des Spannungspfades auf das Spannungs-Verformungsverhalten von gefrorenem Schluff im Hinblick auf die Berechnung von Gefrierschächten

13 (1987) **Uwe Stoffers**
Berechnungen und Zentrifugen-Modellversuche zur Verformungsabhängigkeit der Ausbaubeanspruchung von Tunnelausbauten in Lockergestein

14 (1988) **Gerhard Thiel**
Steifigkeit und Dämpfung von wassergesättigtem Feinsand unter Erdbebenbelastung

15 (1991) **Mahmud Thaher**
Tragverhalten von Pfahl-Platten-Gründungen im bindigen Baugrund,
Berechnungsmodelle und Zentrifugen-Modellversuche

16 (1992) **Rainer Scherbeck**
Geotechnisches Verhalten mineralischer Deponieabdichtungsschichten
bei ungleichförmiger Verformungswirkung

17 (1992) **Martin M. Bizialiele**
Torsional Cyclic Loading Response of a Single Pile in Sand

18 (1993) **Michael Kotthaus**
Zum Tragverhalten von horizontal belasteten Pfahlreihen aus langen Pfählen in Sand

19 (1993) **Ulrich Mann**
Stofftransport durch mineralische Deponieabdichtungen:
Versuchsmethodik und Berechnungsverfahren

20 (1992) **Festschrift anlässlich des 60. Geburtstages von**
Prof. Dr.-Ing. H. L. Jessberger
20 Jahre Grundbau und Bodenmechanik an der Ruhr-Universität Bochum

21 (1993) **Stephan Demmert**
Analyse des Emissionsverhaltens einer Kombinationsabdichtung im Rahmen der
Risikobetrachtung von Abfalldeponien

22 (1994) **Diethard König**
Beanspruchung von Tunnel- und Schachtausbauten in kohäsionslosem Lockergestein
unter Berücksichtigung der Verformung im Boden

23 (1995) **Thomas Neteler**
Bewertungsmodell für die nutzungsbezogene Auswahl von Verfahren zur Altlastensanierung

24 (1995) **Ralph Kockel**
Scherfestigkeit von Mischabfall im Hinblick auf die Standsicherheit von Deponien

25 (1996) **Jan Laue**
Zur Setzung von Flachfundamenten auf Sand unter wiederholten Lastereignissen

26 (1996) **Gunnar Heibrock**
Zur Rissbildung durch Austrocknung in mineralischen Abdichtungsschichten
an der Basis von Deponien

27 (1996) **Thomas Siemer**
Zentrifugen-Modellversuche zur dynamischen Wechselwirkung zwischen Bauwerken
und Baugrund infolge stoßartiger Belastung

28 (1996) **Viswanadham V. S. Bhamidipati**
Geosynthetic Reinforced Mineral Sealing Layers of Landfills

29 (1997) **Frank Trappmann**
Abschätzung von technischem Risiko und Energiebedarf bei Sanierungsmaßnahmen
für Altlasten

30 (1997) **André Schürmann**
Zum Erddruck auf unverankerte flexible Verbauwände

31 (1997) **Jessberger, H. L. (Herausgeber)**
Environment Geotechnics, Report of ISSMGE Technical Committee TC 5
on Environmental Geotechnics

Herausgeber: Th. Triantafyllidis

32 (2000) **Triantafyllidis, Th. (Herausgeber)**
Boden unter fast zyklischer Belastung: Erfahrung und Forschungsergebnisse (Workshop)

33 (2002) **Christof Gehle**
Bruch- und Scherverhalten von Gesteinstrennflächen mit dazwischenliegenden Materialbrücken

34 (2003) **Andrzej Niemunis**
Extended hypoplastic models for soils

35 (2004) **Christiane Hof**
Über das Verpressankertragverhalten unter kalklösendem Kohlensäureangriff

36 (2004) **René Schäfer**
Einfluss der Herstellungsmethode auf das Verformungsverhalten von Schlitzwänden in weichen bindigen Böden

37 (2005) **Henning Wolf**
Zur Scherfugenbänderung granularer Materialien unter Extensionsbeanspruchung

38 (2005) **Torsten Wichtmann**
Explicit accumulation model for non-cohesive soils under cyclic loading

39 (2008) **Christoph M. Loreck**
Die Entwicklung des Frischbetondruckes bei der Herstellung von Schlitzwänden

40 (2008) **Igor Arsic**
Über die Bettung von Rohrleitungen in Flüssigböden

41 (2009) **Anna Arwanitaki**
Über das Kontaktverhalten zwischen einer Zweiphasenschlitzwand und nichtbindigen Böden

Herausgeber: T. Schanz

42 (2009) **Yvonne Lins**
Hydro-Mechanical Properties of Partially Saturated Sand

43 (2010) **Tom Schanz (Herausgeber)**
Geotechnische Herausforderungen beim Umbau des Emscher-Systems
Beiträge zum RuhrGeo Tag 2010

44 (2010) **Jamal Alabdullah**
Testing Unsaturated Soil for Plane Strain Conditions: A New Double-Wall Biaxial Device

45 (2011) **Lars Röchter**
Systeme paralleler Scherbänder unter Extension im ebenen Verformungszustand

46 (2011) **Yasir Al-Badran**
Volumetric Yielding Behavior of Unsaturated Fine-Grained Soils

47 (2011) **Usque ad finem**
Selected research papers

48 (2012) **Muhammad Ibrar Khan**
Hydraulic Conductivity of Moderate and Highly Dense Expansive Clays

49 (2014) **Long Nguyen-Tuan**
Coupled Thermo-Hydro-Mechanical Analysis: Experimental and Back Analysis

50 (2014) **Tom Schanz (Herausgeber)**
Ende des Steinkohlenbergbaus im Ruhrrevier: Realitäa und Perspektiven für die Geotechnik Beiträge zum RuhrGeo Tag 2014

51 (2014) **Usque ad finem**
Selected research papers

52 (2014) **Houman Soleimani Fard**
Study on the Hydro-Mechanical Behaviour of Fiber Reinforced Fine Grained Soils with Application to the Preservation of Historical Monuments

53 (2014) **Wiebke Baille**
Hydro-Mechanical Behavior of Clays - Significance of Mineralogy

54 (2014) **Qasim Abdulkarem Jassim Al-Obaidi**
Hydro-Mechanical Behavior of Collapsible Soils

55 (2015) **Veselin Zarev**
Model Identification for the Adaption of Numerical Simulation Models - Application to Mechanized Shield Tunneling

56 (2015) **Meisam Goudarzy**
Micro and Macro Mechanical Assessment of Small and Intermediate Strain Properties of Granular Material

57 (2016) **Oliver Detert**
Analyse einer selbstregulierenden interaktiven Membrangründung für Schüttkörper auf geringtragfähigen Böden

58 (2016) **Yang Yang**
Analyses of Heat Transfer and Temperature-induced Behaviour in Geotechnics